

https://dspace.org/

Commissioning and Implementation aspect of the Monaco TPS system at CMJAH

Baloyi, Trevor

2025-06
University of the Witwatersrand, Johannesburg
https://hdl.handle.net/10539/47483
Baloyi, Trevor. (2025). Commissioning and Implementation aspect of the Monaco TPS system at CMJAH. [Master's dissertation, University of the Witwatersrand, Johannesburg]. WIReDSpace. https://hdl.handle.net/10539/47483

Downloaded from a DSpace repository. https://dspace.org/

Commissioning and Implementation aspect of the Monaco TPS system at CMJAH

Mr Trevor Baloyi

A research report submitted to the Faculty of Science, University of the Witwatersrand, Johannesburg, in partial fulfilment of the requirements for the Master of Science degree in Medical Physics.

Supervisor: Dr. Sonwabile Ngcezu

(University of the Witwatersrand)

Co-supervisor: Arcilliah Mavundla

(University of the Witwatersrand)

June 2025

DECLARATION

I, Trevor Baloyi, declare that this Research Report represents my own, unaided work. It is submitted in partial fulfilment of the requirements for the Master of Science degree (coursework and research report) in Medical Physics at the University of the Witwatersrand, Johannesburg. This report has not been submitted for any degree or examination at any other university.



(Signature of candidate)

09 day of June 2025 in Soshanguve

ABSTRACT

Introduction: Modern Treatment Planning Systems (TPS), such as Elekta's Monaco TPS, are essential in radiotherapy. Proper commissioning and Quality Assurance (QA) are essential to ensure accurate treatment planning and minimise side effects. This study aimed to validate the Monaco TPS (version 6.1.2.0) through photon beam data collection, analysis and dose calculation algorithm checks, ensuring optimal clinical outcomes and patient safety.

Methodology: The verification of the Monaco TPS commissioning beam data for clinical use with four Elekta Versa HD linear accelerators at Charlotte Maxeke Johannesburg Academic Hospital (CMJAH) was performed in accordance with established dosimetric protocols. Photon beam data were collected using a PTW Beamscan water phantom and a PTW Unidos E electrometer with ionisation chambers and were compared with simulated data from the TPS for validation. Treatment plans for Volumetric Modulated Arc Therapy (VMAT) and 3D Conformal Radiation Therapy (3DCRT) techniques were generated and tested using the CIRS SHANE phantom for dose accuracy across various tissues and Perspex slabs. The Catphan 600 phantom was used for electron density (ED) calibration.

Results: This work showed good agreement for open fields of 10 x 10 cm^2 or larger, but discrepancies were primarily observed in fields, particularly in those less than 5 x 5 cm^2. Collapsed Cone Convolution (CCC) models performed well for wedged fields, with minor limitations in smaller field sizes (FSs). Linac calibration accuracy was confirmed within ±1% and CT scan evaluations validated the ED to Hounsfield unit (ED-HU) curve, ensuring a reliable representation of tissue heterogeneities. Gamma analysis and IMRT/VMAT audits confirmed clinical acceptability. Dose delivery accuracy in prostate cancer treatment using 3D-CRT and VMAT was within ±5%.

Conclusion: This study effectively verifies and validates the commissioned Monaco TPS data at CMJAH, thereby confirming the accuracy of dose calculations and adherence to international commissioning standards for clinical implementation.

Dedication

In memory of my father,

Tikoleni Joseph Baloyi

1949-2007

ACKNOWLEDGEMENTS

I am deeply grateful to my supervisor, Dr. S.A. Ngcezu, for his guidance, patience, encouragement and constructive feedback. It was a privilege to benefit from his outstanding scientific expertise throughout this project. I would like to extend my profound appreciation to Mr. Origin Bila for his significant contributions to the data collection process, which immensely facilitated the successful outcome of this research.

I also extend my appreciation to the University of the Witwatersrand for providing the opportunity to pursue my Master of Science degree and to Dr. S.A Ngcezu for his invaluable supervision.

Additionally, I acknowledge the invaluable contributions of the participating centres, radiation therapists and Medical Physicists (MPs) who generously shared their time and expertise to facilitate data collection. Their support played a crucial role in the successful completion of this study.

I extend my heartfelt appreciation to my mother, Tintswalo Baloyi and brother, Bongani Baloyi, whose unconditional love, support and encouragement provided invaluable motivation throughout my journey.

Finally, I acknowledge the financial support and Psycho-support provided by the Council for Scientific and Industrial Research (CSIR), which enabled the completion of this research.

GLOSSARY

2DCRT	2D Conformal Radiation Therapy
3DCRT	3D Conformal Radiation Therapy
AAA	Anisotropic Analytical Algorithms
AAPM	American Association of Physicists in Medicine
AI	Artificial Intelligence
AXB	Acuros XB
BQ	Beam Quality
BL	Baseline Value
CAX	Central Axis
CC/CCC	Collapsed Cone Convolution
CMJAH	Charlotte Maxeke Johannesburg Academic Hospital
CT	Computer Tomography
DICOM	Digital Imaging and Communications in Medicine
DLG	Dosimetric Leaf Gap
DTA	Distance-To-Agreement
E2E	End-to-End
EBT2	Gafchromic film
ED	Electron Density
EPID	Electronic Portal Imaging Device
EPOM	Effective Point of Measurement
FOV	Field Of View
FS	Field Size
GeV	Gigaelectron volt

HU	Hounsfield Units
IAEA	International Atomic Energy Agency
IEC	International Electrotechnical Commission
IGRT	Image-Guided Radiation Therapy
Linac	Linear Accelerator
MC	Monte Carlo
ML	Machine Learning
MLC	Multi-Leaf Collimator
MP	Medical Physicists
MRI	Magnetic Resonance Imaging
MV	Megavoltage
MU	Monitor Unit
ODI	Optical Distance Indicator
OF	Output Factor
PBC	Pencil Beam Convolution
PDD	Percentage Depth Dose
PET	Positron Emission Tomography
PSQA	Patient-Specific Quality Assurance
PTV	Planning Target Volume
QA	Quality Assurance
QC	Quality Control
RED	Relative Electron Density
RT	Radiation Therapy
SiMPs	Silicon photomultipliers

SRS	Stereotactic Radiosurgery
SBRT	Stereotactic Body Radiation Therapy
SOPs	Standard Operating Procedures
SP	Superposition
SCD	Source-to-Chamber distance
SSD	Source-to-Surface/Skin Distance
TG	Task Group
TPRs	Tissue-Phantom Ratios
TPS	Treatment Planning System
VMAT	Volumetric Modulated Arc Therapy

Table of Contents

DECLARATION ..... **i**
ABSTRACT ..... **ii**
ACKNOWLEDGEMENTS ..... **iv**
GLOSSARY ..... **v**
LIST OF FIGURES ..... **xi**
LIST OF TABLES ..... **xiv**
1. Introduction **1**
1.1. Background 1
1.2. Problem Statement 2
1.3. Motivation of the study 3
1.4. Aim and Objectives 3
1.5. Research Questions 4
1.6. Research Report Outline 5
2. Theoretical Background **6**
2.1. Literature Review 6
2.2. Machine Specification 7
2.3. Commissioning in Radiation Therapy 8
2.3.1. Beam Data Acquisition and Base Model Validation 8
2.3.2. Heterogeneity Correction Validation 8
2.3.3. Dosimetric Leaf Gap (DLG) Measurement 8
2.3.4. Multi-Leaf Collimator (MLC) Transmission and Leaf Position Verification 9
2.3.5. Treatment Plan Verification (End-to-End(E2E) Testing) 9
2.4. Importance of Quality Assurance (QA) 9
2.5. Commissioning Data Verification 9
2.6. Percentage Dose Depth Curves (PDDs) and Dose Beam Profiles 10
2.6.1. Percentage Depth Dose (PDDS) 10
2.6.2. Beam Profiles 11
2.7. Importance of Small Field Commissioning in Photon Beam Therapy 12
2.8. Optimising CT Commissioning for Accurate Treatment Planning in Monaco System: Calibration and Simulation Protocol 13

2.9. Comparing 2D vs. 3D Radiation Therapy: Considerations for Treatment Selection....13
2.10. Understanding Dose Calculation Algorithms in Monaco Treatment Planning.....14
2.11. Modern 3D dose calculation and optimisation 15
2.12. Optimising DLG and MLC Transmission in Monaco TPS for Clinical Accuracy 16
2.13. Balancing Precision and Safety Through IMRT and VMAT Techniques 17
2.14. Versa HD and IGRT features. 17
2.14.1. Mega-voltage cone beam CT (MV CBCT) and X-ray 2D.....18
2.15. 1 D Gamma Analysis 19
3. Materials and Methods.....20
3.1. Materials 20
3.1.1. Scanning Water Tank and Electrometer 21
3.1.2. Detectors 22
3.1.3. Linear accelerator (Linac).....25
3.1.4. Treatment Planning System (TPS).....25
3.1.5. Phantoms employed in this study.....25
3.1.6. Record and Verify (MOSAIQ VERSION 2.81).....29
3.2. Methods.....29
3.2.1. Pre-Scanning Linac checks 30
3.3. Photon Beam Data Collection.....31
3.3.1. Open Field.....32
3.3.2. Physical and motorised wedges 32
3.3.3. Absolute Dose Calculations.....33
3.4. Model validation 34
3.4.1. Heterogeneous Phantom Validation 35
3.4.2. Basic Beam Data Validation 35
3.4.3. MLC and DLG Transmission.....36
3.4.4. VMAT/IMRT Validation (Including 3D Plan Validation).....36
3.4.5. 3D and VMAT for Prostate 39
4. Results and Discussion.....41
4.1. Commissioning data.....41
4.2. Homogeneity Correction.....44

4.3. Base model validation 45
4.3.1. PDDs and Profiles Validation 46
4.3.2. Output Factor Validation 57
4.3.3. Dosimetric Validation 60
4.4. DLG and MLC measurement 62
4.5. 3DCRT and VMAT/IMRT Plan Validation 63
4.5.1. Patient-Specific Quality Assurance (PSQA) 67
5. Conclusion 69
6. References 71
Appendix 1-Beam Data (PDDs) 80
Appendix 2- Beam Data (Beam Profile) 82

LIST OF FIGURES

Figure 1: Schematic diagram of PDD (Bencheikh et al., 2018).....10
Figure 2: Schematic diagram of Dose profile and its components (Beyzadeoglu et al., 2010). 11
Figure 3: Elekta High Dose Rate Digital Linear Accelerator Versa HD. 18
Figure 4: Image of a PTW UNIDOS E electrometer. 22
Figure 5: Detectors used: (a) PTW 0.125cm^3 Semiflex (b) PTW 0.004 cm^3 MicroDiamond (c) PTW 0.07 cm^3 Semiflex 3D field (e) PTW 0.07 cm^3 Semiflex 3D reference and (f) TRUFIX BS equipment. 24
Figure 6: Shane Phantom taken at CMJAH. 26
Figure 7:Setup used for PSQA measurements. 27
Figure 8: The Catphan®600 CT phantom (Zarb and Rainford, 2014). 28
Figure 9:Setup used to acquire the commissioning data with field and reference chamber. ..32
Figure 10: Set-up used to collect measurements for both MLC and DLG. 36
Figure 11: CT scan of the Head & Neck phantom illustrating the locations of the ionisation chamber channels and the respective ionisation chamber positions in various views: (a) Transverse plane, (b) 3-D Display, (c) Sagittal view and (d) Coronal view (Kazantsev et al., 2020). 39
Figure 12: 6MV PDD measurements were performed using a PTW micro-diamond 0.004 cm³ chamber for FSs ranging from 2 × 2 cm² to 4 × 4 cm² and the PTW Semiflex 3D 0.07 cm³ for FSs from 5 × 5 cm² to 40 × 40 cm², all at an SSD of 90 cm. 42
Figure 13:6MV inplane and crossplane profiles for a 5 × 5 cm² FS were measured at depths (see Section 3.1.1) using the PTW Semiflex 0.07 cc detector, with an SSD of 90 cm. 42
Figure 14:6MV inplane and cross-plane half profiles for a 40 × 40 cm² FS were measured at depths (see Section 3.1.1) using the PTW Semiflex 0.07 cc detector, with an SSD of 90 cm.43
Figure 15: (a) Catphan Reference diagram with different materials (C a t p h a n ® 500 and 600 Product Guide) (b) Scanned Catphan at CMJAH. 45
Figure 16: Shows the comparison of CT to RED curves measured with the Catphan phantom and the CIRS Shane phantom, both scanned at CMJAH, with reference to the Monaco TPS RED curve.....45
Figure 17: (a) Comparison of measured and TPS Monte Carlo (MC) percentage depth dose for a 5x5 cm² open field for 6 MV. (b) Comparison of measured and TPS collapsed cone (CC) percentage depth dose for a 10x10 cm² wedged field for 6 MV. (c) Comparison of measured

and TPS Monte Carlo MC percentage depth dose for a 20x20 cm² open field for 6 MV FFF. 48
Figure 18: (a) Comparison of measured and TPS Monte Carlo (MC) percentage depth dose for a 5x5 cm² open field for 10 MV. (b) Comparison of measured and TPS collapsed cone (CC) percentage depth dose for a 5x5 cm² wedged field for 10 MV. 49
Figure 19: (a) Comparison of measured and TPS collapsed cone (CC) percentage depth dose for a 3x3 cm² open field for 15 MV. (b) Comparison of measured and TPS CC percentage depth dose for a 5x5 cm² wedged field for 15 MV. 50
Figure 20: (a) Comparison of measured and TPS collapsed cone (CC) percentage depth dose for a 5x5 cm² open field for 15 MV. (b) Comparison of measured and TPS CC percentage depth dose for a 5x5 cm² wedged field for 15 MV. 51
Figure 21: Comparison of measured and TPS MC open field half profiles for 6MV, 40 × 40 cm² at 1.5 cm depth, showing 1D gamma. (b) Comparison of measured and TPS CC wedged field profiles for 6MV, 10 × 10 cm² at 1.5 cm depth, Showing 1D gamma. (c) Comparison of measured and TPS MC open field half profiles for 6MV FFF, 40 × 40 cm² at 1.3 cm depth, showing 1D gamma. 52
Figure 22: (a) Comparison of measured and TPS MC open field half profiles for 10MV, 40 × 40 cm² at 2.5 cm depth, showing 1D gamma. (b) Comparison of measured and TPS CC wedged field profiles for 10MV, 40 × 30 cm² at 2.5 cm depth, Showing 1D gamma. 53
Figure 23: (a) Comparison of measured and TPS CC open field half profiles for 15MV, 10 × 10 cm² at 2.69 cm depth, showing 1D gamma. (b) Comparison of measured and TPS CC wedged field profiles for 15MV, 40 × 30 cm² at 2.69 cm depth, Showing 1D gamma. 54
Figure 24: (a) Comparison of measured and TPS CC open field half profiles for 18MV, 3 × 3 cm² at 3.0 cm depth, showing 1D gamma. (b) Comparison of measured and TPS CC wedged field profiles for 18MV, 10 × 10 cm² at 3.0 cm depth, Showing 1D gamma. 55
Figure 25: (a) Compares the measured Open Field Output Factors (OFs) with those calculated for the specified wedged FSs. (b) Illustrates the deviations between the measured and calculated OF values. 59
Figure 26: Compares the measured Wedged Field Output Factors (OFs) with those calculated for the specified FSs. (b) Illustrates the deviations between the measured and calculated OF values. 60
Figure 27: DLG measurement using the sweeping gap technique, which accounts for MLC end-of-leaf transmission, shows a linear relationship in the collected data. This analysis

provided initial DLG values specific to each energy: 0.50 mm for 6MV, 0.51 mm for 6MV FFF, 0.47 mm for 10MV, 0.49 mm for 10MV FFF and 0.93 mm for 15MV. 63

LIST OF TABLES

Table 1: Detector Characteristics and Assign Activities for VersaHD Linac Commissioning. 23
Table 2:CIRS Shane phantom design with associated volumes and TPS constraints. 38
Table 3: Gamma analysis pass rate for various open fields for measured and MC PDDs 56
Table 4: Gamma analysis pass rate for various open fields for measured and TPS MC PDDs. 56
Table 5: Gamma analysis pass rate for various open fields for measured and TPS CC PDDs 56
Table 6: Gamma analysis pass rate for various open fields for measured and TPS MC Profiles. 57
Table 7: Gamma analysis pass rate for various open fields for measured and TPS CC Profiles. 57
Table 8: Calculated dose at dmax for standard reference conditions using SSD techniques. .61
Table 9: Calculated dose at dmax for wedge fields using SSD techniques. 62
Table 10: Recorded values for DLG and MLC transmission. 62
Table 11: Comparison between the measured and calculated doses using the Monte Carlo (MC) algorithm for the CIRS Shane phantom with 6 MV photon beams. 64
Table 12: Comparison between the measured and calculated doses using the Monte Carlo (MC) algorithm for the CIRS Shane phantom with 6 MV FFF photon beams. 65
Table 13: Comparison between the measured and calculated doses using the Monte Carlo algorithm for the CIRS Shane phantom with 10 MV photon beams. 66
Table 14: Result for VMAT plans on a Perspex phantom. 67
Table 15: Results for 3D plans on a Perspex phantom. 67
Table 16: PSQA results for both sites: Head & Neck and Prostate. 68

1. Introduction

1.1. Background

Radiation therapy (RT) centres worldwide rely on modern TPSs to simulate the characteristics of the radiation source and to calculate the dose distribution within the patient, based on the modelled treatment geometry and patient anatomy (Garibaldi *et al*., 2017). One of these systems is Elekta's Monaco TPS, a sophisticated treatment planning tool that has been utilised for nearly two decades (Gardner *et al*., 2019). Proper commissioning and interpretation of the Monaco TPS are essential to ensure accurate and efficient operation, requiring skilled personnel with a thorough knowledge of the system (Clements *et al*., 2018).

Commissioning a modern radiation TPS involves a variety of tests and measurements to establish the system's accuracy and reliability. This includes dose calculation and verification, validation of beam modelling accuracy and extensive evaluation of overall system performance (Geurts *et al*., 2022). The commissioning process for TPS is continuously refined to align with advancements in technology and evolving best practices, ensuring accurate and safe dose calculations.

Analysis of photon beam data forms an important aspect of commissioning a TPS. The accuracy of the measurement data collected and subsequent modelling of the radiation beam impacts upon the precision and accuracy of the dose calculation. It is important to understand the numerous factors affecting the photon beam data: energy of radiation, size and shape of the field and the distance from the source of radiation. Photon beam data interpretation is an expert activity, requiring a high degree of skill in the use of specialised equipment, such as ionisation chambers and dosimeters and an ability to carry out difficult calculations with Monte Carlo (MC) simulations (IAEA-TECDOC-1583, 2008).

The accuracy of dose calculation is essential in RT, as it determines the effectiveness of the treatment and the potential for side effects (Keall *et al*., 2000). The Monaco TPS (version 6.1.2.0) uses numerous dose calculation algorithms, including the Pencil Beam (PB) model and the CCC.

CCC methods and MC algorithms are used to calculate the dose distribution to heterogeneous materials. These algorithms consider multiple factors, including the energy and angle of the radiation beam, the patient's anatomical characteristics and the size and shape of the radiation field. Dose calculation accuracy further depends on the reliability of the input data,

the system parameter, configuration settings and the complexity of the treatment plan (Martino *et al*., 2021).

Measuring photon beam data, modelling beams and verifying the accuracy of the dose calculation algorithm are some of the phases included in the Monaco TPS commissioning procedure. For the commissioning process to be accurate and repeatable, a consistent procedure must be followed. This includes adhering to recognised protocols, such as those recommended by global organizations such as the IAEA and AAPM, for the commissioning process and regularly conducting QA testing to maintain the ongoing accuracy of the TPS (Van Dyk *et al*., 2006).

1.2. Problem Statement

Although accurate dose calculation is a well-established requirement in radiation therapy (Keall *et al*., 2000), it must be supported by rigorous commissioning and verification processes to ensure clinical reliability. At Charlotte Maxeke Johannesburg Academic Hospital (CMJAH), concerns have been raised about the completeness of the Monaco commissioning. While the Monaco TPS at CMJAH was initially commissioned according to manufacturer guidelines, these protocols did not fully incorporate several site-specific Quality Assurance (QA) procedures and internationally recommended validation steps (Fraass *et al*., 1998; Das *et al*., 2008; Smilowitz *et al*., 2015) .As a result, questions remain regarding the completeness and robustness of the current commissioning process, particularly in the context of advanced treatment techniques that rely on precise dose modelling.

This gap does not imply that the system is inherently inaccurate; however, it introduces uncertainty about whether the existing beam models and calculation algorithms perform reliably under diverse clinical conditions. Complex dose calculation algorithms such as MC and CCC are sensitive to input data quality, configuration settings, and patient-specific anatomical variations (Papanikolaou *et al*., 2004; Martino *et al*., 2021). Without comprehensive verification of these components, there is a risk of systematic deviations in dose delivery, which could affect both tumour control and normal tissue sparing.

Therefore, a thorough review and re-verification of the Monaco TPS commissioning data at CMJAH is necessary. This includes evaluating photon beam modelling accuracy, validating system performance against international standards (e.g., AAPM MPPG 5.a, TG-53, TG-106, TG-218, IAEA TRS-398) and implementing a robust framework tailored to local clinical

workflows. Strengthening the verification process will improve confidence in the TPS's performance, support safe and effective treatment planning and align the institution's practices with global best standards.

1.3. Motivation of the study

TPS form the computational backbone of modern radiation therapy, enabling accurate dose calculation and optimal tumour control while minimising damage to surrounding healthy tissue (Garibaldi *et al*., 2017). The Monaco TPS, known for its advanced dose calculation algorithms MC modelling capabilities, offers clinicians a powerful tool for achieving these goals. However, the reliability of its output is critically dependent on how well the system is commissioned, verified and maintained (Clements *et al*., 2018).

At CMJAH, the Monaco TPS was implemented using standard commissioning protocols provided by the manufacturer. While these protocols established a baseline for clinical use, they did not fully incorporate several internationally recommended Quality Assurance (QA) procedures necessary to validate system performance under local clinical conditions steps (Fraass *et al*., 1998; Das *et al*., 2008; Smilowitz *et al*., 2015).This partial implementation may result in reduced confidence in the TPS's predictive accuracy, particularly for complex, heterogeneous treatment scenarios (Brock *et al*., 2017).

This study is motivated by the need to strengthen and standardise the verification process of the Monaco TPS at CMJAH. By conducting a comprehensive review of existing commissioning data and implementing additional validation procedures in accordance with international guidelines such as AAPM MPPG 5.a, TG-53, TG-106, TG-198, TG-218, and IAEA TRS-398, this work aims to close the existing QA gaps and improve the system's reliability.

Furthermore, the study seeks to establish a reproducible, audit-ready commissioning framework that can be applied during future TPS upgrades, beam model adjustments, or institutional audits. It also aims to enhance staff confidence in the system's dose calculation accuracy, support safer patient treatments and raise the overall standard of care delivered within the department.

1.4. Aim and Objectives

This study aims to verify and validate the commissioned data of the Monaco TPS, version 6.1.2.0, at CMJAH through comprehensive dosimetric analysis, QA testing, and benchmarking

against international guidelines, with a specific focus on open and wedged fields and CT-to-density conversion accuracy.

The study includes**:**

- Assessment of the accuracy of Monaco TPS dose calculations for open and wedged photon fields using the MC and CC algorithms across various field sizes by comparing calculated and measured beam characteristics at clinically relevant photon energies (6 MV, 6 MV FFF, 10 MV, 15 MV and 18 MV) and evaluating agreement through gamma analysis with 3%/3 mm criteria.
- Interpretation of CT number to Relative Electron Density (RED) curve validation using Catphan and Shane phantoms and assess the influence of RED accuracy on dose calculation within heterogeneous tissues.
- Validation of Multi-leaf Collimators (MLC) parameters, including Dosimetric Leaf Gap (DLG) and leaf transmission factors, using ionisation chamber measurements and sweeping gap techniques and evaluating their impact on TPS dose modelling.
- Verification of reference dosimetry and calibration consistency for different energies using IAEA TRS-398 protocol, ensuring beam output accuracy and SSD-based dose delivery accuracy.
- Validation of the algorithms by conducting End-to-End (E2E) testing and Patient-Specific Quality Assurance (PSQA) using the PTW Octavius 4D system, following AAPM Task Group-218, for (3D Conformal Radiotherapy) 3D-CRT and (Volumetric Modulated Arc Therapy) VMAT treatment plans.

1.5. Research Questions

This study will explore the following research questions.

- Which commissioning and reference datasets are essential to achieve accurate clinical implementation of the Monaco TPS?
- What validation protocols are required to rigorously assess the accuracy of dosimetric calculations and dose delivery for all radiation oncology patients treated at CMJAH?

1.6. Research Report Outline

Chapter One introduces the key modalities employed in cancer treatment, specifically focusing on the technological advancements in RT. It outlines the purpose and motivation behind the study and the primary research questions that will be explored throughout the research report.

Chapter Two presents the literature review, which delves into the principles of TPS-related dosimetry, focusing on the Monaco TPS. It reviews relevant concepts, definitions and the challenges associated with commissioning photon beams and VMAT plans. It also examines previous studies on dosimetric validation techniques, including the use of Perspex phantoms and other measurement tools.

Chapter Three contains this study's materials and methodology, including phantoms, measurement devices and software tools. It describes the methodology employed for commissioning the Monaco TPS, including the setup of photon beam parameters, dosimetric measurements and data analysis procedures. Special emphasis is placed on the processes for validating dose distributions and machine performance.

Chapter Four details the results and discusses them by presenting the findings of the commissioning. It includes dose measurements, gamma analysis results and measured and calculated data comparisons. The discussion interprets these results in the context of the study objectives and evaluates the performance of the Monaco TPS in clinical settings.

Chapter Five gives the Conclusion and Recommendations. This concluding chapter summarises the study's key findings, provides conclusions based on the results and offers recommendations for future work. It reflects on the implications of the study for clinical practice and suggests areas for further research or improvements in the commissioning process.

2. Theoretical Background

The development of the medical linear accelerator, commonly known as the Linac, has been fundamental to the advancement of external beam radiation therapy. Introduced in the 1950s, Linacs were designed to overcome the challenges posed by earlier technologies such as orthovoltage X-ray machines and cobalt-60 units. These earlier machines had limited tissue penetration, uneven dose distribution and raised safety concerns due to their continuous radioactivity. Linacs produce megavoltage photon beams by accelerating electrons with microwave radiofrequency fields and directing them onto a high atomic number target to generate bremsstrahlung radiation. Over time, Linac technology has significantly improved by incorporating features like computer-controlled gantries, variable energy selection, onboard imaging systems and MLC, all of which have enhanced the precision and adaptability of radiation treatment (Chandrasekaran, 2012).

These technological improvements have enabled advanced treatment techniques, including 3D-CRT, Intensity-Modulated Radiation Therapy (IMRT), and VMAT. The success of these techniques largely depends on the accuracy of pre-treatment dose calculations. TPS simulates how radiation beams interact with the patient's anatomy. To achieve this, the systems must accurately model specific machine characteristics, such as energy spectra, jaw positions, Multi-Leaf Collimator (MLC) transmission and Dosimetric Leaf Gaps (DLG). Modern systems like Monaco, which utilise MC algorithms, require detailed commissioning based on measured data from the Linac. This process ensures that dose calculations closely match the actual radiation delivered during treatment, which is critical for both treatment effectiveness and patient safety (Chandrasekaran, 2012).

2.1. Literature Review

The development and commissioning of the TPS have greatly advanced the precision and safety of RT. In the 1950s, dose calculations were performed manually using basic tools like isodose curves and geometric models, limiting accuracy. A breakthrough came with the first computer-based TPS in the 1970s, allowing more precise calculations and forming the basis of modern treatment planning (Conway *et al*., 1998). The technology progressed in the 1980s with the introduction of 3D TPS, which integrated CT scans to allow for personalised treatment planning based on patient anatomy (Zhao and Xing, 2023).

In the 1990s, the demand for more advanced TPS increased with the development of complex radiation techniques like IMRT and VMAT. Recent studies highlight the critical need for

comprehensive data collection during TPS commissioning to ensure accurate radiation beam modelling and effective integration of imaging data, ultimately improving radiotherapy capabilities and patient outcomes (Dogan *et al*., 2017;Fraass *et al*., 1998)

Key data types include beam characteristics such as profiles, Percentage Depth Doses (PDDs) and Output Factors (OFs), which are essential for accurately characterizing radiation beam behaviour (Khan, 2014). Additionally, machine-specific data allows the TPS to replicate the unique characteristics of the Linacs used in clinical practice. Data on and MLC transmission are vital for reducing dose errors in complex treatment techniques like IMRT and VMAT (Kim *et al*., 2018). Furthermore, PSQA data is critical for verifying that planned doses match delivered doses, ensuring patient safety (Goodall *et al.*, 2023b). The integration of imaging data, including CT number calibration and image registration, significantly enhances treatment precision, while consistent beam output is essential for reproducibility and accuracy in treatment delivery (Brock *et a*l., 2017).

Therefore, Commissioning TPS is essential as it ensures that the system can accurately model radiation beams, calculate precise dose distributions and integrate imaging data effectively. Key aspects of TPS commissioning have been extensively examined in the literature, highlighting their impact on treatment accuracy and safety.

2.2. Machine Specification

The Versa HD Linacs purchased by CMJAH can deliver electron beams with energies of 4, 6, 8, 9, 12 and 15 MeV, as well as photon beams of 6 MV, 6 MV FFF, 10 MV, 10 MV FFF, 15 MV and 18 MV. The machine's largest FS is 40 x 40 cm^2 and it is determined by two sculpted diaphragms that are mounted orthogonally to the MLC. There are no diaphragms or backup jaws because the MLCs replace the jaws in an orthogonal orientation. The projection width over all leaves of the 80 pair inter-digitising MLCs is 5 mm at the isocenter. The Agility collimator has tungsten MLCs that are 9 cm thick and have a leaf speed of 3.5 cm/s with a maximum speed of 6.5 cm/s. The Rubicon optical tracking system monitors the exact positioning of the leaves. The MLCs have a narrow tongue and groove interleaf gap of less than 0.1 mm to reduce interleaf leakage and are defocused from the source. The Agility collimator has an isocenter clearance of 45 cm and a primary collimator speed of 9 cm/s. The Rubicon optical tracking system monitors the exact positioning of the leaves. Unless otherwise indicated, all measurements are to be made according to International Electrotechnical

Commission (IEC) 1217 using a collimator and gantry angle of 0 degrees (Narayanasamy *et al.,* 2016*)*.

2.3. Commissioning in Radiation Therapy

Commissioning is a foundational step in the implementation of radiation therapy systems, particularly the TPS and Linac. It refers to the process of collecting, inputting and validating beam data to ensure the accuracy and safety of dose calculation and treatment delivery. According to Fraass et al. (Fraass *et a*l., 1998), commissioning establishes the Baseline (BL) performance of a radiotherapy system, ensuring that it meets the clinical and technical requirements before patient treatments commence. The AAPM and other international bodies emphasise that comprehensive commissioning is essential for the clinical reliability of any radiotherapy setup, including conformal, intensity-modulated and arc-based techniques (IAEA, 2001; Fraass *et al*., 1998).

2.3.1. Beam Data Acquisition and Base Model Validation

The commissioning process begins with beam data acquisition, where a comprehensive set of measurements is obtained from the Linac. This includes OFs, PDD curves and lateral beam profiles for various field sizes and depths (Khan, 2014). These measurements are then sent to the vendor and used to construct a beam model within the TPS. The base model validation is performed by comparing TPS-generated dose distributions with measured data in water or solid phantoms. This step ensures that the calculated dose closely matches the true delivered dose under reference conditions.

2.3.2. Heterogeneity Correction Validation

In clinical scenarios, patients often present with heterogeneous tissues, such as lungs and bones, which can significantly affect dose deposition. The TPS must accurately account for variations in tissue density to ensure dose accuracy. Heterogeneity correction is validated using specially designed phantoms containing lung- or bone-equivalent materials (Antunes *et al*., 2023). MC and convolution/superposition algorithms are often assessed in this context due to their ability to model complex scatter and attenuation phenomena.

2.3.3. Dosimetric Leaf Gap (DLG) Measurement

The DLG parameter accounts for the rounded geometry of MLC leaves and the associated transmission during dynamic treatments. DLG is measured using the sweeping gap technique, wherein various gap widths are created between opposing MLCs and the dose is measured at the isocentre (LoSasso *et al.*, 1998). These results are linearly extrapolated to determine the

theoretical zero-dose gap. Accurate DLG values are crucial for ensuring that IMRT and VMAT plans deliver dose as predicted by the TPS.

2.3.4. Multi-Leaf Collimator (MLC) Transmission and Leaf Position Verification

Accurate modelling of MLC characteristics is essential in modern radiotherapy (Saez *et al*., 2023). This includes verifying the transmission through closed leaves, the end-leaf leakage and the positional accuracy of leaf movement. Measurements are typically conducted with radiochromic film or ion chambers and results are compared with TPS predictions. Errors in MLC modelling can lead to dose discrepancies, especially in regions with high modulation or steep dose gradients.

2.3.5. Treatment Plan Verification (End-to-End(E2E) Testing)

E2E testing simulates the entire treatment workflow using anthropomorphic or slab phantoms to verify plan integrity from imaging through delivery. This test ensures that all subsystems, including imaging, TPS, data transfer and beam delivery, function harmoniously. It is especially important for new modalities or techniques and serves as the final check before clinical implementation (Gallo *et al*., 2015).

2.4. Importance of Quality Assurance (QA)

While commissioning provides the initial verification, ongoing QA ensures the system maintains its integrity over time. QA practices include periodic machine calibration, software checks and PSQA, particularly for complex plans. Guidelines such as AAPM TGs (e.g., TG-53, TG-119, MPPG 5.a) outline protocols to detect deviations in beam output, geometry and dosimetric accuracy (Ezzell *et al*., 2009). Routine QA complements commissioning by monitoring machine performance and maintaining treatment accuracy and patient safety.

2.5. Commissioning Data Verification

To verify that TPS-calculated dose distributions match the measured data, gamma index analysis is widely employed. This method simultaneously evaluates the dose difference (DD) and distance-to-agreement (DTA) between the measured and calculated dose maps. A point passes the gamma test if it falls within a specified dose DD (e.g., 3%) and distance threshold (e.g., 3 mm), typically denoted as the 3%/3 mm criteria (Das *et al*., 2022). Gamma analysis provides a quantitative measure of agreement and is integral to both commissioning and routine PSQA. A high gamma passing rate (e.g., > 95%) indicates that the TPS accurately models the treatment beam and can be trusted for clinical use.

2.6. Percentage Dose Depth Curves (PDDs) and Dose Beam Profiles

PDDs and dose profiles are critical for accurate dosimetric measurements in RT and impact both treatment precision and patient safety. PDD provides insights into the distribution of radiation dose with depth, which is essential for understanding radiation penetration into tissues (Krisnanjani *et al*., 2024;Poudel *et al*., 2023;Ali *et al*., 2023). In contrast, dose profiles describe the spatial distribution of the dose, which is essential for precise treatment planning and implementation (Thrower *et al*., 2023).

2.6.1. Percentage Depth Dose (PDDS)

Photon beam commissioning in RT necessitates accurate PDD data collection to inform treatment planning and delivery (Brooks *et al*., 2024). PDD measurements (Fig 1) offer crucial insights into dose distribution characteristics within a medium like water, aiding in determining essential parameters such as D_{max}, surface dose and dose attenuation with depth (Roy *et al*., 2023). Precise modelling of dose distributions by TPS relies on accurate PDD data to ensure the accurate delivery of the prescribed dose to the tumour while minimising exposure to healthy tissue. Discrepancies in PDD data have been shown to introduce substantial inaccuracies in dose calculations, potentially compromising treatment efficacy and patient safety *(*Brooks *et al*., 2024). Therefore, meticulous attention to collecting and utilising PDD data during commissioning is paramount to guarantee the effectiveness and safety of RT treatments.

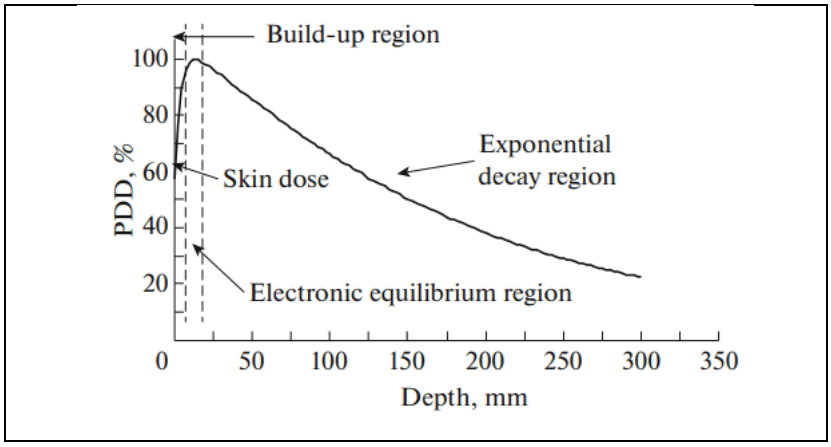


Figure 1: Schematic diagram of PDD (Bencheikh *et al*., 2018).

Regular comparison of current photon beam performance with baseline PDD data collected during commissioning is crucial for ongoing QA in RT (Liu *et al*., 2023). This continuous verification process aids in detecting variations in beam characteristics, including changes in Linac output and energy, ensuring the consistency and reliability of the photon beam (Tsai *et*

al., 2024*)*. By promptly identifying and correcting deviations from baseline PDD data, the integrity of treatment delivery is maintained, enhancing patient outcomes through precise and safe dose delivery (Liu *et al*., 2023). Implementing a robust QA program that includes regular comparison of PDD data allows for the early detection of any deviations, ultimately improving the quality and accuracy of RT treatments (Liu *et al*., 2023).

2.6.2. Beam Profiles

Accurate beam profile (Fig. 2) measurements are crucial for the commissioning and QA of photon beams in RT and provide important information about dose distribution properties such as beam symmetry, flatness and penumbra. These measurements play a critical role in validating the TPS algorithms and ensuring accurate dose distribution modelling and treatment delivery (Portela and Mourão, 2023). Studies have utilised tools such as plastic scintillation fibres, SiPMs and high positional resolution scanning devices to achieve precise and repeatable beam profiling in the 1 GeV range, which significantly contributes to the safety and effectiveness of radiotherapy by minimising errors in dose calculations and improving treatment results (Portela and Mourão, 2023). Advances in beam profiling techniques highlight the importance of precise and reliable measurements to avoid discrepancies that could lead to substantial inaccuracies in dose calculation and treatment delivery and highlight the critical role of precise beam profiles in improving patient care and treatment effectiveness.

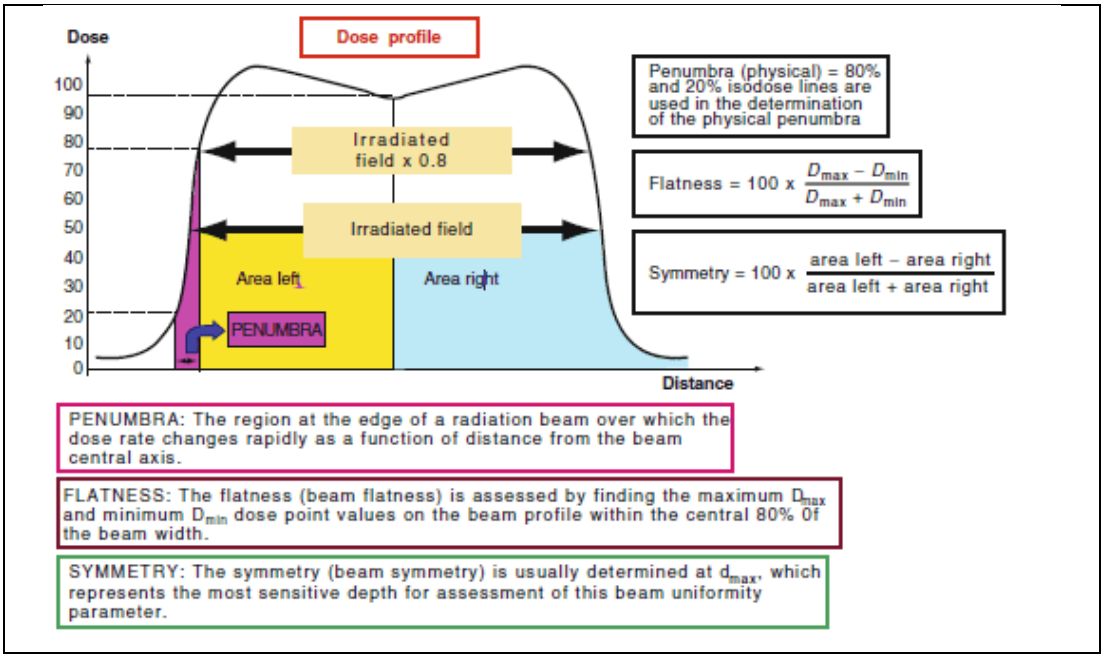


Figure 2: Schematic diagram of Dose profile and its components (Beyzadeoglu *et al*., 2010).

Furthermore, regular monitoring of beam profiles helps maintain the consistency and reliability of the photon beam over time. According to a report by the AAPM (Klein *et al*., 2009), routine profile measurements are integral to detecting any deviations in beam characteristics that may arise due to equipment changes or aging. By comparing current profile data with baseline measurements, MPs can identify issues such as shifts in beam symmetry or changes in flatness, allowing for timely corrective actions. This ongoing verification process ensures that RT remains accurate and effective, ultimately contributing to high-quality patient care and optimised treatment outcomes.

2.7. Importance of Small Field Commissioning in Photon Beam Therapy

Precision in Dose Calculations

Small field commissioning is essential for ensuring precise dose calculations in advanced radiotherapy techniques such as IMRT, (Stereotactic Body Radiation Therapy) SBRT and (Stereotactic Radiosurgery) SRS *(*Teixeira and Prata, 2023*;*Goodall *et al*., 2023a). These small fields, often smaller than ≤ 4 x 4 cm², exhibit unique dosimetric properties such as altered scattering conditions and reduced lateral electronic equilibrium, requiring accurate commissioning to ensure that the TPS accurately models these features (Ding and Das, 2023;Da Silva *et al*., 2022). Proper commissioning is critical for high-precision treatments targeting small, well-defined areas, as it allows the TPS to address the specific dosimetric challenges of small fields and ultimately improve the accuracy and effectiveness of radiotherapy in these modern techniques.

Impact on Treatment Planning

The accuracy of the commissioning of smaller fields directly influences treatment planning quality. Detailed measurements of dosimetric parameters such as OFs and tissue-phantom ratios (TPR) are essential for validating and adapting TPS models. These adjustments minimise uncertainties in dose calculation and lead to more effective and precise treatment plans, as Fraass et al. (Fraass *et al*., 1998).

Verification and QA

Strict QA protocols, particularly for high-precision treatments such as SRS and SBRT, rely heavily on the accurate commissioning of small fields. Precise measurements and modelling help identify and mitigate potential errors in dose administration, ensuring the safety and

effectiveness of these treatments. This rigorous QA is essential to maintaining high standards in RT, as highlighted in AAPM TG Report 101 (Benedict *et al*., 2010)

2.8. Optimising CT Commissioning for Accurate Treatment Planning in Monaco System: Calibration and Simulation Protocol

To ensure accurate and reliable image capture for TPSs, commissioning Computed Tomography (CT) involves several essential processes. These procedures are of utmost importance as they directly influence the precision and quality of the treatment plans generated during the commissioning of the Monaco TPS.

Ensuring that the CT scanner is properly calibrated is the primary step in commissioning CT. This involves verifying the accuracy of the CT codes assigned to different tissue types. The CT scanner is validated and calibrated using calibration phantoms containing materials with known CT numbers. Discrepancies can be identified and corrected by comparing the CT numbers obtained from the phantom with the established values. Proper calibration is essential to obtain accurate tissue density information during the treatment planning phase (Fraass *et al*., 1998).

The next stage involves the creation of the CT simulation protocol. This entails specifying the precise settings for image acquisition, such as slice thickness, the Field of View (FOV) and image matrix size. The TPS used, in this case, Monaco, has specific requirements that must be considered when designing the CT simulation protocol. It is crucial to adhere to defined methods to ensure uniformity and repeatability of CT images across multiple patient scans. Additionally, this stage involves enhancing image quality and minimising artifacts to enhance the precision of treatment planning.

2.9. Comparing 2D vs. 3D Radiation Therapy: Considerations for Treatment Selection.

The field of RT has evolved significantly, progressing from basic two-dimensional radiotherapy (2DRT) to more advanced techniques like 3DCRT, which offer greater treatment accuracy. While 2DRT typically relied on simple beam arrangements and anatomical landmarks, it sometimes incorporated 2D imaging methods such as planar X-rays for treatment verification. In contrast, 3DCRT uses advanced imaging modalities like CT, MRI, and PET to visualise the tumour in three dimensions, enabling more precise and conformal dose delivery with reduced

exposure to surrounding healthy tissues. Numerous studies have demonstrated that this level of precision leads to fewer side effects and better results, especially for the treatment of tumours which are near critical structures (Huq, 2010;Brock *et al*., 2017). However, the advantages of 3DCRT come at a cost; it is more complex and involves the use of advanced TPSs, accurate CT and advanced delivery techniques such as VMAT and IMRT. It elevates the levels of training and spending required which may translate to higher out-of-pocket expenses for the patients (Afrin and Ahmad, 2020;Agrawal *et al*., 2020). Nevertheless, the clinical occurrence of 3DCRT therapy has been justified on its benefits such as decreased risks for patients and better control of the tumour over a long period (Mohindra *et al*., 2019).

The commissioning process for TPS in 3D CRT is essential for ensuring accurate dose calculations and patient safety. Effective commissioning involves validating TPS algorithms against clinical scenarios, as demonstrated by studies that assess beam modelling parameters and their impact on dose accuracy, revealing that complex plans are more sensitive to modelling errors (Brooks *et al*., 2024). Current research continues to explore ways to reduce the cost and complexity of 3DCRT, including the development of more affordable TPS and the integration of Machine Learning (ML) and Artificial Intelligence (AI) to streamline treatment planning. These advancements aim to further enhance treatment precision, reduce planning time and broaden the accessibility of high-quality RT, especially in resource-limited settings (Kang *et al*., 2024).

2.10. Understanding Dose Calculation Algorithms in Monaco Treatment Planning

During the commissioning of photon beams in TPS, various dose calculation algorithms are utilised to ensure accurate dose delivery. Different algorithms, such as MC, PBC, anisotropic analytical algorithms (AAA), Superposition (SP) and Clarkson algorithms, are evaluated for accuracy in dose calculations (Saini *et al*., 2022;Kavousi *et al*., 2019). Monaco TPS by Elekta has only three of the stated algorithms, which are MC, CC and PBC. Among these algorithms, the MC algorithm demonstrates superior accuracy in dose calculations, making it the preferred choice for complex treatment planning scenarios (Kavousi *et al*., 2019).

The MC algorithm calculates dose by simulating all physical interactions in radiation transport, making it highly accurate in handling dose calculations in radiotherapy. Studies comparing dose calculation algorithms (AAA, Acuros XB (AXB), CCC and MC) show that MC, along with AXB, exhibits better accuracy than AAA and CCC, especially in heterogeneous media

and for superficial doses (Rostami *et al*., 2023;Gondré *et al*., 2021;Chandrasekaran, 2012). MC's ability to account for charged-particle equilibrium disruptions in heterogeneous anatomical structures like lung, air cavities, bone and soft tissue sets it apart from other algorithms, ensuring precise dose calculations for improved clinical outcomes (Fu *et al*., 2020). Additionally, advancements like the CT-MCDL network have enhanced MC's efficiency by accelerating dose calculations while maintaining high accuracy levels, making it a valuable tool in radiotherapy treatment planning.

2.11. Modern 3D dose calculation and optimisation

Modern 3D dose calculation techniques enhance the precision of radiation delivery, ensuring optimal treatment plans for cancer patients. The commissioning process involves rigorous testing and verification of the TPS algorithms, dose calculation models and optimization algorithms to ensure their reliability and accuracy in clinical practice.

In modern 3D dose calculation, sophisticated algorithms are employed to calculate the dose distribution within a patient's anatomy accurately. These algorithms take into account various factors such as tissue heterogeneity, multiple radiation beams and patient-specific parameters. One commonly used algorithm is the convolution-superposition algorithm, which combines a convolution algorithm to model the primary photon fluence and a superposition algorithm to model the scatter and secondary photon fluence. This algorithm has been widely validated and is considered a benchmark for accurate dose calculation in clinical practice (Ahnesjö, 1989).

Dose optimization in modern TPSs involves finding the best radiation beam arrangement and intensity modulation to achieve the desired treatment goals while minimising the dose to healthy tissues. This process is typically performed using optimization algorithms based on mathematical optimization techniques such as linear programming, quadratic programming or simulated annealing. These algorithms iteratively modify the beam weights and intensities to achieve the desired dose distribution and conformality. Variety of objective functions can be used to guide the optimization process, including minimising the dose to organs at risk, maximising target dose coverage and achieving dose homogeneity within the target volume (Spirou and Chui, 1998).

2.12. Optimising DLG and MLC Transmission in Monaco TPS for Clinical Accuracy

The transmission from an MLC system in addition to the DLG settings is vital in the commissioning of photon beams within the Monaco TPS. These elements are key contributors in the precision and safety of a VMAT and IMRT treatment plan. Adjusting MLC transmission maps for instance, for the tongue and groove or the tip of the leaf regions help to improve how the MLC is represented in the TPS. Different MLC transmission maps when utilised improve the accuracy and consistency of dose calculations and subsequently enhance the planning and measurement systems (Hussein *et al*., 2023). Furthermore, the DLG adjustment which is the minimum segment width of the MLC is important in treatment in the treatment plan design. Treatment times can be optimised using DLG adjustments without it affecting the treatment results thereby increasing clinical efficiency (Zhou *et al*., 2022).

The DLG and MLC transmission are critical parameters in the dose calculation algorithm of a TPS, particularly for treatment plans involving complex MLC leaf motions. The accuracy of dose calculations is particularly sensitive to variations in DLG, as this parameter incorporates the effect of additional x-ray transmission resulting from the rounded tips of the leaves. Because DLG values depend on the quality of the beam, the type of MLC and the position of leaves among others, it is very crucial to find the most suitable DLG for each beam energy for correct dose delivery in a variety of clinical cases. Often, a single DLG is used for purposes of modelling the gap between the opposing leaves, however, several investigations have established that DLG is not a constant value and that spatial variations exist with respect to DLGs and not all plans can adopt a single DLG value (Zhou *et al*., 2022;Hussein *et al*., 2023).

To accurately measure DLG for different photon energies, the sweeping gap technique provided by vendors is commonly used in clinical settings. The analysis revealed sizable discrepancies in dose calculations, suggesting that a more accurate and robust approach is essential. This study re-evaluated the vendor's calculation method and found inconsistencies when compared to film-based measurements described by LoSasso et al. (LoSasso *et al*., 1998), indicating that the iterative process for optimizing DLG can be time-consuming without reliable reference values.

2.13. Balancing Precision and Safety Through IMRT and VMAT Techniques

It is feasible to attain a highly conformal dose distribution, characterised by a steep dose gradient, for complex target volumes with concave surfaces through the application of IMRT and VMAT. There are risks associated with developing patient planning and delivery techniques (such IMRT/VMAT). The capacity of the delivery and planning system to precisely deliver the planned dose to the target determines the clinical outcome of IMRT. High dose gradients caused by IMRT planning in close proximity to vital organs and tumours result in strict quality control standards for radiation beam modelling (Sharma *et al*., 2017).

Implementing comprehensive QA programs, like VMAT QA plan verification, is crucial to ensure accurate dose calculations and minimise uncertainties in treatment. Commissioning these advanced techniques is essential to guarantee safe and effective RT for patients.

2.14. Versa HD and IGRT features.

Advanced Linacs, such as the Elekta Versa HD (Fig 3), are equipped with Image-Guided Radiotherapy (IGRT) capabilities and support for advanced techniques like VMAT and SBRT. These features facilitate highly conformal treatments by improving target accuracy and minimising radiation exposure to surrounding healthy tissues(Benedict *et al*., 2010).

IGRT refers to the integration of imaging before or during treatment delivery to improve tumour localisation and patient positioning accuracy. Techniques such as cone beam computed tomography (CBCT), kilovoltage (kV) imaging, and megavoltage (MV) imaging allow clinicians to visualise anatomical changes, including tumour shrinkage, organ motion, or setup deviations, and to make real-time adjustments to treatment delivery (Van Herk *et al*., 2000).By incorporating IGRT, RT becomes more adaptive and robust against daily anatomical variations.

While TPS commissioning is not dependent on the linear accelerator itself, accurate modelling of the Elekta Versa HD's characteristics, including high dose rate flattening filter free (FFF) beams, beam shaping with the Agility MLC, and stereotactic dose delivery, is essential for clinical precision. TPS such as Monaco ensure that these advanced delivery techniques are accurately modelled, enabling precise dose calculations and optimal clinical outcomes. Additionally, integrated IGRT features support adaptive workflows, further enhancing patient safety and target conformity (Van Herk *et al*., 2000).



Figure 3: Elekta High Dose Rate Digital Linear Accelerator Versa HD.

IGRT is particularly vital for high precision therapies such as SBRT, but it also improves outcomes in conventional techniques like IMRT and 3DCRT (Benedict *et al*., 2010). With growing technological complexity, Qualified Medical Physicists (QMPs) play a central role in developing and maintaining QA programs that uphold safety and treatment accuracy (Fontenot *et al*., 2014).

Guidance documents and AAPM TG reports provide recommendations for commissioning and QA of IGRT systems (Fattori *et al*., 2022b).These include tests for imaging system performance, geometric fidelity, and motion management (Wijesooriya *et al*., 2017). However, distinctions between minimum standards and best practices are often unclear, which can lead to inconsistencies in clinical implementation (Zhou *et al*., 2022).For example, AAPM TG 119 provides test cases for validating IMRT and VMAT accuracy, but further guidance is needed to improve standardisation of IGRT QA procedures.

2.14.1. Mega-voltage cone beam CT (MV CBCT) and X-ray 2D

Modern accelerators, such as Elekta's Versa HD and Varian's TrueBeam , come with two different imaging systems: (a) a Megavoltage (MV) electronic portal imaging device (EPID), which has its own flat-panel image detector (b) a kilovoltage x-ray imager, which mounts a traditional x-ray tube on the gantry with an opposing flat-panel image detector and. Mega-Voltage Cone Beam CT (MV CBCT) is a type of imaging technology used in RT to provide 3D images of the patient's anatomy (Reitz *et al*., 2008).

MV-CBCT is utilised for tumour localization and patient positioning verification before treatment (Abuhaimed and Martin 2023;Suwanraksa *et al*., 2023) CBCT provides static volumetric images, limiting its ability to capture intra-fractional changes (Scholey et al., 2022). To address this limitation, deep learning methods like CycleGAN have been employed to enhance MV-CBCT image quality and HU accuracy, making the generated synthetic CT (sCT) suitable for Adaptive Radiotherapy (ART) (Bayat *et al*., 2022). Additionally, the implementation of a 3D deep convolutional neural network allows for the synthesis of MVCT datasets from MRI, demonstrating the feasibility of MRI-MVCT-only treatment planning (Zhao *et al*., 2021). These advancements enable more accurate dose calculations and treatment planning by incorporating patient-specific anatomical information, enhancing the potential for adaptive strategies in radiotherapy.

2.15. 1 D Gamma Analysis

The gamma index (Γ) quantifies the agreement between an evaluated (or simulated) dose D_e reference dose (D_r) by determining the minimum. Euclidean distance between these doses within their respective distribution. For a specific evaluated dose D_e, Γ is calculated by comparing it to all reference doses D_r using the following formula:

$$\Gamma = \sqrt{(\frac{\Delta D}{\delta D})^2 + (\frac{\Delta d}{\delta d})^2} \quad (1)$$

Where ΔD is the DD between D_r & D_e and Δd is the spatial distance between their positions, d_r & d_e . The parameters δD and δd represent the percentage DD and DTA, respectively. These are often reported together as $\delta D/\delta d$. The most used criteria are 3% for DD and 3mm for DTA (Das *et al*., 2022;AL-Sa'd *et al*., 2013). A given D_e is considered acceptable if less than 1 (Anetai *et al*., 2022).

The Γ integrates DD and DTA to calculate a dimensionless value for each point within the assessed dose distribution. The reference dose distribution, considered the 'gold standard', is typically derived from measurements, such as those from ionisation chambers (single point), line profiles (1D), film measurements (2D) or gel dosimetry and MC simulations (3D). The evaluated dose distribution, often the predicted TPS dose distribution, is compared against this reference to assess the accuracy of the dose modelling (Hussein *et al*., 2017).

3. Materials and Methods

This chapter thoroughly describes the material preparation, equipment commissioning, data acquisition techniques and validation processes used to implement the TPS at CMJAH, with a specific focus on its integration with four Elekta Versa HD linear accelerators. All four machines were beam-matched during initial commissioning, ensuring consistent beam characteristics and allowing for shared beam data in treatment planning and verification.

The methodology began with the acquisition of photon beam data for specified energies using dosimetric tools such as ionisation chambers, electrometers and water phantoms. Beam data collection and treatment plan verification for 6 MV, 6 MV FFF, 10 MV and 15 MV photon energies were performed on Linac 1 (L1), while 18 MV data were acquired using Linac 3 (L3). Linac 4 (L4) was used for DLG and MLC transmission measurements, taking advantage of the matched configuration to ensure consistent and representative data across all linacs.

Commissioning involved detailed measurements of PDD curves, beam profiles, and OFs, following IAEA and AAPM protocols to ensure high dosimetric accuracy. These measurements enabled a comprehensive beam model characterisation across various field sizes and clinical scenarios. MLC systems were essential for precise beam shaping and supported the advanced planning capabilities of the Monaco TPS.

The final section of this chapter presents the validation of the Monaco TPS through rigorous E2E testing. This process used Perspex and the CIRS SHANE phantom to replicate clinical treatment conditions and assess the system's dose calculation accuracy under controlled conditions.

3.1. Materials

This section introduces the key materials used in the commissioning to ensure The VersaHD Linacs served as the primary radiation sources. At the same time, the PTW MEDPHYSTO Navigation Software and the PTW FREIBURG Electrometer were critical for data management and measurement precision. Various ionisation chambers were employed to measure radiation dose accurately and the TRUFIX BS equipment ensured proper device positioning during measurements.

A Canon Aquillion LB CT scanner was used with the Catphan 600 phantom for imaging and dosimetric verification to ensure geometric accuracy. Furthermore, the 4D Octavius system facilitated dynamic dose verification, while the CIRS Head & Neck Shane Phantom was

integral to conducting E2E testing of the TPS. This section provides a scientific overview of each material's function, some of its characteristics and their contribution to the overall commissioning process.

3.1.1. Scanning Water Tank and Electrometer

The PTW MP3-M water tank (PTW, Freiburg, Germany) was utilised for the measurements. The system operates in stepping mode and provides a scanning range of 50×50×40 cm^3. The scanning speed ranges from 0.1 to 50 mm/s, providing for versatile data acquisition. The minimum scanning step (resolution) in stepping mode is 0.1 mm, ensuring high precision in dosimetric measurements. The obtained beam data were analysed using the MEPHYSTO mc^2 (version 4.4) program, a comprehensive tool for beam data analysis and QA in radiotherapy. It verifies critical dosimetric parameters, such as PDD curves, beam profiles and OFs, for accurate TPS configuration. With its user-friendly interface, it integrates seamlessly with water phantom systems like the PTW MP3-M, offering real-time data acquisition, smoothing and filtering. The software also includes advanced correction algorithms for precise calibration, making it essential for the commissioning and QA of Linac and TPS. Several ionisation chambers of varying sizes (see table 1) were used alongside the water tank for field measurements, with a 0.07 cm^3 chamber serving as the reference.

The PTW UNIDOS E electrometer (Fig 4) was essential for accurately measuring key parameters during the commissioning process. It was used to measure OFs, MLC and DLG transmission and to verify dose measurements. The electrometer provided precise ionisation current readings, which were critical for the accurate modelling of the TPS and for ensuring the reliability of dose calculations validation.



Figure 4: Image of a PTW UNIDOS E electrometer.

3.1.2. Detectors

A range of ionisation chambers (see Fig 5) was employed in this study, each chosen for its suitability to specific dosimetric needs. The PTW 0.07 cm^3 Semiflex ionisation chamber was used for large photon fields due to its high collection efficiency and relatively larger sensitive volume, ideal for measuring dose profiles, PDDs and OFs. For small field dosimetry, the microDiamond detector was preferred for its superior spatial resolution and minimal volume-averaging effects, particularly in high-gradient regions, making it highly effective for FSs under 5x5 cm^2. Additionally, the 0.6 cm^3 Farmer-type and 0.125 cm^3 ionisation chambers were essential for specialised applications, including point dose measurements and MLC verification, due to their high sensitivity and precision in complex dosimetric scenarios.

Table 1: Detector Characteristics and Assign Activities for VersaHD Linac Commissioning.

Type	Model	Diameter	Sensitive Volume	Type of material	Activities Performed
Cylindrical Ionisation Chambers	PTW Farmer Chamber TM 30006	2.3 mm	0.6 cm^3	Aluminium	Dose Measurements
	PTW Semiflex 3D TM 31021	4.8 mm	0.07 cm^3	Aluminium	PDD, Profile and OF (Photon FS ≥5x5)
	PTW Semiflex TM 31010	5.5 mm	0.125 cm^3	Aluminium	Independent dose measurements, Verification Measurements
Diamond detector	PTW MicroDiamond TM 60022	Active sensitive area:3.8 mm^2	0.004 cm^3	Synthetic Single diamond	PDD, Profile and OF (Photon FS ≤ 3x3)
2D Array Detector	PTW OCTAVIUS 1500	27 x 27 cm^2 (Active Area)	N/A	Vented Ionisation Chambers	Plan Verification, IMRT and VMAT QA

The TRUFIX BS basic equipment was employed to maintain consistent and precise positioning of these dosimetric devices during data collection, further ensuring the accuracy and reproducibility of the measurements across various conditions.

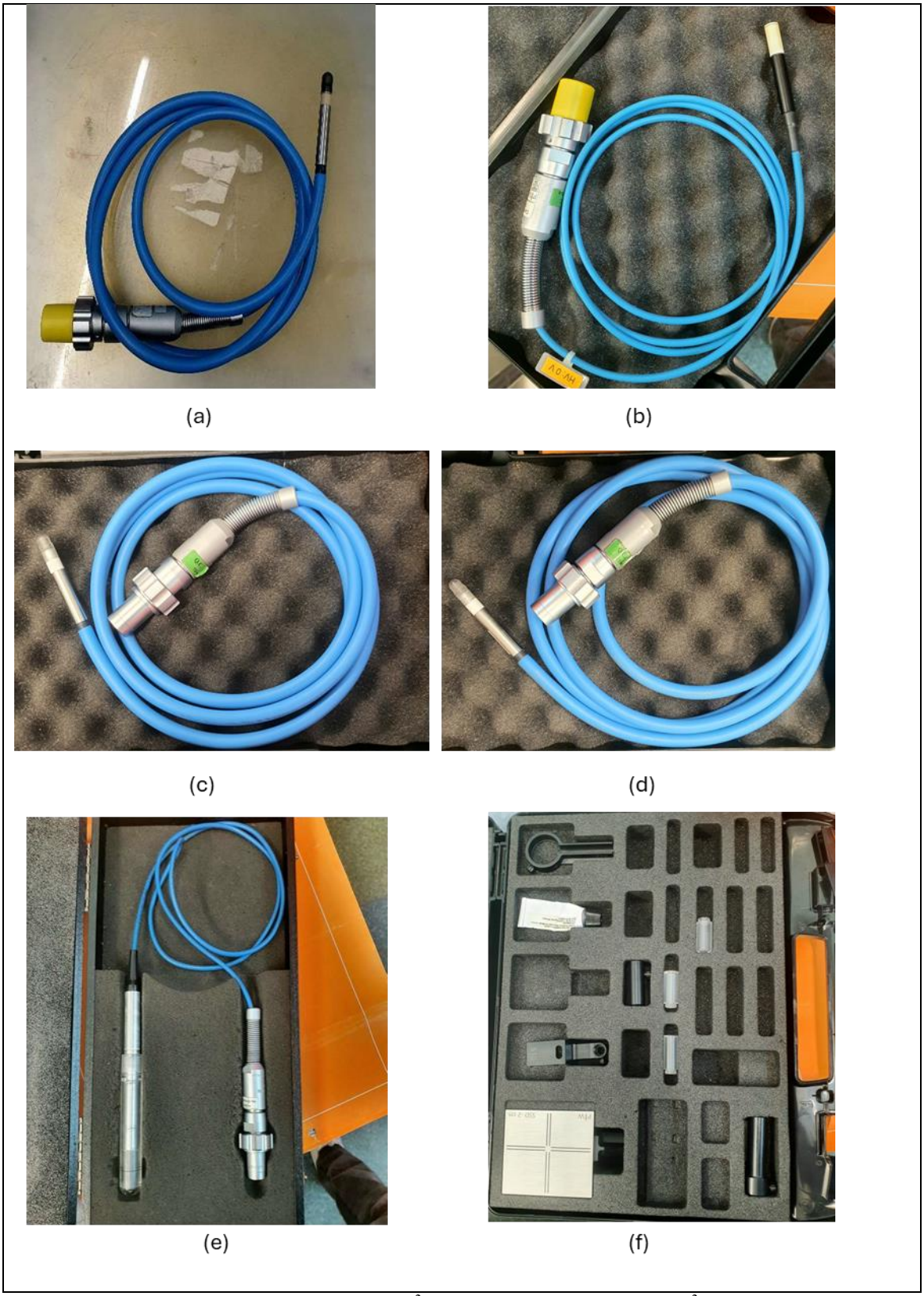


Figure 5: Detectors used: (a) PTW 0.125cm^3 Semiflex (b) PTW 0.004 cm^3 MicroDiamond (c) PTW 0.07 cm^3 Semiflex 3D field (e) PTW 0.07 cm^3 Semiflex 3D reference and (f) TRUFIX BS equipment.

3.1.3. Linear accelerator (Linac)

The Versa HD (HD Oncology Systems, Crawley, UK) Linac delivers beams of radiation with a wide energy spectrum and different FSs. This advanced radiotherapy system is equipped with high-definition beam-shaping capabilities, allowing for precise dose delivery. Measurements acquired from the Linac were used for comparison with the corresponding calculated dose values generated by the TPS, thereby facilitating validation and commissioning processes.

3.1.4. Treatment Planning System (TPS)

The Elekta Monaco TPS (version 6.1.2.0) was used as the primary software platform for this study. The system models both photon and electron beams in RT, utilising advanced algorithms mentioned in section 2.10, for precise dose calculations (Zhou *et al*., 2022). For electron therapy, the Monaco TPS employs both PBC and MC algorithms to ensure accurate dose calculations. The system was utilised for contouring, treatment plan generation, dose distribution analysis, and comparison with measured data (Hussain & Muhammad, 2017). Key capabilities of the Monaco TPS include importing imaging data from CT, MRI and PET scans, efficient contouring of treatment volumes, accurate dose calculations and integrated dose optimisation. The system also features an expert function to assist in customised treatment planning.

3.1.5. Phantoms employed in this study.

CIRS Shoulder Head, & Neck E2E Verification Phantom (SHANE)

In radiotherapy QA, phantoms are critical for validating TPSs, particularly in the context of complex anatomical structures. The CIRS SHANE Phantom (Fig. 6) is an example of advances in this field, offering a heterogeneous design that closely mimics human anatomy, including intra- and extracranial features as well as thoracic vertebrae. This phantom can be utilised for comprehensive E2E verification of VMAT plans by enabling precise placement of dosimetric tools, such as radiochromic films and ion chambers, essential for accurately calibrating and measuring radiation doses delivered to patients (Mukwada *et al*., 2024;Jeong *et al*., 2011). The integration of such sophisticated phantoms increased the reliability of treatment delivery and ultimately improved patient safety and treatment efficiency by ensuring that radiotherapy was delivered as planned (Raina *et al*., 2022).

Therefore, the development and use of heterogeneous phantoms such as the CIRS SHANE phantom represented a significant advance in the field of QA in radiotherapy. Specifically, key measurements with this phantom include dose distribution verification using radiochromic

films, point dose measurements via ion chambers and alignment checks with imaging systems (CT, MRI, X-ray). These features make the phantom a valuable tool for ensuring safe and accurate radiotherapy delivery.

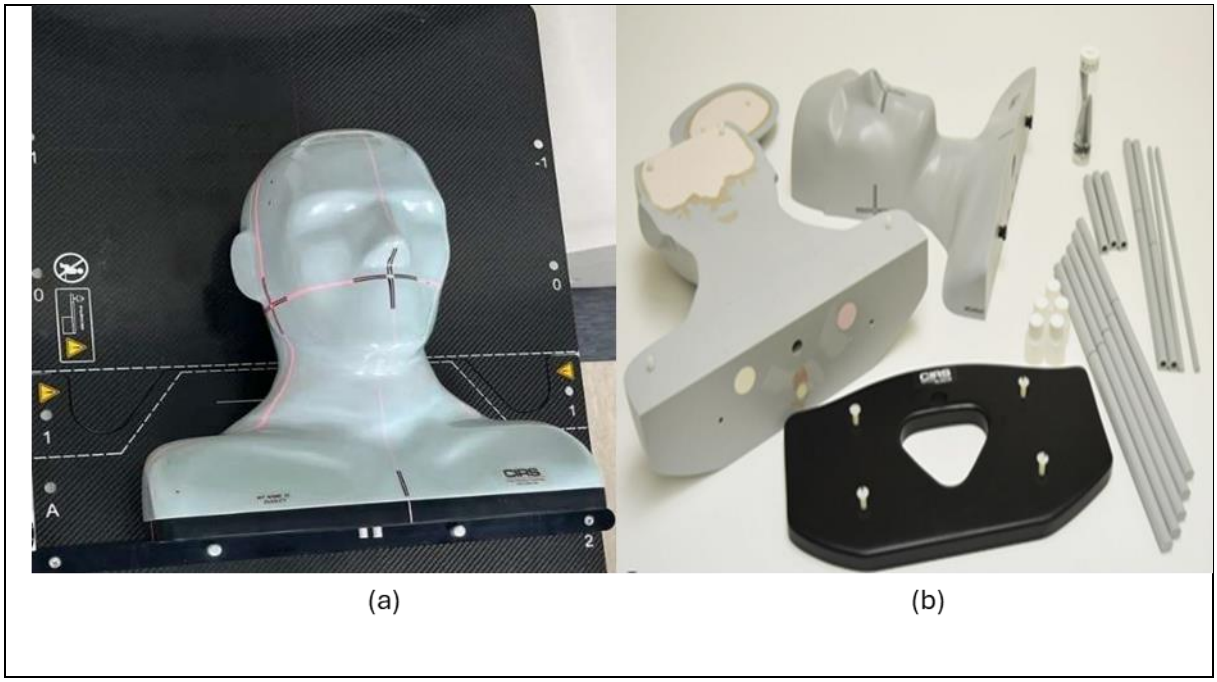


Figure 6: Shane Phantom taken at CMJAH.

4D Octavius

The study utilised the Octavius 4D System (Fig. 7) by PTW, equipped with the Octavius 1500 Detector Array for PSQA (Shin *et al*., 2024). The system was equipped with a Cylindrical Phantom, designed to house the detector array and precisely mimic the patient setup. The phantom's dimensions are typically 32 cm in diameter and made from a tissue-equivalent material such as polystyrene or PMMA, providing realistic scattering and attenuation properties. The cylindrical shape allows for a uniform geometry, ideal for accommodating both coplanar and non-coplanar beam evaluations (Shin *et al*., 2024).

The Octavius 1500 Detector Array is a 2D ionisation chamber array consisting of 1500 ion chambers, each with a detector size of 4.4 mm x 4.4 mm x 3 mm and a spacing of 7.1 mm between chambers (Stelljes *et al*., 2015). These chambers are embedded at a depth of 5 mm within the phantom to accurately measure dose distributions at clinically relevant depths. The array spans a 27 cm x 27 cm detector matrix, providing a wide field of view for treatment plan verification (Shin *et al*., 2024).

The detector array is known for its high spatial resolution, making it suitable for detecting small deviations in complex treatment plans. The measurement time for each detector is within

milliseconds, ensuring real-time dose recording. The gamma index analysis, performed during irradiation, compares the measured doses to the planned distributions, enabling precise identification of deviations and ensuring accuracy and safety (Shin *et al*., 2024).

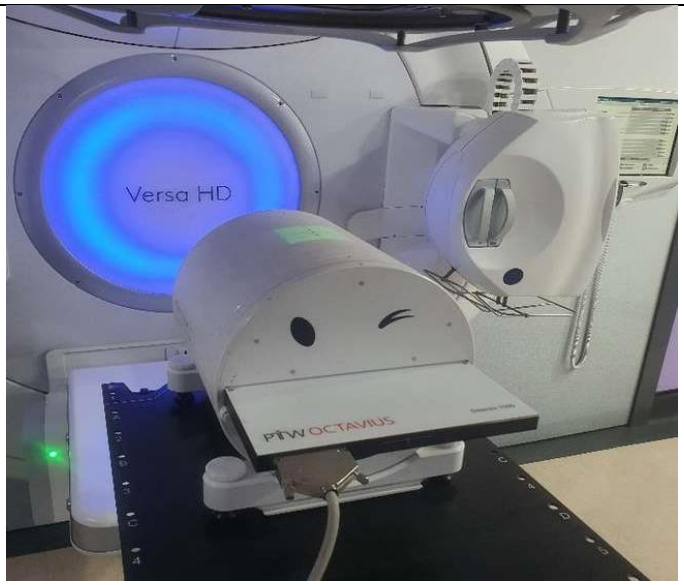


Figure 7:Setup used for PSQA measurements.

RW3 Slab Phantom

In this study, the RW3 slab phantom, a water-equivalent synthetic resin (Goettingen White Water), utilised for RT dosimetry. It was ideal for QA tests, such as MLC transmission and DLG measurements. The phantom's density (1.045 g/cm³) closely mimicked human tissue, ensuring accurate dose measurements (Asgari *et al*., 2015). The slabs, typically measuring 30 cm by 30 cm, were available in various thicknesses (e.g., 1mm, 2mm, 5mm, 10mm), allowing for flexible setups to create appropriate buildup and backscatter conditions. RW3 was used to measure radiation leakage through the MLC leaves and determine DLG values using the sweeping gap technique. Its stability and uniformity were crucial for obtaining precise dosimetric evaluations during the study.

Perspex Slabs Phantom

Perspex (polymethyl methacrylate, PMMA) was utilised as the base phantom material in those E2E studies on 3DCRT because of its tissue-like density, consistent radiation attenuation and profound mechanical strength. Being composed of carbon, hydrogen and oxygen, PMMA is characterised by a density of approximately 1.19 g/cm³ (Huszank *et al*., 2019) which closely approximately that of human tissue what makes it perfectly suitable for dosimetric and QA measurements.

The Perspex slabs, measuring 30 cm × 30 cm and available in thicknesses of (1 , 2 , 3 and 10 mm), facilitated flexible configurations for establishing buildup and backscatter conditions. Its reproducible radiation attenuation characteristics, high mechanical strength and effective atomic number Z_{eff} akin to human soft tissue contributed to accurate dose calculations and reliable measurement outcomes, enabling precise calibration and direct comparison with TPS calculations. Thus, Perspex was an ideal choice for achieving accurate dosimetric results in the study.

Catphan 600

The Catphan 600 phantom (Fig. 8) was used for CT number calibration to ensure accurate HU measurements across various tissue densities. It contains specialised inserts, such as Low-Density Polyethylene (LDPE) for fat, Polystyrene for soft tissue, Acrylic (PMMA) for denser soft tissues and Teflon (PTFE) to simulate bone, covering a wide range of HU values (Gulliksrud *et al*., 2014). Additionally, a Water-Equivalent Material with an HU of 0 serves as a reference, while an Air Insert with an HU of -1000 is used to verify low-density imaging. The phantom also includes Bone-Like Material (Hydroxyapatite) in two densities for testing bone imaging accuracy. Its cylindrical design with a diameter of 30 cm and a height of 20 cm allows for installation in standard CT scanners for comprehensive testing of CT number accuracy, low contrast detectability and spatial resolution. By comparing the scanner's readings to known HU values of the inserts, ensures accurate calibration and compliance with regulatory standards (Samei *et al*., 2019). This makes the Catphan 600 an essential tool for maintaining high-quality diagnostic imaging.

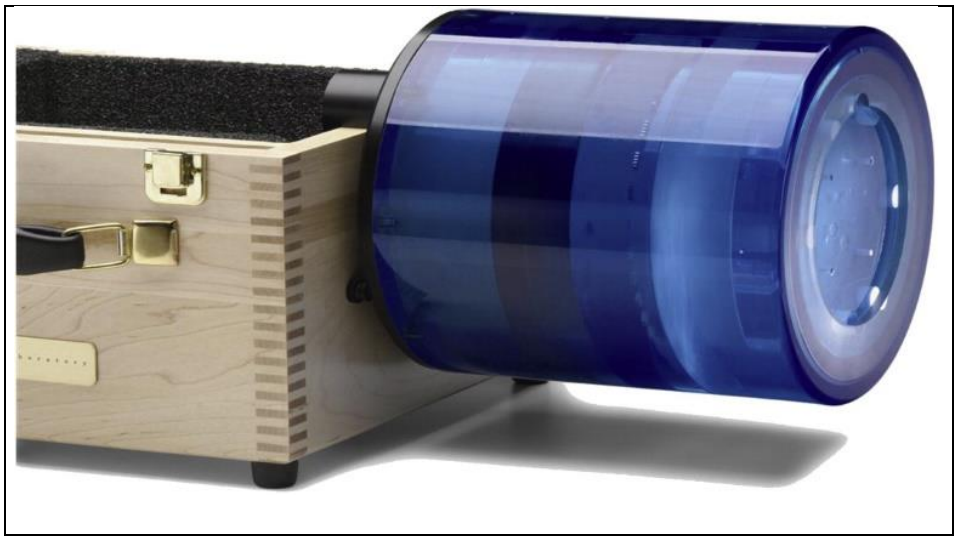


Figure 8: The Catphan®600 CT phantom (Zarb and Rainford, 2014).

3.1.6. Record and Verify (MOSAIQ VERSION 2.81)

MOSAIQ version 2.81, developed by Elekta, is a comprehensive Record and Verify (R&V) system designed to promote patient well-being and treatment accuracy in radiotherapy. It streamlines the documentation and verification of treatment parameters by integrating with TPS, facilitating real-time data tracking and automating radiation delivery checks. In this study, MOSAIQ 2.81 was used to record and monitor essential dosimetric and positional data, ensuring the accurate execution of prescribed treatment plans. Its seamless integration with imaging modalities and Linacs helped reduce human error and optimise the overall safety and effectiveness of radiation delivery, as supported by guidelines from the AAPM (Fraass *et al*., 1998).

3.2. Methods

When commissioning a TPS, several critical steps were taken to ensure its accuracy and reliability. Initially, the installation and configuration of the TPS were checked by cross-referencing the data and parameters with those specified by the vendor. Then, data entry tests were followed by phantom measurements to verify that the TPS accurately computed dose distributions for various machine setups and treatment techniques. The next step was the validation of TPS dose calculation algorithms against measurements for different clinical situations. Furthermore, the accuracy of beam modelling was validated by comparisons of measured and calculated dose distributions for a range of beam energies and field sizes. To determine the overall effectiveness of the TPS, a comprehensive overall evaluation based on real patient scenarios (E2E test) was performed. To verify that the clinical use of the TPS was safe and effective, it was important that all records were well maintained and that all proper guidelines, such as the AAPM TG 53 guidelines, were followed.

In addition, the development and maintenance of a continuous QA process is crucial to ensure the accuracy and reliability of the TPS system in the long term. Regular QA tests, performed after frequent updates of dose calculation algorithms and swift model tuning upon software update releases, ensure deviations caused by those modifications are detected and corrected. In this section, the methods followed in this study are presented to achieve the objective presented above.

3.2.1. Pre-Scanning Linac checks

Before beam data acquisition, the optimum functioning of the Linac from which beam data will be acquired needs to be ensured. Amongst other checks, the checks below were performed before any scanning was done.

Presented below is a summary of a few tests, including mechanical tests, that ensure acceptable functioning on the Linac before beam data measurements are performed.

During the commissioning of the Linac, mechanical checks were conducted to ensure that the light and digital readout fields were properly aligned. This was achieved by positioning graph paper at a distance of 100 cm from the crosshairs. The FS tolerances adhered to TG-142 guidelines, allowing for a 2 mm variation for symmetrical jaws and 1 mm for single asymmetric jaw configurations. Furthermore, measurements assessed the coincidence of the Optical Distance Indication (ODI) and mechanical front pointer alignment at various source-to-skin distances (SSDs) between 80 &100 cm. The recommended tolerance for the ODI, as per TG-142, was 1 mm. The study employed Gafchromic EBT2 film to assess the alignment between radiation and light fields at various SSDs. The film was positioned at a 90-degree angle to the beam axis, ensuring it met TG-142's recommended tolerance of 2 mm. This setup ensured accurate dosimetric assessments, demonstrating the effectiveness of Gafchromic EBT2 film in such applications.

Mechanical/Radiation isocentricity

To evaluate the alignment of the radiation isocentre with the mechanical isocentres of the gantry, couch, and collimator, a star-shot analysis was conducted. This assessment was repeated at various gantry, couch, and collimator angles to ensure comprehensive coverage. In accordance with TG-55 guidelines, the film was scanned utilising a Vidar scanner (Vidar Systems Corp., Herndon, VA). Visual inspection and TG-142 recommendations dictated a radiation tolerance of 2 mm diameter for mechanical isocentricity testing.

Nondosimetric Testing

The series of non-dosimetric tests followed the recommendations provided by AAPM TG-53. The primary focus areas included developing CT numbers to ED curves, generating contours, and ensuring the precision of 3D expansions. The procedure also included creating tolerance tables for Elekta Inc.'s Mosaiq oncology record and verification system integration. In addition, an assessment was carried out on the data transfer from Monaco to Mosaiq, taking into account different patient and phantom orientations.

Monaco TPS generated CT to ED curves by scanning a Catphan 600 and a SHANE Phantom at various CT kilovoltage peak (kVp) values (Sharma *et al*., 2020b). Additionally, automatic rigid image registration accuracy can be evaluated using datasets from AAPM TG-132, including CT, CBCT, MRI and PET scans with specified offsets. These offsets were compared to the transformation matrix in the TPS, highlighting the importance of precise image registration for accurate treatment planning and delivery (Sharma *et al*., 2020b). The study emphasised the significance of proper alignment and registration of multimodality images to ensure the reliability of dose calculations and treatment outcomes, especially when dealing with diverse imaging modalities and patient datasets.

3.3. Photon Beam Data Collection

For PDD and beam profile measurements, data were acquired at a constant SSD of 90 cm for various FSs using PTW MEPHYSTO software, following the required measurements in water as specified by Elekta. A 0.07 cm^3 Semiflex 3D ion chamber served as both the field and reference chamber. The chamber was initially aligned with the crosshairs using a TRUFIX thimble and the alignment was verified using paper to ensure it was level with the water surface at all four corners of the water tank. After verifying the alignment, the chamber was positioned at the vertical level of the Linac isocentre using PTW's TRUFIX system. Initially, the chamber was set to the zero position with its centre at the water surface. It was then adjusted to the effective point of measurement (EPOM) by raising it by 1.2 mm. The FS was set accordingly and a reference chamber, which corrects for beam perturbations, was positioned at the edge of the field to ensure it did not shadow the field chamber.

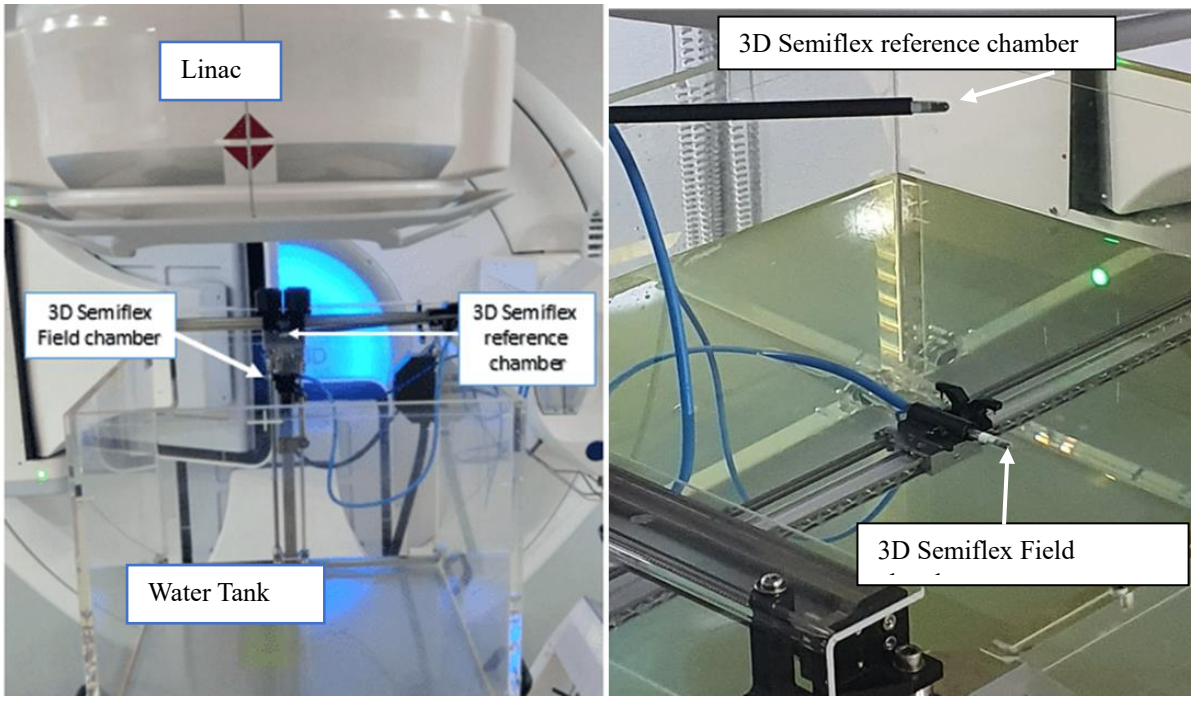


Figure 9:Setup used to acquire the commissioning data with field and reference chamber.

3.3.1. Open Field

PDDs and OFs for multiple FSs were measured for open fields and the OFs normalised to 1 for a 10 × 10 cm² field. In-plane and cross-plane scans were also taken using different depths and FSs. The Central Axis (CAX) depth dose measurements and OFs were made for the following FSs: 2 x 2 cm², 3 x 3 cm², 4 x 4 cm², 5 x 5 cm², 7 x 7 cm², 10 x 10 cm², 15 x 15 cm², 20 x 20 cm², 30 x 30 cm², 40 x 40 cm², 40 x 5 cm² and 5 x 40 cm². Only profile scans, cross-plane and in-plane, were performed at the square fields mentioned above at depths of d_{max}, 5, 10 and 20 cm.

Diagonal scans were performed at angles of 45 and 135 degrees within a maximum open FS of 40 × 40 cm³. The scans were performed at a depth of 10 meters with a geometric field extent of 2 cm. The scanning step size was 3 mm. There were two approaches to the absolute dose measurement. The FS was 10 x 10 cm², the depth 10 cm and the SSD 100 cm. For the second setup, the SSD was 90 cm and all the remaining parameters were kept unaltered.

3.3.2. Physical and motorised wedges

For the wedge fields of 10 x 10 cm² size, the OFs were normalised to 1. Comprehensive diagonal profiles were obtained at a depth of 10 cm for the largest available wedge FS in which the geometric field was extrapolated by 2 cm and measured at 3 mm intervals. Measurements of CAX depth dose distributions, profiles and OFs were made for various FSs ranging from 5

x 5 cm² to 10 x 10 cm², 15 x 15 cm², 20 x 20 cm² and to the largest possible FS of 40 x 30 cm². Profile scans were carried out in both the in-plane and cross-plane orientations at selected depths (see Section 3.3.1).

The wedge transmission factor was determined by calculating the ratio of absolute dose with the wedge to absolute dose for an open field for the same 10 x 10 cm² FS.

3.3.3. Absolute Dose Calculations

The dosimetry was determined under two different reference conditions. The first condition included a FS of 10 x 10 cm² with an SSD of 100 cm and a depth of 10 cm for open and wedged fields. The second condition used a FS of 10x10 cm² with an SSD of 90 cm and a depth of 10 cm for open fields only. A 0.6 cm^3 farmer-type ionisation chamber was aligned with the crosshairs, checked with paper and ensured that it was level with the water surface at all four corners of the water tank. The chamber was then positioned so that its centre was level with the water's surface. Connected to an electrometer, the chamber measured the charge for 100 monitor units (MU) delivered. The absorbed dose to water (D_{zref}) at z_{ref} was calculated using the equation below:

$$D_{z_{ref}} = M_Q \times N_{D,w,Q} \times k_{Q,Q_0} \tag{2}$$

Where M_Q is the reading of the dosimeter at quality Q, corrected for influence qualities as shown in the equation below, $N_{D,w,Q0}$ is the calibration factor of the absorbed dose to water for a dosimeter at a reference Beam Quality (BQ), $k_{Q,Q0}$ is the BQ correction factor.

$$M_Q = M_1 \times k_{TP} \times k_{pol} \times k_{elec} \times k_s \tag{3}$$

The charges obtained were used to determine the *kpol*. To correct for polarity (k_{pol}), the charge values at ± 400 V were recorded for all energies at 100 MU using the same setup as above. The charges obtained were used to determine the *kpol*.

$$k_{pol} = \frac{|M_+| + |M_-|}{2M} \tag{4}$$

Where M_+ is the electrometer value for positive polarity, M- is the electrometer value for negative polarity and M is the charge value derived from the routinely applied polarity setting.

To correct for ion recombination *(k_s)*, the charge value at 400 V and 200 V at 100 MU was measured using the same setup as above. The charges obtained were used to determine k_s.

$$k_s = a_0 + a_1\left(\frac{M_1}{M_2}\right) + a_2\left(\frac{M_1}{M_2}\right)^2 \quad (5)$$

M_1 represents the electrometer reading at normal voltage, while M_2 represents the electrometer reading at reduced voltage. The constants aj were derived from Table 4.VII in TRS 398.

To correct for pressure and temperature k_{TP}., the room pressure and temperature were recorded and the equation below was used to calculate k_{TP}.

$$k_{TP} = \left(\frac{273{,}2 + T}{273{,}2 + T_0}\right)\left(\frac{P_0}{P}\right) \quad (6)$$

k_{TP} is the correction factor for pressure and temperature, where P and T denote the pressure and temperature at the time of measurement, respectively, and P_0 and T_0 represent the temperature and pressure during calibration.

Given that the ionisation chamber and the electrometer were calibrated as a single unit, the calibration factor for the electrometer (k_{elec}) was determined to be 1.

To correct the BQ factor, the $TPR_{20,10}$ was measured under the following reference conditions: a source-to-chamber distance (SCD) of 100 cm, a FS of 10 × 10 cm^2, defined at the isocenter (chamber plane), the charge was measured at depths of 10 cm and 20 cm for all energies.

Then the obtained D_{zref} was utilised to calculate the absorbed dose D_{zmax} utilising equation 2 for the SSD method and equation 7 for the SAD method. The obtained D_{zref} was subsequently utilised to calculate the absorbed dose D_{zmax} utilising equation 7 below for the SSD method

$$D_{Z_{max}} = \frac{100 D_{z_{ref}}}{PDD_{z_{ref}}} \quad (7)$$

Where PDD (z_{ref}) is the percentage depth dose at z_{ref} normalised to z_{max}.

3.4. Model validation

Model validation in RT ensures the accuracy and reliability of the beam models and other components of the TPS system in predicting dose distributions in patients (Giada *et al*., 2023). This validation process involves rigorous comparisons between model predictions and experimental data to evaluate performance and quantify uncertainties. By validating models, the RT term can optimise treatment plans, calculate precise dose distributions and maintain high standards of patient safety (Giada *et al*., 2023).

Benchmarking with established measurements and performing sensitivity analyses are integral to validating radiotherapy models. These practices validate the reliability of models and contribute to continuous improvements in patient outcomes and care. By ensuring that computational models accurately reflect clinical realities and account for variability in treatment scenarios, clinicians can confidently use these tools to enhance the effectiveness and precision of RT interventions.

According to the AAPMs MPPG 5.a report (Fraass *et al*., 1998), validating a photon beam model involves several critical aspects to guarantee the accuracy and reliability of the dose calculations in the TPS. The three main types of validation tests are presented in the following sections, including an additional focus on 3D plan validation.

3.4.1. Heterogeneous Phantom Validation

The validation of TPS for accurate dose calculations in heterogeneous media involves using phantoms with inserts of various materials like lung, bone and soft tissue to simulate different tissue densities in the human body. This process ensures that the TPS can effectively handle the complex interactions of photon beams with tissues of different densities and compositions, providing precise dose distributions in clinically relevant scenarios. Heterogeneous corrections were performed using the Catphan and CIRS Shane phantoms, which are crucial for ensuring accurate dose calculations for TPS.

The Catphan and CIRS Shane phantoms were positioned on the CT scanner couch and scanned using standard clinical protocols to ensure consistent imaging parameters. The acquired CT images were then analysed for uniformity, spatial resolution, low-contrast detectability and HU accuracy, focusing on specific modules simulating various tissues like air, lung, water, liver and bone within the phantoms. The measured HUs were converted to HU-to-RED curves for comparison with the RED curve obtained from Monaco software.

3.4.2. Basic Beam Data Validation

This initial step involves verifying the fundamental dosimetric data used to configure the TPS. Measurements such as PDDs, profiles and OFs for a variety of FSs are acquired using a water phantom. These measurements are then compared with those calculated by the TPS or independently measured data to verify the fundamental dosimetric data used to configure the TPS. The goal is to ensure that the TPS accurately models the primary characteristics of the photon beam, including its energy, symmetry and FS dependence.

3.4.3. MLC and DLG Transmission

The transmission of the MLC was independently for each MLC leaf banks. Leaves were positioned at the far right for one field and at the far left for the other to ensure a bank of leaves blocked each measurement. The calibrated MLC transmission value was determined by averaging the transmission values of both blade banks. Measurements were performed for all photon energies utilising a PTW Semiflex 31010 0.125cm^3 ionisation chamber positioned at a depth of 10 cm in an RW3 phantom. As outlined by AAPM TG No. 50 (Boyer *et al*., 2001b), MLC transmission values are expected to remain below 2%.



Figure 10: Set-up used to collect measurements for both MLC and DLG.

To determine the DLG factor, accounting for leaf-end transmission, we used the sweeping-gap technique with DICOM plan files provided by Elekta. This method involved sweeping various MLC gaps (5, 10, 20 and 30 mm) across a rectangular field, delivering 200 monitor units (MU). Output readings for each MLC gap were measured using the PTW 0.125 cm^3 Semiflex ionisation chamber, with the measurements influenced by both gap size and inherent leaf transmission. The contribution from MLC leaf transmission was isolated by correcting the output readings. These corrected readings were then plotted against the corresponding MLC gap sizes and a linear fit was applied to the data. The x-intercept of the fitted line, representing the point where the corrected output reading reached zero, indicated the theoretical MLC gap size at which the field was dosimetrically fully closed.

3.4.4. VMAT/IMRT Validation (Including 3D Plan Validation)

The third step involves creating and evaluating complex clinical treatment plans, including 3D plans, IMRT and VMAT. For 3D plan validation, clinically representative treatment plans are created in the TPS and the calculated dose distributions are compared with measured doses

using patient-specific phantoms or independent dosimetric systems such as film, ion chamber arrays or 3D dosimeters. This validation step ensures that the TPS accurately replicates clinical conditions and can precisely deliver the planned dose.

The study by (Clark *et al*., 2019) was used as a reference for the CIRS SHANE phantom dataset acquired using the Canon Aquillion LB CT scanner at CMJAH to mimic an IMRT plan for a patient with a nasopharyngeal tumour. The CT data structure sets were imported into the Monaco TPS to verify the CT export and TPS import protocols and ensure accuracy and completeness by comparing individual structure volumes to predetermined values specific to the CIRS SHANE Phantom (see table 2). The aim of this process was to validate the CT dataset and TPS import procedures for IMRT planning and highlight the importance of accurate data processing and consistency in treatment planning (Alfitra *et al*., 2024;Xing *et al*., 2022).

Table 2:CIRS Shane phantom design with associated volumes and TPS constraints.

Structure name	Description	Nominal volume, cm^3	Min volume, cm^3	Max volume, cm^3
PTV_7000	Nasopharynx primary plan target	88.5	87.6	89.4
PTVn1_6000	Involved nodes plan target volume	411.6	397.2	426.0
PTVn2_5400	Elective nodes plan target volume	260.3	244.7	275.9
SpinalCord	Spinal cord organ at risk	24.9	22.8	27.0
SpinalCord_03	Spinal cord Plan Risk Volume 3mm	55.1	50.1	60.1
BrainStem	Brain stem organ at risk	43.9	42.6	45.2
BrainStem_03	Brian stem Plan Risk Volume 3mm	72.5	71.4	73.6
Parotid_L	Contralateral left parotid	19.7	18.9	20.5
Parotid_R	Ipsilateral right parotid	23.4	22.5	24.3
IC_PTV_7000	Ion chamber volume in nasopharynx	0.13	0.1	0.2
IC_PTVn1_6000	Ion chamber volume in involved nodes	0.13	0.1	0.2
IC_PTVn2_5400	Ion chamber volume in elective nodes	0.13	0.1	0.2
IC_SpinalCord	Ion chamber volume in spinal cord	0.13	0.1	0.2
Channel_1	Channel for IC_PTV_7000	42.0	37.8	46.2
Channel_2	Channel for IC_PTVn1_6000	42.0	37.8	46.2
Channel_3	Channel for IC_PTVn2_5400	42.0	37.8	46.2
Channel_4	Channel for IC_SpinalCord	42.0	37.8	46.2

QA procedures for patient-specific IMRT/VMAT plans were performed on optimised plans, verified using a PTW Octavius 4D phantom with a 1500-chamber array in conjunction with PTW Verisoft software (version 7.2) and the results were recorded.

The SHANE system measurements used a 0.125 cm^3 ionisation chamber validated for pretreatment dose verification in advanced techniques. The chamber was inserted in one of four designated SHANE measurement channels using a special chamber cavity rod identified by the prefix IC, as shown in Table 2. The chamber was fully inserted into the cavity rod to ensure precise placement. In accordance with IAEA recommendations, the chamber cable was secured

to the treatment table with adhesive tape to prevent movement during measurements. The remaining SHANE channels were filled with material matching the density of the phantom. This procedure was repeated for the irradiations in the other three channels to ensure consistency and accuracy of the measurements.

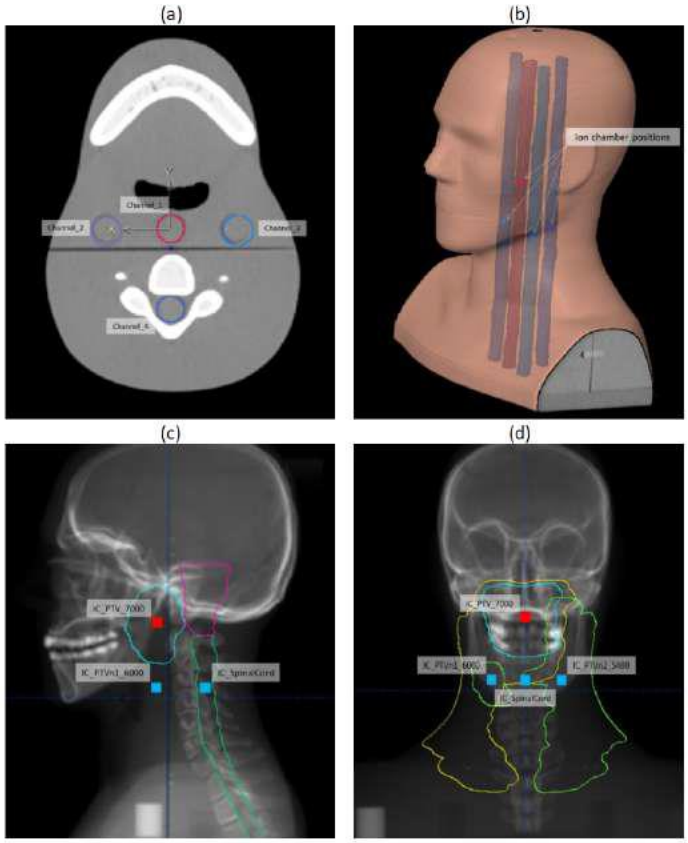


Figure 11: CT scan of the Head & Neck phantom illustrating the locations of the ionisation chamber channels and the respective ionisation chamber positions in various views: (a) Transverse plane, (b) 3-D Display, (c) Sagittal view and (d) Coronal view (Kazantsev *et al*., 2020).

3.4.5. 3D and VMAT for Prostate

In the study on prostate cancer treatment, slabs with a 4.5 cm buildup and 7.5 cm backscatter were utilised to mimic tissue conditions for both VMAT and 3D-CRT plans, ensuring a consistent and realistic model for evaluating dose distribution (Santos *et al*., 2023). The VMAT plans delivered a total dose of 60 Gy in 30 fractions, while the 3D plans prescribed 80 Gy delivered in 40 fractions, with beams directed from lateral, anterior and posterior angles. These slabs provided a consistent and realistic model for evaluating dose distribution specific to prostate cancer treatment.

The 4.5 cm buildup slab was chosen to replicate the superficial tissue layers surrounding the prostate, ensuring that the radiation beams reached the dose buildup region, where maximum energy deposition occurs. This thickness was critical for achieving electronic equilibrium, which is essential for accurate dose calculation in prostate cancer treatment. The 7.5 cm backscatter slab, placed behind the buildup layer, simulated the scattering effects within deeper tissues, providing a realistic representation of how radiation interacts with the prostate and surrounding structures.

For the VMAT plans, the slabs were configured to evaluate how the modulated arcs delivered the prescribed dose to the prostate, ensuring precise dose distribution across the buildup and backscatter regions. In the 3D-CRT plans, the slabs were used to assess dose deposition from beams delivered at lateral, anterior and posterior angles, considering the fixed-angle nature of 3D-CRT in prostate cancer treatment. Dose calculations were performed using a TPS and were validated through dosimetric measurements conducted within the slabs using a 0.6 cm^3 chamber, ensuring the accuracy and effectiveness of the treatment plans.

4. Results and Discussion

During the commissioning of the MONACO TPS, a series of measurements were carried out, including beam profiles, PDDs and OFs, to ensure the accuracy and reliability of the system. This document presents selected commissioning results, including beam data acquisition, base model validation, heterogeneity correction and model validation. A series of charts and results are displayed to highlight specific cases or notable deviations from expected results.

4.1. Commissioning data

Beam scanning was done using a PTW MP3-M Water Tank and PTW MEPHYSTO mc² software, following MPPGA 5.A, TG-53 guidelines and the Elekta document Measurements included open-field profiles, PDDs, OFs and absolute doses: all taken at a constant SSD of 90 cm. Additionally, wedged fields and diagonal scans were performed, where wedge transmission factors are crucial for photon CC beam models. Detectors were selected based on field size (see section 3.1.2.). Prior to integration into the Monaco TPS, all data entries necessary for beam modelling underwent rigorous verification.

The 6 MV photon energy was selected for detailed analysis due to its smoother and less noisy beam characteristics; data for other photon energies, including PDDs and beam profiles, are provided in Appendix 1 and Appendix 2, respectively. Figure 12 presents measured PDDs for various FSs, showing consistent and reliable data. In contrast, Figure 13 displays beam profiles at depths (see Section 3.1.1), emphasising the stable dose distribution of the 6 MV beam. Comprehensive data on beam profiles, PDDs and OFs were collected across FSs from 2 × 2 cm² to 40 × 40 cm², with 6 MV noted for its superior quality, smooth profiles and reduced noise.

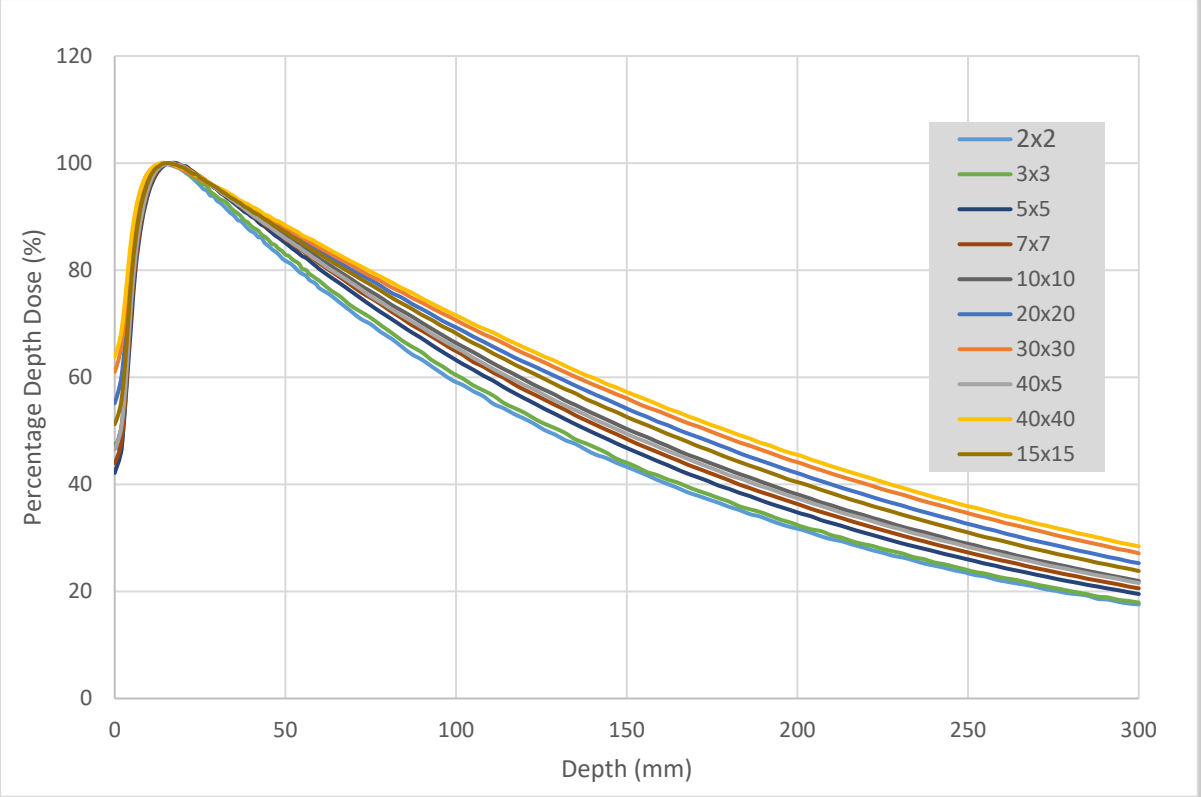


Figure 12: 6MV PDD measurements were performed using a PTW micro-diamond 0.004 cm³ chamber for FSs ranging from 2 × 2 cm² to 4 × 4 cm² and the PTW Semiflex 3D 0.07 cm³ for FSs from 5 × 5 cm² to 40 × 40 cm², all at an SSD of 90 cm.

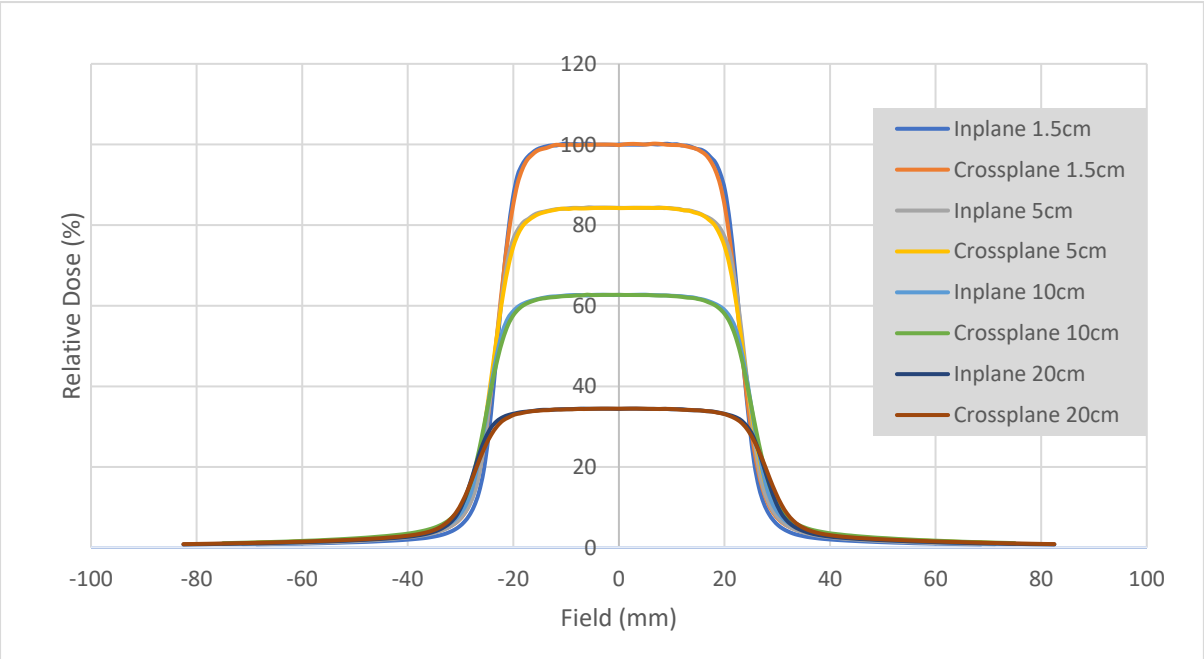


Figure 13:6MV inplane and crossplane profiles for a 5 × 5 cm² FS were measured at depths (see Section 3.1.1) using the PTW Semiflex 0.07 cc detector, with an SSD of 90 cm.

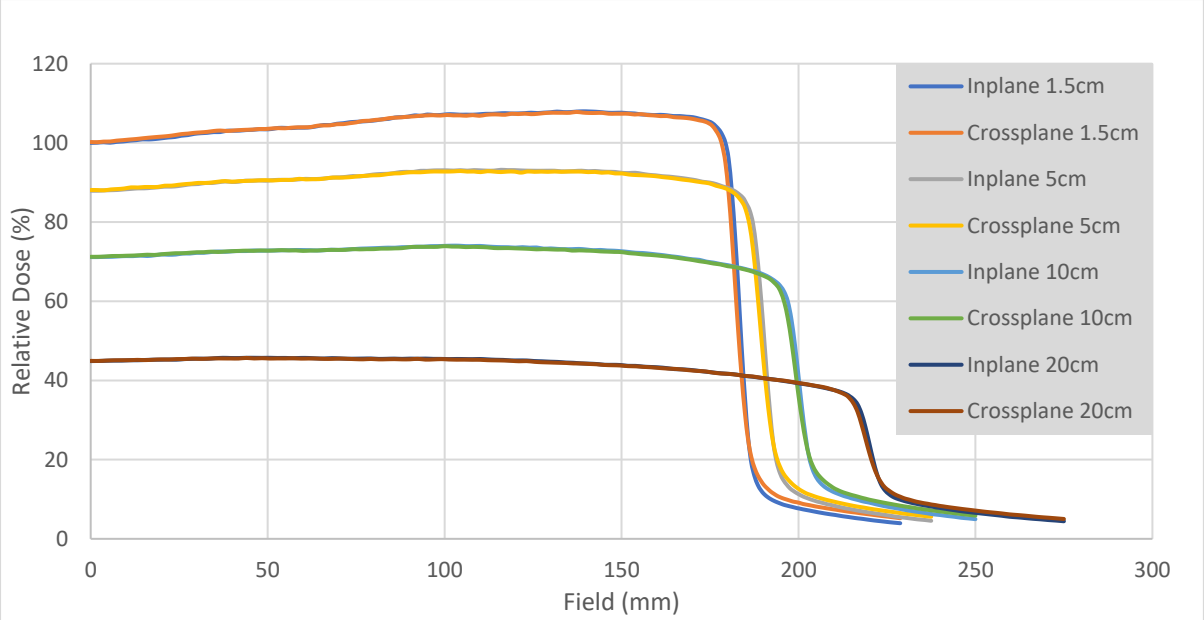


Figure 14:6MV inplane and cross-plane half profiles for a 40 × 40 cm² FS were measured at depths (see Section 3.1.1) using the PTW Semiflex 0.07 cc detector, with an SSD of 90 cm.

4.2. Homogeneity Correction

The evaluation involved scanning a Catphan phantom with known EDs, utilising a Canon Aquillion LB CT scanner and importing the images into the Monaco TPS. When converting the CT numbers to RED values using Monaco's HU to RED calibration curve, we found that the RED values were consistently lower than expected (see Figure 16). This discrepancy was particularly evident in the low HU region, where the measured values were lower than the known electron densities

The Catphan phantom used in the study might not be optimised for homogeneous corrections, potentially leading to deviations in ED calibration accuracy (Ese *et al*., 2023;Slama *et al*., 2023;Visbal., 2023) . The study by Zehra Ese et al. highlights the challenges in CT number mapping to electron density, especially for high-atomic number materials, affecting radiotherapy TPSs (Ese *et a*l., 2023). Luke A. Slama et al. discuss the importance of curvature correction factors for accurate, independent monitor unit calculations in electron treatments, emphasising the impact of body contour on dose calculations (Slama *et al*., 2023). Additionally, Jorge Homero Wilches Visbal's work underscores the significance of phantom design in simulating monoenergetic PDDs for electron beam spectrum reconstruction, indicating the influence of phantom materials on calibration accuracy (Visbal., 2023). These findings collectively suggest that the choice of phantom materials and structure plays a crucial role in achieving precise ED calibration and accurate dose calculations in radiotherapy applications.

Despite these discrepancies, the data from the Shane phantom, which is also not specifically designed for homogeneity corrections, largely agreed with the RED values calculated by the Monaco TPS. This alignment suggests that the Monaco TPS can reliably convert CT data to RED values, even when using phantoms that are not ideal for homogeneous corrections. In addition, gamma analysis using a 3%/3 mm passing criterion demonstrated that overall agreement was within clinically acceptable limits. This shows that although the Catphan phantom is not perfect for homogeneous corrections, the Monaco TPS still provides reliable accuracy in converting CT data into RED values, ensuring precise dose calculations for effective and safe radiotherapy treatments.

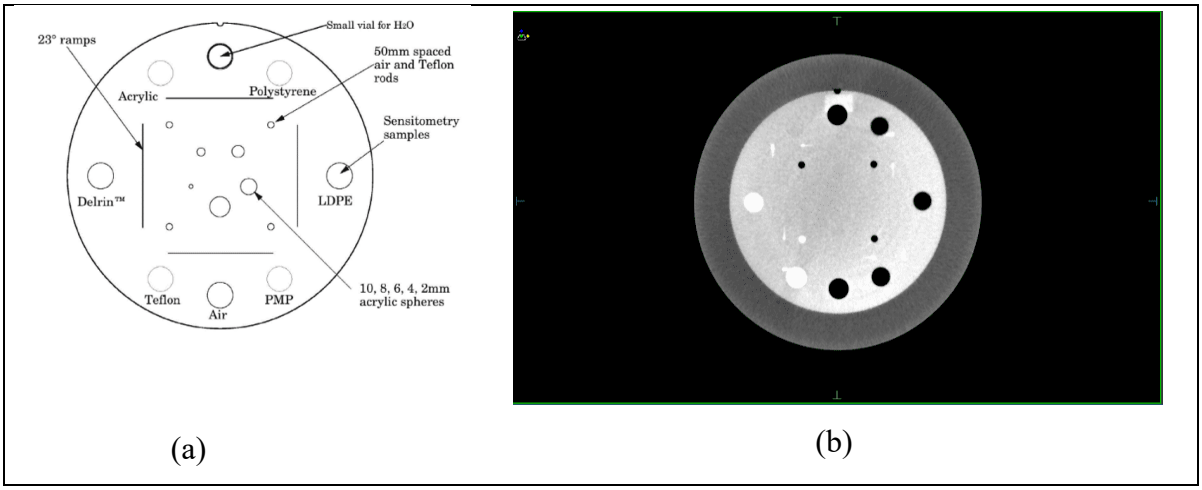


Figure 15: (a) Catphan Reference diagram with different materials (C a t p h a n ® 500 and 600 Product Guide) (b) Scanned Catphan at CMJAH.

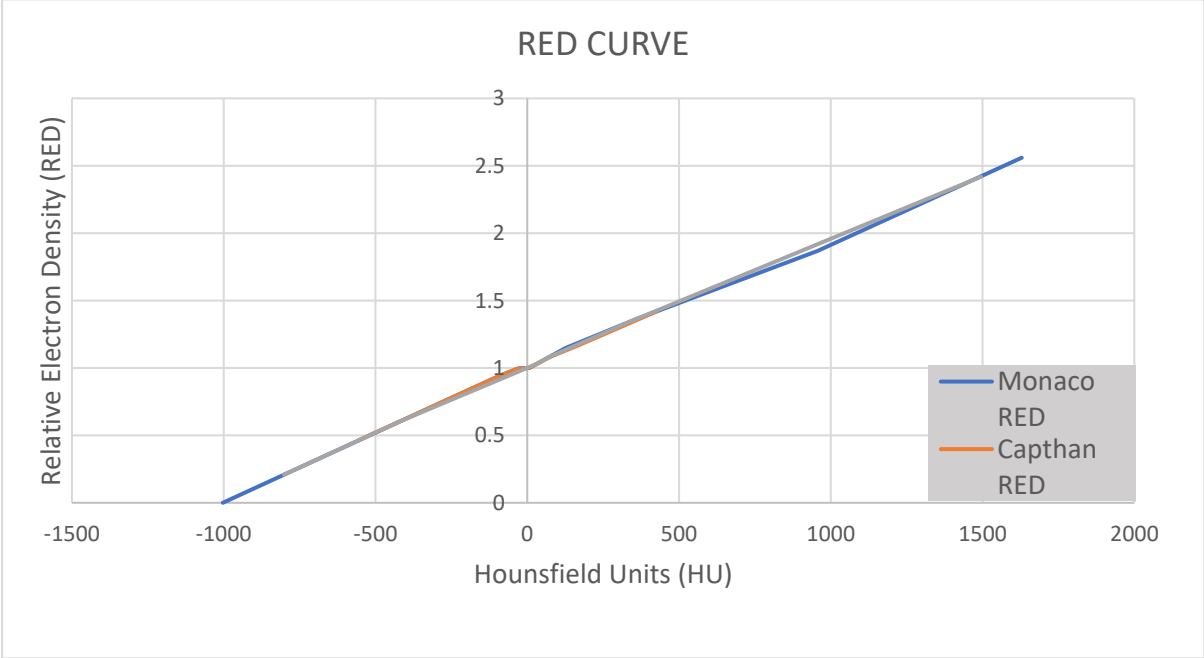


Figure 16: Shows the comparison of CT to RED curves measured with the Catphan phantom and the CIRS Shane phantom, both scanned at CMJAH, with reference to the Monaco TPS RED curve.

4.3. Base model validation

All calculations in this study were performed utilising the Monaco TPS (version 6.1.2.0). The Versa HD Linac used in this study generates photon energies of 6 MV (with flattening filter), 6 FFF (6 MV flattening filter free), 10 MV (with flattening filter), 10 FFF (10 MV flattening filter free), 15 MV and 18 MV. MC models were generated for each energy and modality. Additionally, CC. Models were developed for the 15 MV and 18 MV photon beams, both with and without wedges. In the Monaco TPS, CC models can be used to replicate the effects of an actual motorised wedge, while MC models cannot.

4.3.1. PDDs and Profiles Validation

A CT scan of air was performed and then imported into the Monaco TPS by Elekta. Within this system, a cubic volume measuring 50 x 50 x 50 cm^3 was defined in air. This volume was assigned an ED of 1.0 for MC simulations. For CC, the option to treat the entire patient as water was selected as one of the parameters under the calculation properties to simplify tissue heterogeneity effects, ensuring more consistent dose calculations by assuming uniform electron density. Dose calculations for open and wedge fields were executed utilising a fine dose grid resolution of 0.3 cm. The values of 0.5% statistical uncertainty in MC simulations for 6 MV and 1.0% for 10 MV were chosen to appropriately balance the precision of calculation and computational efficiency. The lower uncertainty for the 6 MV reflects its higher frequency of use in clinical applications for which high accuracy is needed, whereas the higher uncertainty for 10 MV optimises the calculation time with very little effect on accuracy for this less frequently used energy. The Monaco TPS analysed the resulting dose for the opened and wedged fields.

This section focuses on comparing the dose distributions calculated by the Monaco TPS to the measured data from the Linac using gamma analysis, which employs a DD criterion of 3% and a DTA criterion of 3 mm. The analysis was performed in photon beam relative mode. The results showed that the Monaco TPS achieved high accuracy as its reference metrics closely matched the measured data, confirming its stability under monitored conditions.

This section explores the PDDs and beam profiles for open and wedged fields for MC and CC calculations, respectively, compared to measurement data. MC calculations were performed for open FSs of 3 x 3 cm^2, 5 x 5 cm^2, 10 x 10 cm^2, 20 x 20 cm^2 and 40 x 40 cm^2, while measurements were taken for wedged FSs of 5 x 5 cm^2, 10 x 10 cm^2, 20 x 20 cm^2 and 40 x 30 cm^2 The difference between CC, MC simulations and measured data is explained in percent as the dose is relative (%) due to the fact that the study compares the absolute doses calculated by various algorithms for both CC and MC after delivering the same number of MUs. The number of MUs given per beam determines the dose of each irradiated point. The MC/CC PDDs and beam profiles were calculated using 100 MUs, while the absolute dose measurements were made using relative measurements, OFs and the absolute dose that the accelerator is set to deliver at the isocenter under base shaft conditions.

A high degree of correlation was found between the measured and MC-calculated open-field PDDs and beam profiles. Furthermore, the results met the 3%/3 mm gamma passing criteria

proposed by Venselaar and colleagues, thereby validating the accuracy of the MC calculations for open field beam profiles across various FSs and depths (Venselaar *et al*., 2001). The detailed analysis reveals that the MC method predicts higher doses for smaller FSs (3 x 3 cm², 4 x 4 cm² and 5 x 5 cm²) and lower doses for FSs exceeding the reference size (10 x 10 cm²). Generally, there was good agreement between MC/CC-calculated and measured doses, except in the build-up region of PDDs and at the beam edges in beam profiles. MC predicted lower doses in the build-up region due to the finite size of the ionisation chamber used for measurements and wall thickness effects. Uncertainties in dose voxels along the CAX increased with depth.

The plots illustrating the PDDs for the selected FSs mentioned above are displayed in Figures 17 and 24. The PDDs and beam profiles for wedged and opened s match very closely. Except for small fields due to various factors such as loss of lateral charged particle equilibrium, source occlusion, volume averaging and differences in detector composition compared to the challenges in small field dosimetry arise from the hindrance of the source size and collimation system, the lack of electronic balance and the size differences between detectors and beam sizes. The OFs calculated by MC simulations were higher than measured values for FSs smaller than 10 x 10 cm² but were lower for larger fields. This discrepancy is attributed to inadequate jaw modelling.

In this study, a gamma index pass rate of 90% was established as the benchmark for successful agreement between measured and calculated dose distributions (Nguyen et al., 2016). Fields that failed to meet the 90% threshold are highlighted in red in the tables below. However, it is noteworthy that another study referenced within this analysis reported a pass rate of 79% for other fields (Hrbacek et al., 27). The figures below show the PDDs and dose profiles for the fields with lower pass rates. These results illustrate how the dose distribution deviated from the expected values, particularly in the smaller FSs.

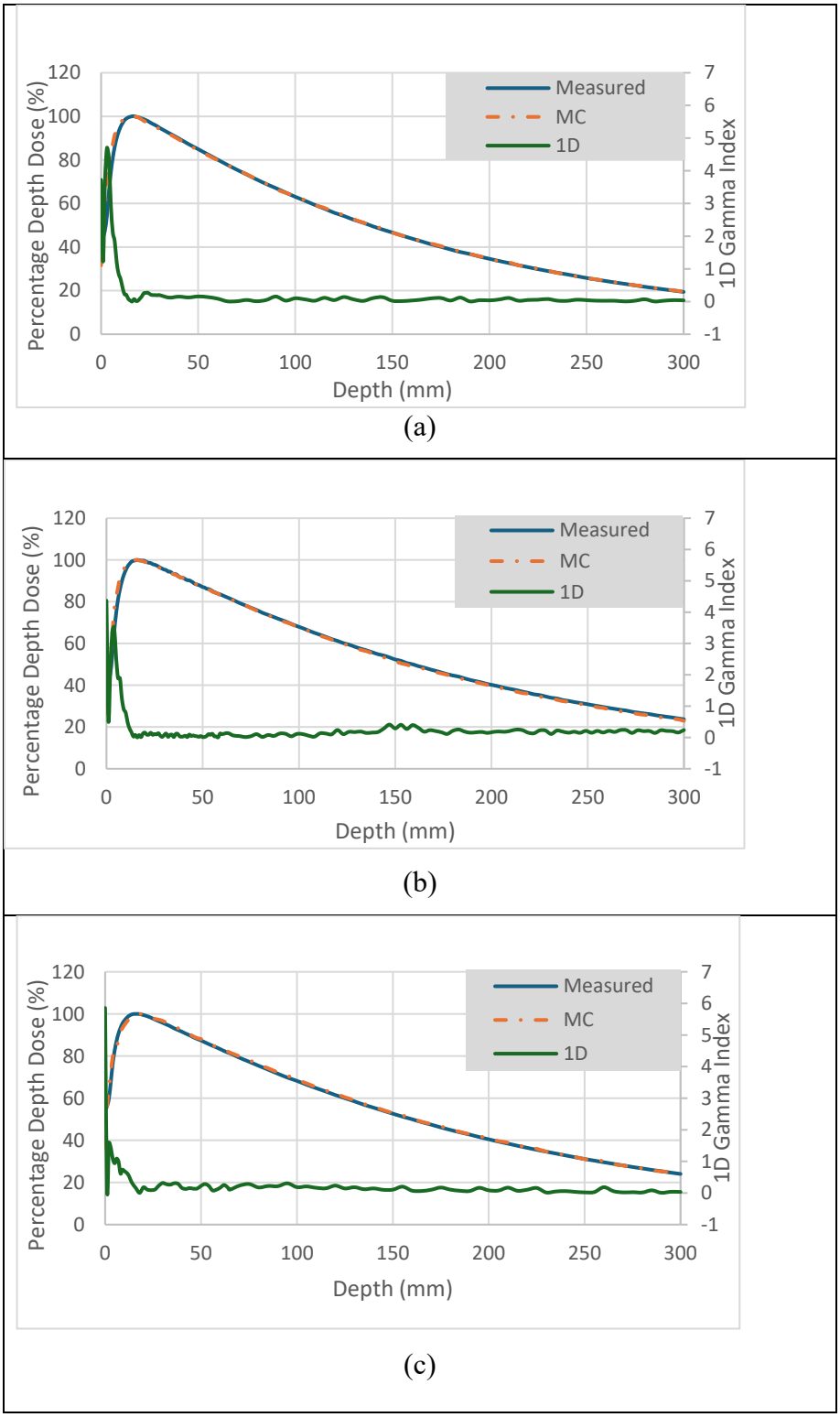


Figure 17: (a) Comparison of measured and TPS Monte Carlo (MC) percentage depth dose for a 5x5 cm² open field for 6 MV. (b) Comparison of measured and TPS collapsed cone (CC) percentage depth dose for a 10x10 cm² wedged field for 6 MV. (c) Comparison of measured and TPS Monte Carlo MC percentage depth dose for a 20x20 cm² open field for 6 MV FFF.

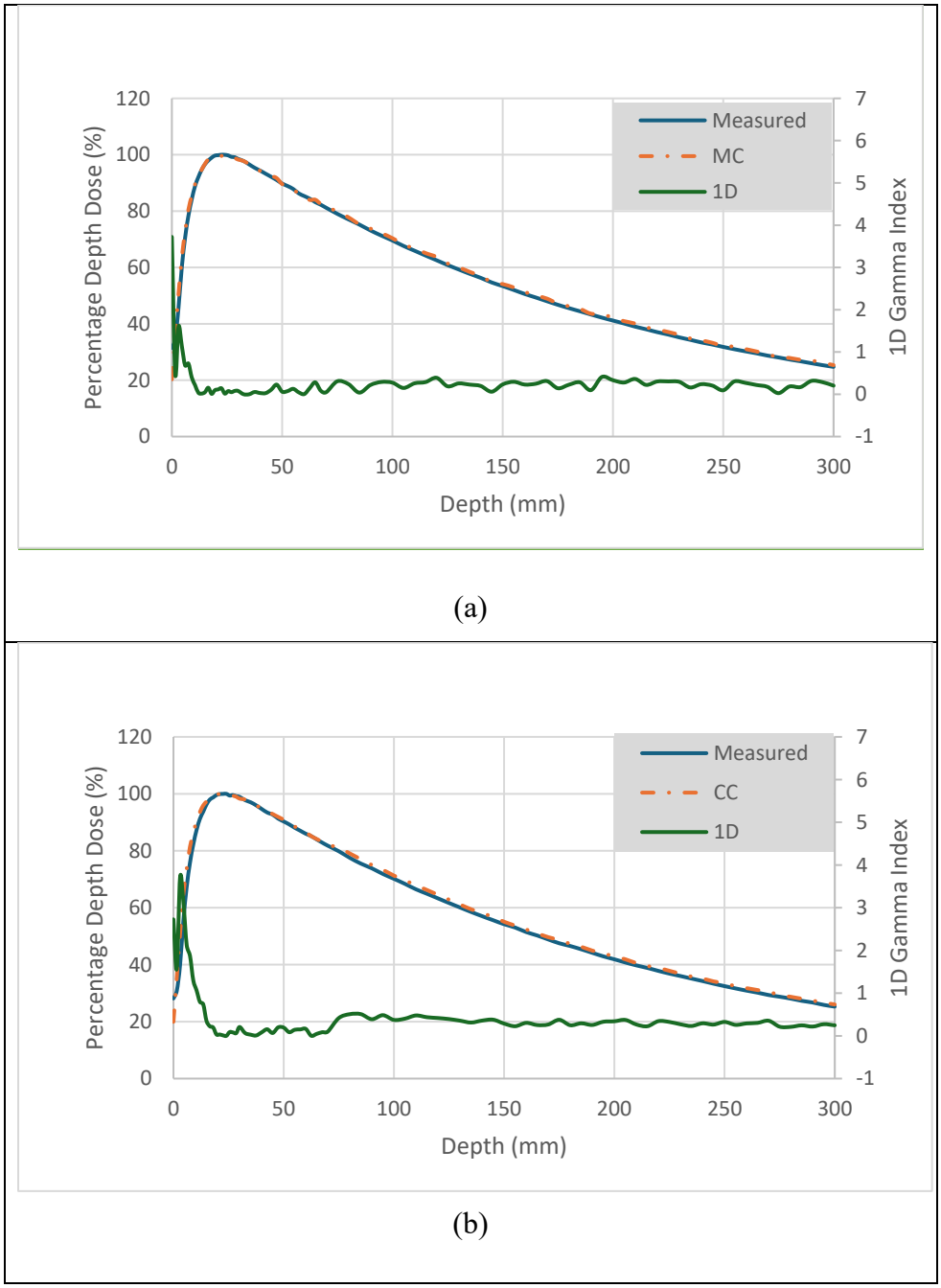


Figure 18: (a) Comparison of measured and TPS Monte Carlo (MC) percentage depth dose for a 5x5 cm² open field for 10 MV. (b) Comparison of measured and TPS collapsed cone (CC) percentage depth dose for a 5x5 cm² wedged field for 10 MV.

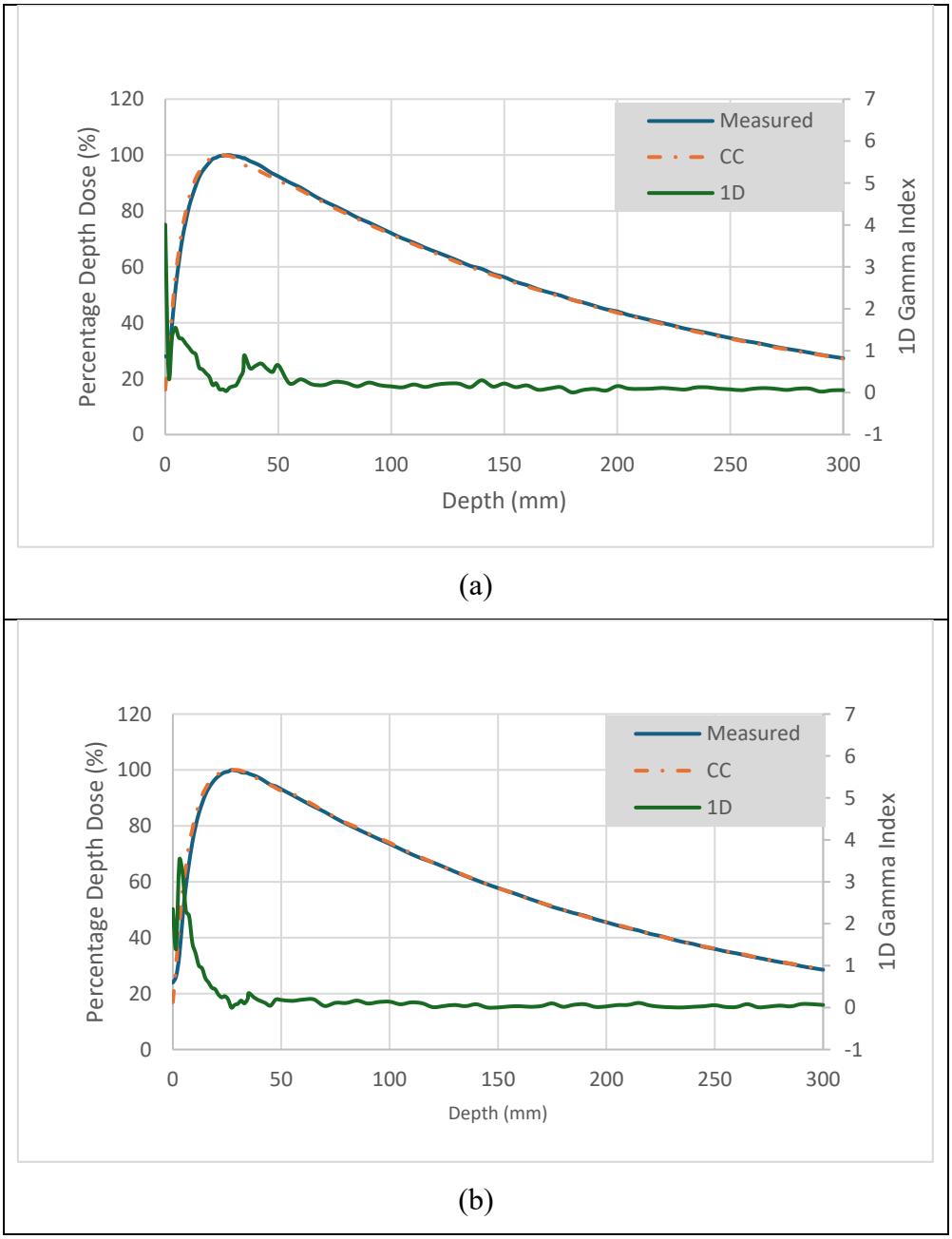
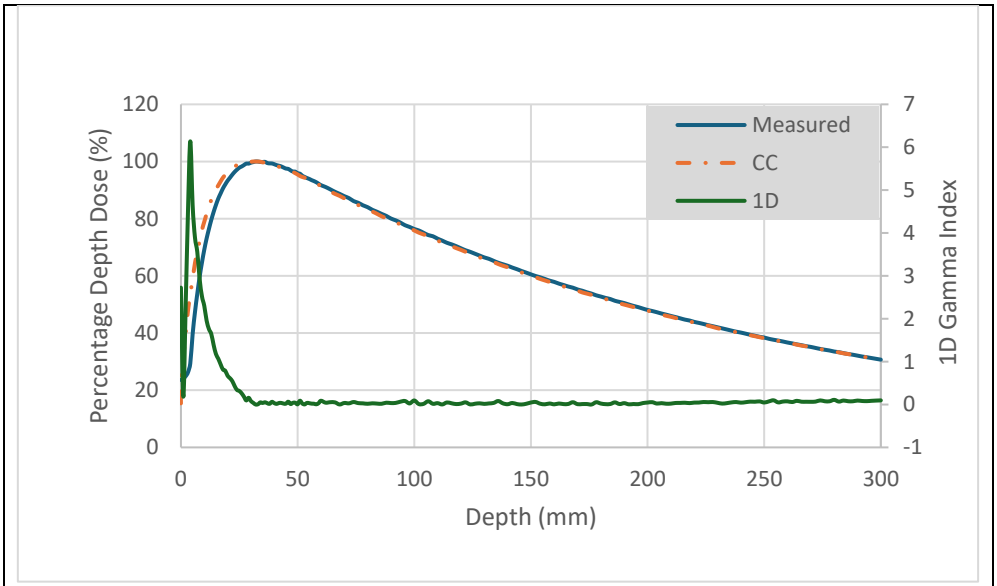
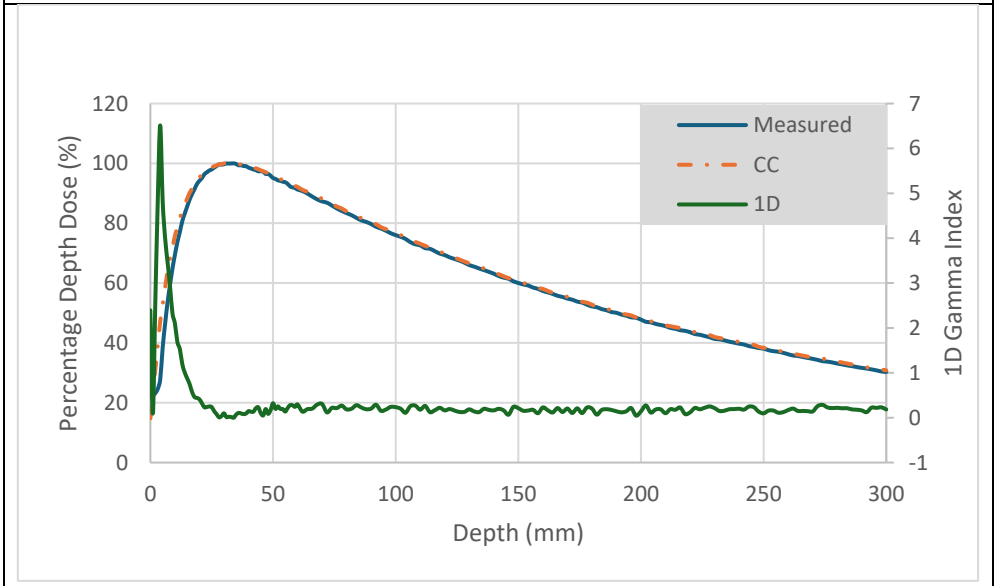


Figure 19: (a) Comparison of measured and TPS collapsed cone (CC) percentage depth dose for a 3x3 cm² open field for 15 MV. (b) Comparison of measured and TPS CC percentage depth dose for a 5x5 cm² wedged field for 15 MV.

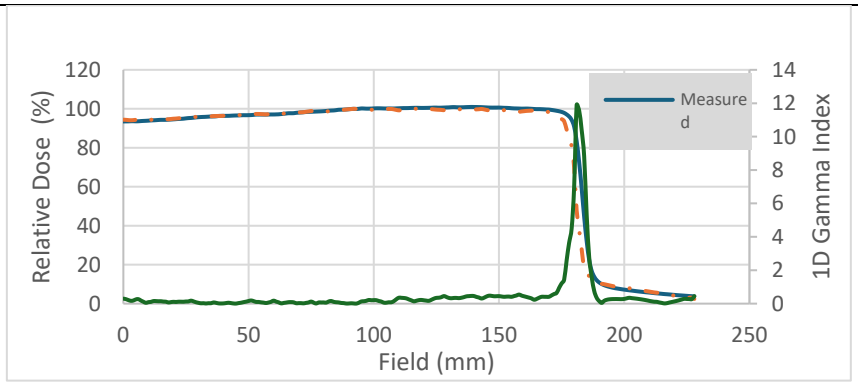


(a)

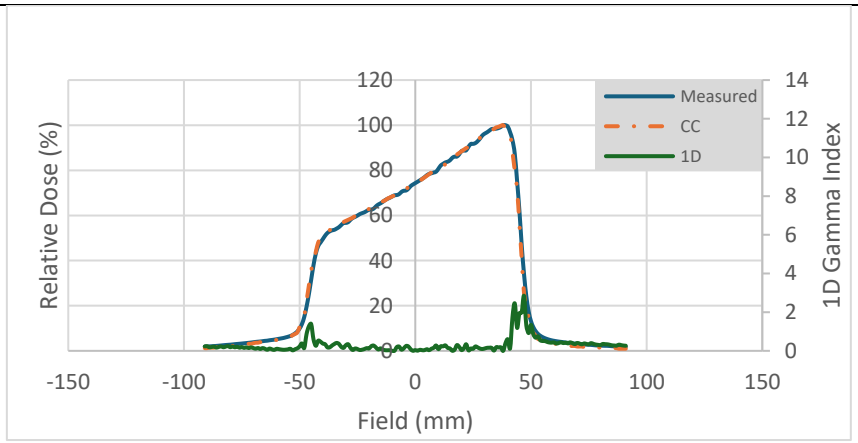


(b)

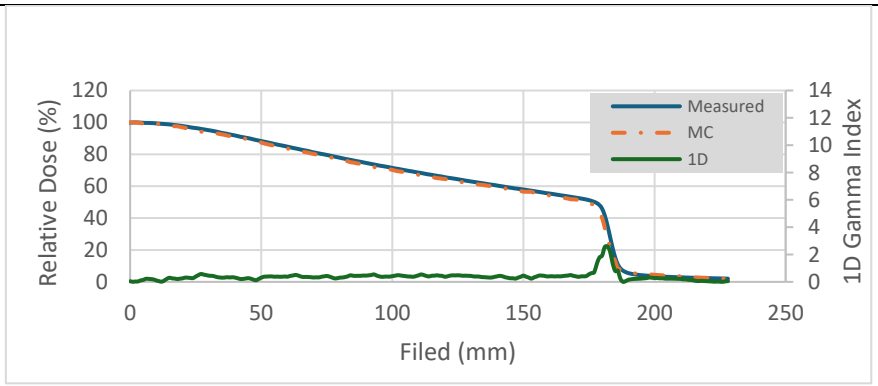
Figure 20*:* (a) Comparison of measured and TPS collapsed cone (CC) percentage depth dose for a 5x5 cm² open field for 15 MV. (b) Comparison of measured and TPS CC percentage depth dose for a 5x5 cm² wedged field for 15 MV.



(a)



(b)



(c)

Figure 21: Comparison of measured and TPS MC open field half profiles for 6MV, 40 × 40 cm² at 1.5 cm depth, showing 1D gamma. (b) Comparison of measured and TPS CC wedged field profiles for 6MV, 10 × 10 cm² at 1.5 cm depth, Showing 1D gamma. (c) Comparison of measured and TPS MC open field half profiles for 6MV FFF, 40 × 40 cm² at 1.3 cm depth, showing 1D gamma.

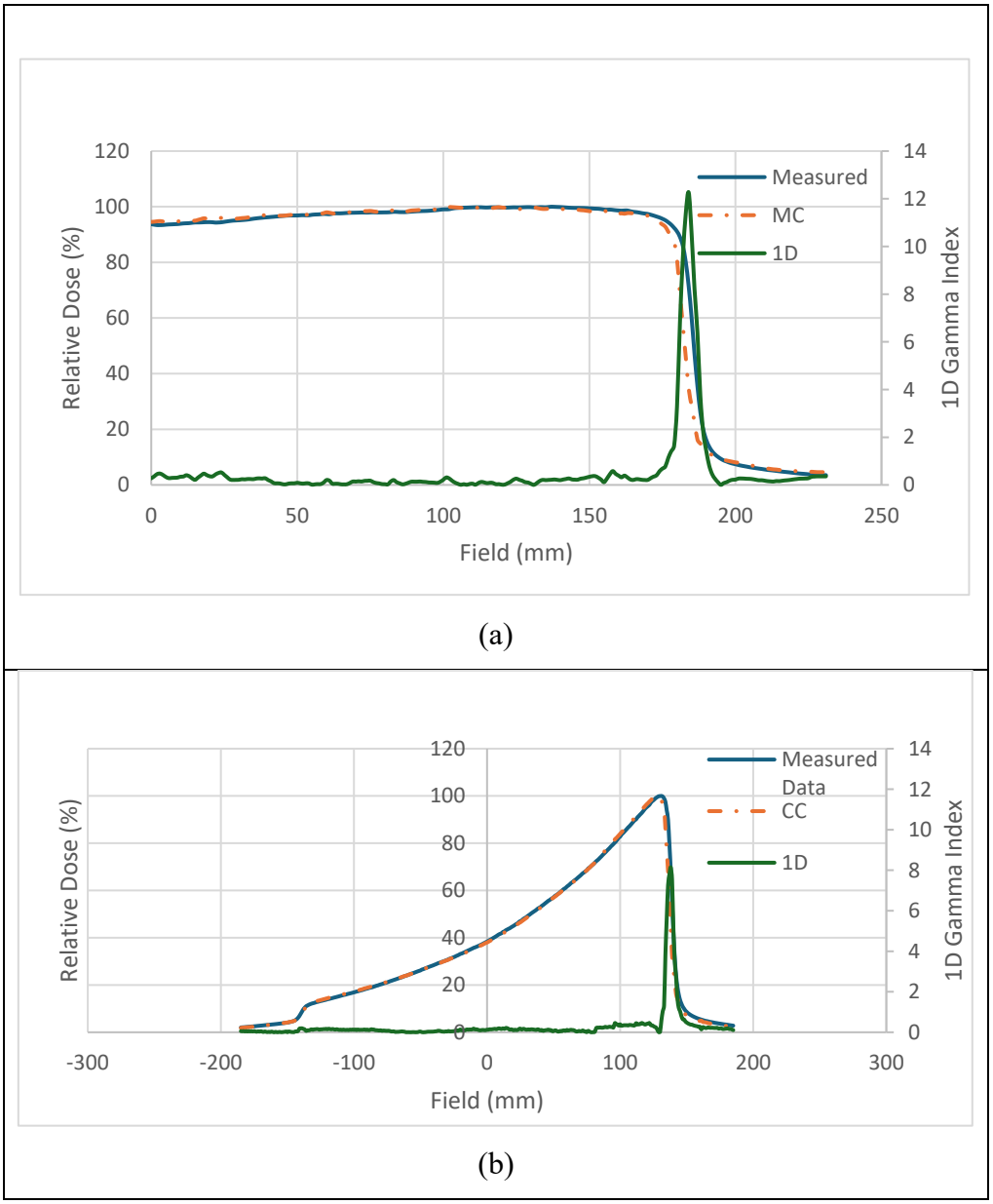


Figure 22: (a) Comparison of measured and TPS MC open field half profiles for 10MV, 40 × 40 cm² at 2.5 cm depth, showing 1D gamma. (b) Comparison of measured and TPS CC wedged field profiles for 10MV, 40 × 30 cm² at 2.5 cm depth, Showing 1D gamma.

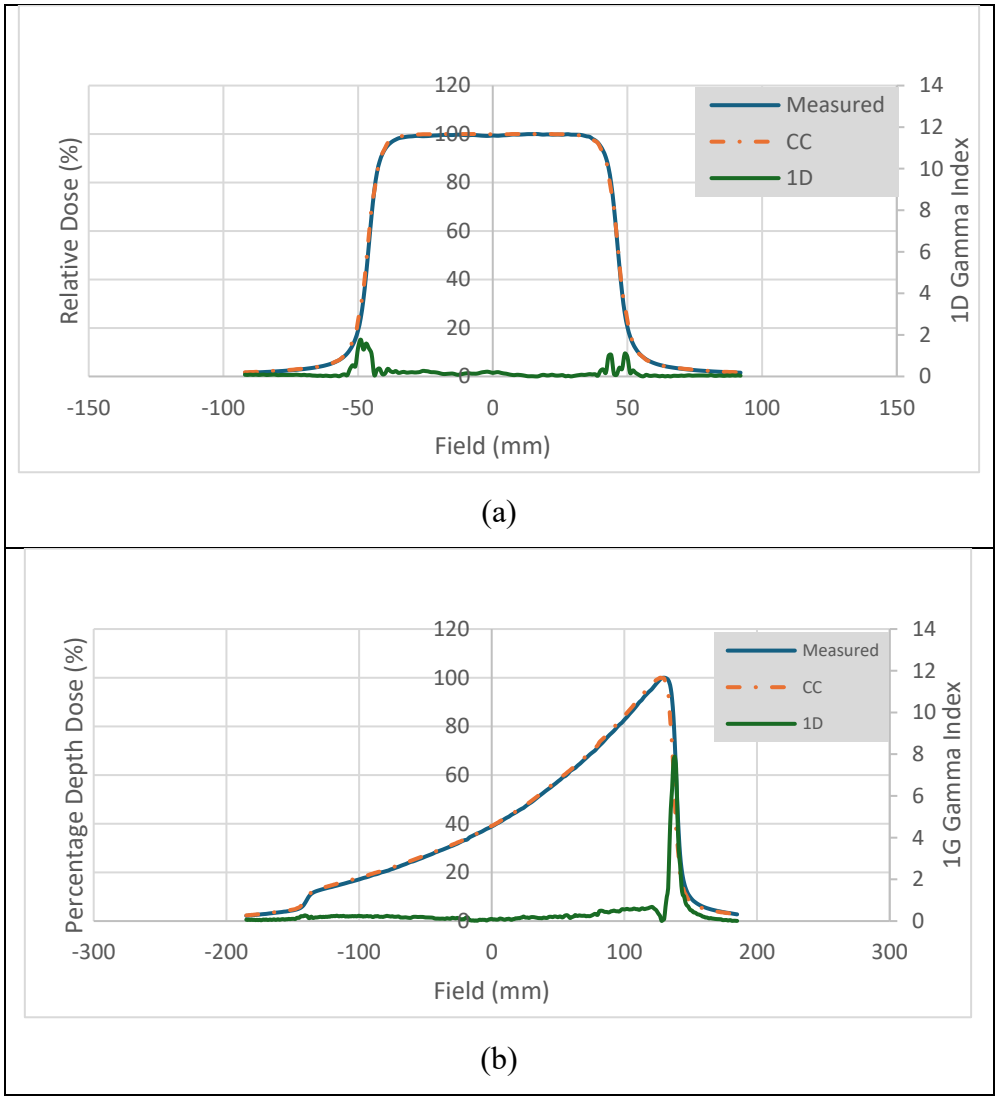


Figure 23: (a) Comparison of measured and TPS CC open field half profiles for 15MV, 10 × 10 cm² at 2.69 cm depth, showing 1D gamma. (b) Comparison of measured and TPS CC wedged field profiles for 15MV, 40 × 30 cm² at 2.69 cm depth, Showing 1D gamma.

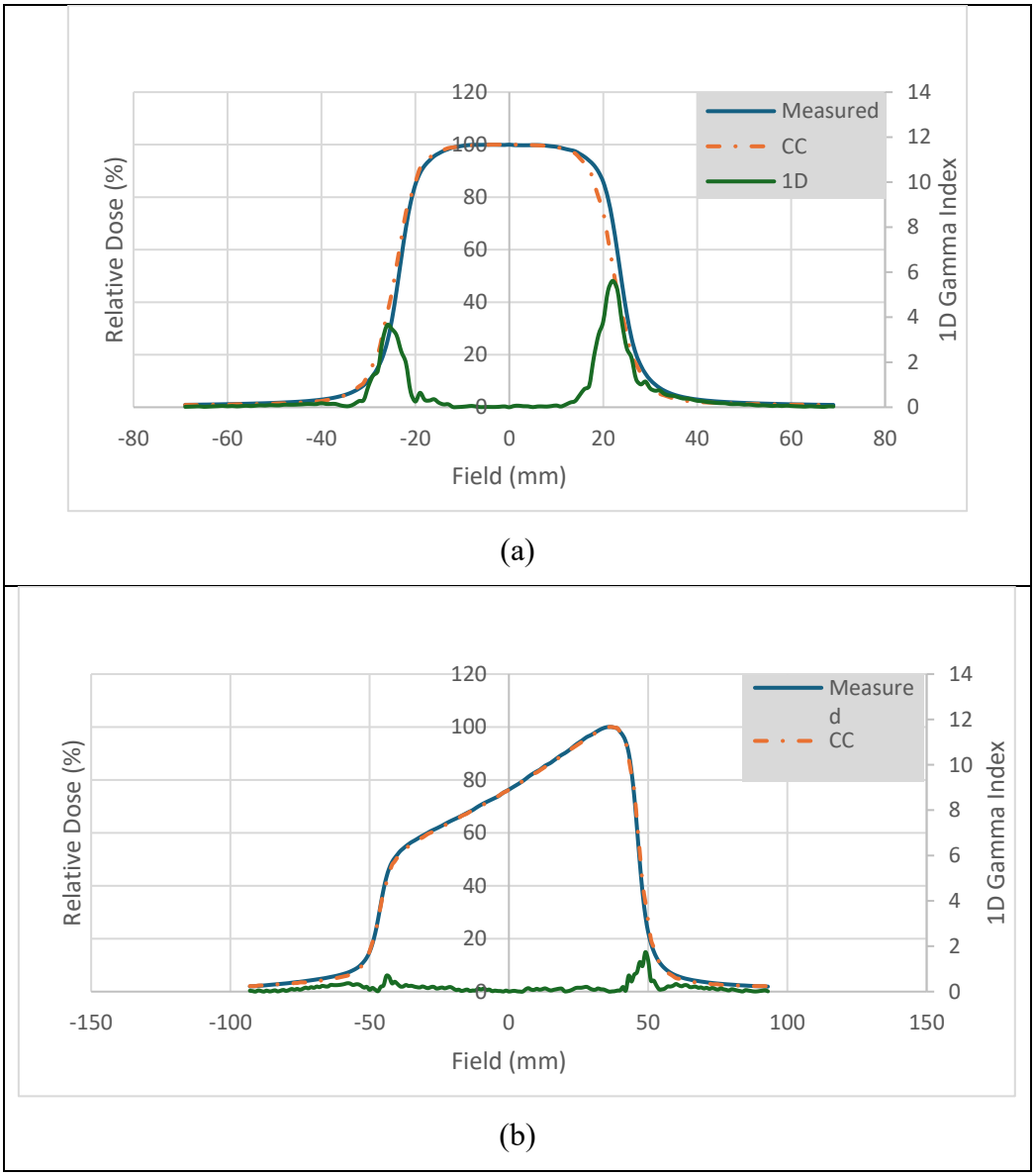


Figure 24: (a) Comparison of measured and TPS CC open field half profiles for 18MV, 3 × 3 cm² at 3.0 cm depth, showing 1D gamma. (b) Comparison of measured and TPS CC wedged field profiles for 18MV, 10 × 10 cm² at 3.0 cm depth, Showing 1D gamma.

Table 3: Gamma analysis pass rate for various open fields for measured and MC PDDs

Energy (MV)	Field sizes (cm^2)				
	3x3	5x5	10x10	20x20	40x40
6	95.74 %	89.41 %	92.20 %	94.33 %	97.16 %
6 FFF	94.19 %	95.35 %	95.35 %	94.19 %	95.35 %
10	98.80 %	96.39 %	97.57 %	96.39 %	90.80 %

Table 4: Gamma analysis pass rate for various open fields for measured and TPS MC PDDs.

Energy (MV)	Field sizes (cm^2)				
	3x3	5x5	10x10	20x20	40x40
15	91.36 %	91.36 %	93.83 %	95.06 %	98.77 %
18	95.03 %	91.16 %	92.82 %	93.37 %	93.92 %

Table 5: Gamma analysis pass rate for various open fields for measured and TPS CC PDDs

Energy (MV)	Field sizes (cm^2)			
	5x5	10x10	20x20	40x30
6	95.04 %	94.33 %	97.87 %	97.14 %
10	90.36 %	92.77 %	95.18 %	98.78 %
15	88.89 %	97.53 %	98.77 %	98.75 %
18	92.27 %	93.92 %	94.48 %	97.56 %

Table 6: Gamma analysis pass rate for various open fields for measured and TPS MC Profiles.

Energy (MV)	Algorithm	Field Sizes (cm^2)					Overall (1D) Pass
		3x3	5x5	10x10	20x20	40X40	
6	MC	90.83 %	90.51 %	94.54 %	94.55 %	93.95 %	92.88%
6 FFF	MC	88.24 %	97.08 %	98.91 %	97.44 %	96.94 %	95.72 %
10	MC	90.08 %	97.12 %	97.84 %	96.73 %	93.49 %	95.05 %
15	CC	87.60 %	99.28 %	95.68 %	95.99 %	96.26%	94.96 %
18	CC	81.90 %	85.61 %	93.58 %	97.49 %	94.76 %	90.67 %

Table 7: Gamma analysis pass rate for various open fields for measured and TPS CC Profiles.

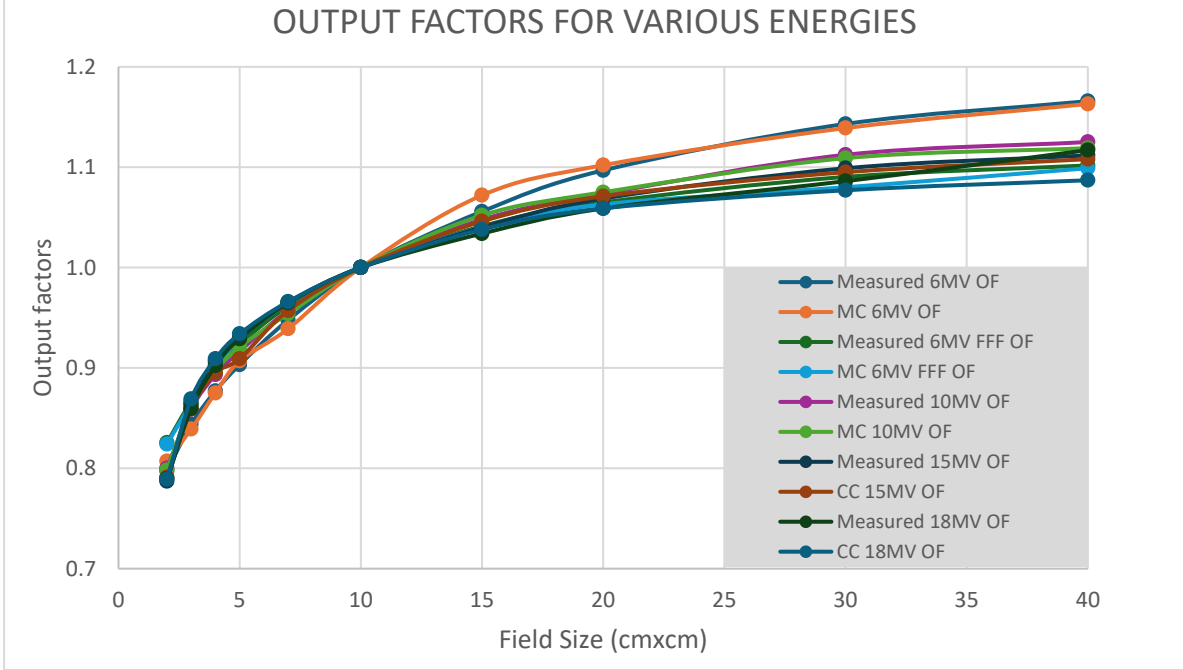
Energy (MV)	Algorithm	Field Sizes (cm^2)				Overall (1D) Pass
		5X5	10X10	20X20	40X30	
6	CC	86.86 %	94.54 %	97.82 %	97.00 %	94.06 %
10	CC	98.56 %	96.76 %	97.45 %	96.23 %	97.25 %
15	CC	90.09 %	98.38 %	96.77 %	96.23 %	95.37 %
18	CC	92.90 %	97.86 %	99.64 %	98.39 %	97.20 %

4.3.2. Output Factor Validation

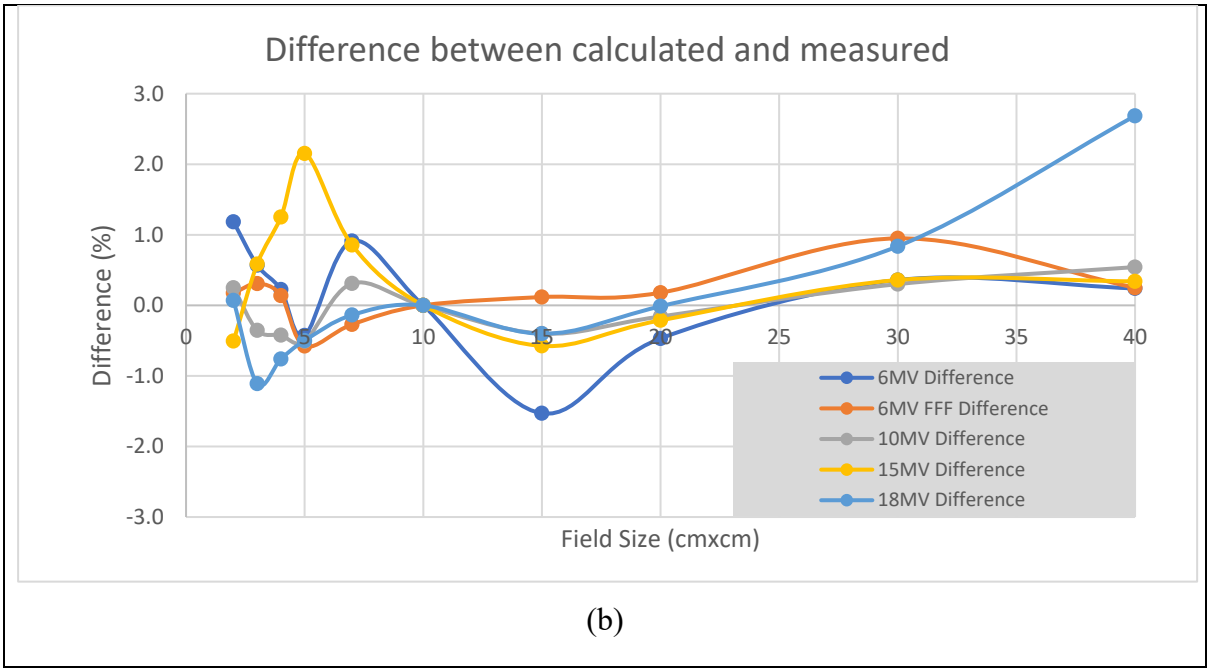
Figure 25a provides an overview of the OFs for open fields across five different energies, measured at an SSD of 90 cm and a depth of 10 cm. The figure demonstrates that the OFs obtained from MC simulations are higher than the measured OFs for FSs smaller than the

reference size of 10 × 10 cm². In contrast, the MC-calculated OFs are lower for larger FS than the measured values. Conversely, the OFs from the CC simulation for all the energies closely match the measured values. Figure 25b illustrates the discrepancies in OFs derived from MC and CC simulations for the Elekta system. As shown in Figure 25a, the most significant deviations between the calculated OFs and the MC/CC data occurred for 15 MV and 18 MV energies, with observed differences of 2.15% and 2.69%, respectively, at a FS of 5 × 5 cm² for 6 MV and at a FS of 40 x 40 cm². According to the AAPM TG 198 report (Hanley *et al.*, 2021), which provides tolerances for dosimetry and states that OFs variations between measured and calculated values should be within a ±2% margin for consistency and quality control in radiotherapy planning.

Figure 26a provides an overview of the OFs for wedge fields across four different energies, measured at an SSD of 90 cm and a depth of 10 cm. This figure depicts the discrepancies between the OFs derived from CC simulations for the Elekta system. As illustrated in Figure 26b, the most pronounced deviations between the calculated OFs and the CC data were observed for 6 MV and 18 MV energies, with differences of 2.19% and 2.45%, respectively. These deviations were noted at a field FS of 40 × 30 cm² for 6 MV and 15 × 15 cm² for 18 MV.

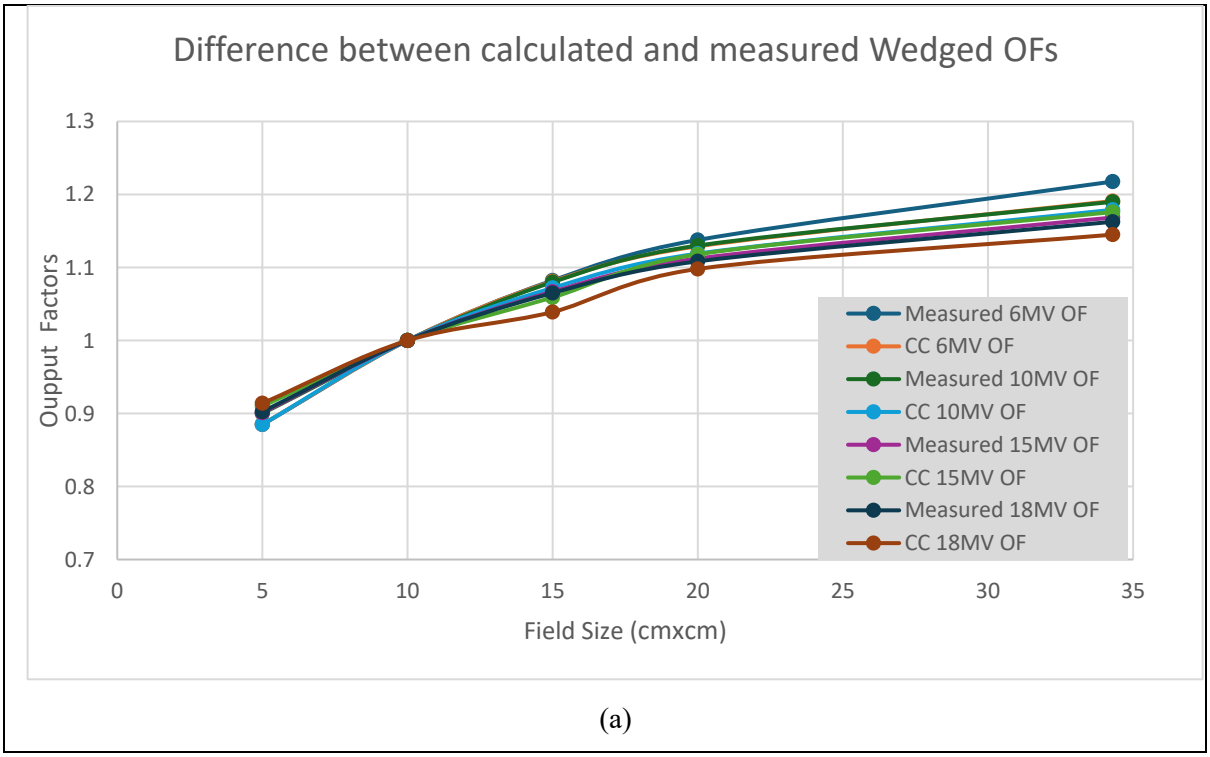


(a)

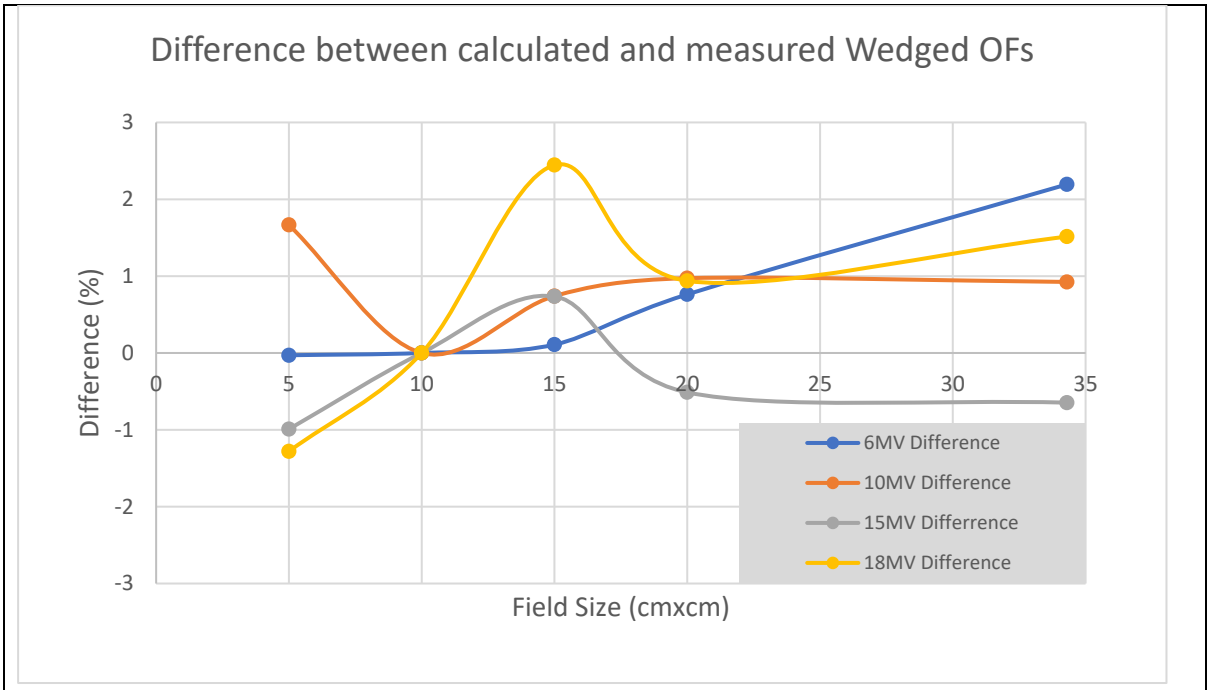


(b)

Figure 25: (a) Compares the measured Open Field Output Factors (OFs) with those calculated for the specified wedged FSs. (b) Illustrates the deviations between the measured and calculated OF values.



(a)



(b)

Figure 26: Compares the measured Wedged Field Output Factors (OFs) with those calculated for the specified FSs. (b) Illustrates the deviations between the measured and calculated OF values.

4.3.3. Dosimetric Validation

Reference dosimetry for each energy was conducted following the IAEA TRS-398 protocol to verify the proper calibration of the Linacs, utilising a PTW 0.6 cm^3 Farmer chamber for dose measurements. The calibration checks were performed in a PTW BeamScan water tank under reference conditions, confirming that the Linacs were calibrated accurately to deliver the predetermined doses. The measured doses are closely aligned with the expected values, with deviations within acceptable limits, ensuring the accuracy and reliability of the Linac systems in clinical settings (IAEA, 2001).

Dosimetry was performed using the SSD technique for both open and wedge fields. The results obtained are shown in the following Tables 8-9. The results were compared to 1 Gy/MU for the open-field SSD technique because the machine was calibrated with the SSD technique. This means that for reference conditions of 100 SSD and a FS of 10 x 10 cm^2, the dose at dmax should be 1 Gy per 100 MU. The highest deviation between the calculated dose at dmax and the baseline value (BL) was 0.77%, well within the acceptable limit of 1%. The dose calculated at dmax for the SAD technique is shown in Table 8 below. The dose for 6, 6 FFF, 10 FFF and 18 energies was above 1 Gy/MU, which corresponds to the calibration of the device. This was to be expected since the machine was calibrated using the SSD method. For wedge fields, the

calculated dose at d_{max} using SSD techniques consistently measured below 0.28 Gy per 100 MU, as shown in Table 9. The attenuation introduced by the wedge reduces the beam intensity, resulting in an expected dose per 100 MU expected remains below 1 Gy. Currently, no established tolerance limits exist for the calculated dose at dmax for wedged fields.

Table 8: Calculated dose at dmax for standard reference conditions using SSD techniques.

Energy (MV)	Measured Dose (Gy)	Expected Dose (Gy)	Difference (%)
6	1.0031	1.000	0.31
6 FFF	1.0006	1.000	0.06
10	0.993	1.000	0.70
10 FFF	1.0077	1.000	0.77
15	0.9997	1.000	0.03
18	1.0022	1.000	0.22

Table 9: Calculated dose at dmax for wedge fields using SSD techniques.

Energy (MV)	Measured Dose (Gy)
6	0.26
6FFF	0.24
10	0.23
10 FFF	0.25
15	0.27
18	0.27

4.4. DLG and MLC measurement

The optimization of MLC leaf transmission factors, as detailed in Table 10, consistently achieved results below the 0.5% threshold, in line with prior studies (Schneider *et al*., 2023) and well within the 2% threshold recommended by AAPM TG No. 50 (Boyer *et al*., 2001a). Figure 27 displays the measured DLG values for 6MV, 6MV FFF, 10MV, 10MV FFF and 15MV photon beams using the sweeping-gap technique. The ionisation chamber readings were recorded for progressively smaller gap sizes, with corrections applied for MLC leaf transmission, measured with the leaves fully closed. A linear fit was applied to the data to estimate the theoretical negative gap size that would yield a zero-ionisation chamber reading. The absolute value of this negative gap corresponds to the DLG, which represents the transmission at the leaf ends when the MLC is closed. The sweeping-gap method, performed under controlled conditions, provided a rough estimate of the optimal DLG values for these photon energies.

Table 10: Recorded values for DLG and MLC transmission.

Energy (MV)	MLC Transmission	DLG (mm)
6	0.40%	0.50
6 FFF	0.27%	0.51
10	0.41%	0.47
10 FFF	0.25%	0.49
15	0.40%	0.93

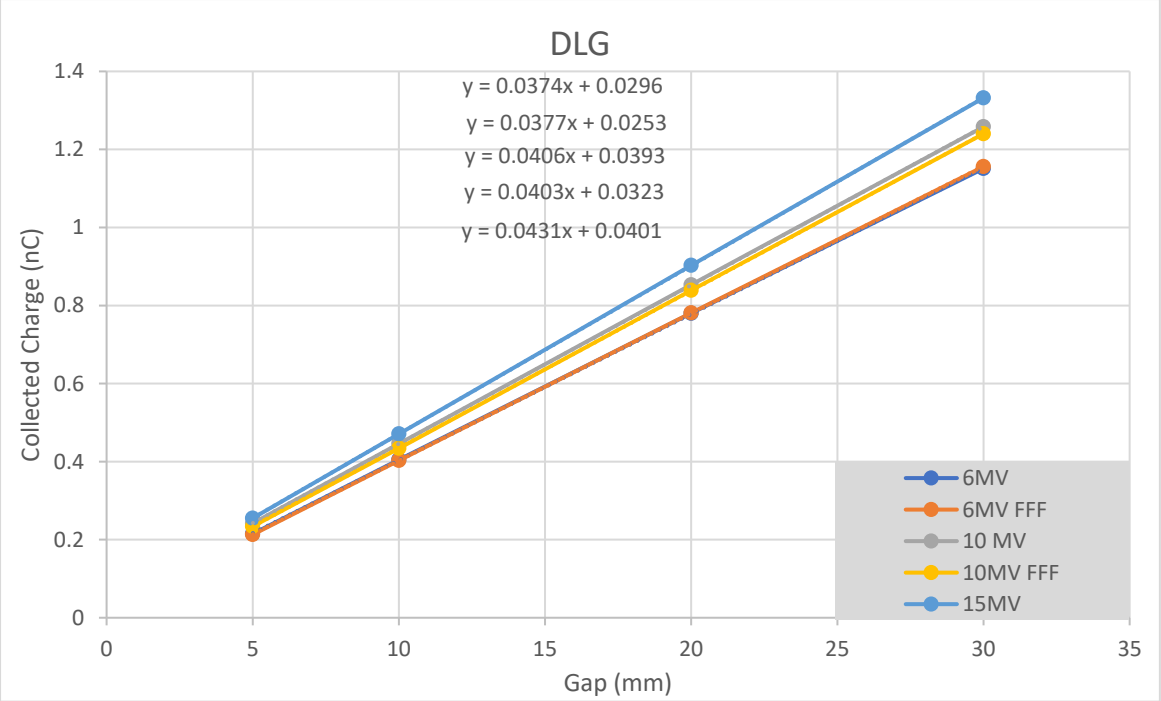


Figure 27: DLG measurement using the sweeping gap technique, which accounts for MLC end-of-leaf transmission, shows a linear relationship in the collected data. This analysis provided initial DLG values specific to each energy: 0.50 mm for 6MV, 0.51 mm for 6MV FFF, 0.47 mm for 10MV, 0.49 mm for 10MV FFF and 0.93 mm for 15MV.

4.5. 3DCRT and VMAT/IMRT Plan Validation

The IAEA audit methodology for IMRT/VMAT dosimetry, as described in Table 2 (section 3.4.3), involved comparing calculated and measured point doses for different chamber positions. The study included a tolerance of 5% for Planning Target Volume (PTV) volumes and 7% for the spinal cord volume (Clark *et al*., 2019) . In each case, the difference between the calculated and measured dose for all energies was within the limits stated above.

Table 11: Comparison between the measured and calculated doses using the Monte Carlo (MC) algorithm for the CIRS Shane phantom with 6 MV photon beams.

Volume structure corresponding to the chamber's position.	TPS calculated mean dose (Gy)	Mean measured dose (Gy)	Difference (%)
IC_PTV_7000 PTV_7000 (nasopharynx), isocentre, red channel no 1	2.264	2.205	2.61
IC_PTVn1_6000 PTVn1_6000 (involved nodes), 5 cm inferior to isocentre, blue channel no 2	2.109	2.130	-1.0
IC_PTVn2_5400 PTVn2_5400 (elective nodes), 5 cm inferior to isocentre, blue channel no 3	1.943	1.935	0.4
IC_SpinalCord IC_SpinalCord, 5 cm inferior to isocentre, blue channel no 4	1.051	1.035	1.5

Table 12: Comparison between the measured and calculated doses using the Monte Carlo (MC) algorithm for the CIRS Shane phantom with 6 MV FFF photon beams.

Volume structure corresponding to the chamber's position.	TPS calculated mean dose (Gy)	Mean measured dose (Gy)	Difference (%)
IC_PTV_7000 PTV_7000 (nasopharynx), isocentre, red channel no 1	2.352	2.325	1.15
IC_PTVn1_6000 PTVn1_6000 (involved nodes), 5 cm inferior to isocentre, blue channel no 2	2.341	2.295	1.96
IC_PTVn2_5400 PTVn2_5400 (elective nodes), 5 cm inferior to isocentre, blue channel no 3	2.124	2.100	1.30
IC_SpinalCord IC_SpinalCord, 5 cm inferior to isocentre, blue channel no 4	0.777	0.750	1.5

Table 13: Comparison between the measured and calculated doses using the Monte Carlo algorithm for the CIRS Shane phantom with 10 MV photon beams.

Volume structure corresponding to the chamber's position.	TPS calculated mean dose (Gy)	Mean measured dose (Gy)	Difference (%)
IC_PTV_7000 PTV_7000 (nasopharynx), isocentre, red channel no 1	2.321	2.370	-2.11
IC_PTVn1_6000 PTVn1_6000 (involved nodes), 5 cm inferior to isocentre, blue channel no 2	2.254	2.370	-4.89
IC_PTVn2_5400 PTVn2_5400 (elective nodes), 5 cm inferior to isocentre, blue channel no 3	2,186	2.28	-4.12
IC_SpinalCord IC_SpinalCord, 5 cm inferior to isocentre, blue channel no 4	1.039	1.050	-1.1

The evaluation of dose delivery accuracy in prostate cancer treatment using 3D-CRT and VMAT reveals important insights into treatment efficacy and safety. Both techniques were assessed with a prescribed dose of 60 Gy in 20 fractions for VMAT and 80 Gy in 40 fractions for 3D-CRT, focusing on the PTV cantered on slabs. The dosimetric measurements conducted using a 0.6 cm^3 chamber aimed to ensure that the delivered dose remained within a clinically acceptable range of ±5% of the planned dose from the TPS (Miften *et al*., 2018) . This tolerance level is crucial for balancing effective treatment while minimising side effects, as both techniques demonstrated comparable accuracy in dose delivery.

Table 14: Result for VMAT plans on a Perspex phantom.

Energy (MV)	TPS Mean Dose (Gy)	Measured Mean Dose (Gy)	Difference (%)
6	2.999	2,91	2.97
6 FFF	2.971	2.86	3.74
10	3.063	2.94	4.02

Table 15: Results for 3D plans on a Perspex phantom.

Energy (MV)	TPS Mean Dose (Gy)	Measured Mean Dose (Gy)	Difference (%)
6	2.004	2.000	0.2
10	2.003	2.000	0.1
15	2.006	2.030	-1.2
18	2.004	1.965	1.9

4.5.1. Patient-Specific Quality Assurance (PSQA)

The PSQA for Head & Neck and prostate plans was conducted using the PTW Octavius 4D phantom in accordance with the AAPM TG 218 protocol. A DTA criterion of 3 mm, DD threshold of 3% and a 5% dose suppression for normalization of the measured dose distribution were applied. The passing criteria were set at ≥ 95% to ensure clinical safety and accuracy. This threshold aligns with the literature to account for minor variances between the TPS

calculations and the measured dose. The results, presented in Table 16, indicate that all plans across the tested energies met or exceeded the 95% passing threshold.

Table 16: PSQA results for both sites: Head & Neck and Prostate.

Energy (MV)	Plans VMAT (%)	
	Head & Neck	Prostate
6	97.1	100
6 FFF	97.9	95.9
10	95.8	97.0

5. Conclusion

This study assessed the accuracy of dose calculations for open and wedged fields using both MC and CC models within the Monaco TPS, while specifically employing the CC model for wedged fields. MC simulations, executed with a fine grid resolution of 0.3 cm and statistical uncertainties of 0.5% for 6 MV and 1.0% for 10 MV, demonstrated excellent agreement with measured data for open fields for PDDs, beam profiles and OFs, particularly for FSs greater than 5 x 5 cm². This finding underscores the reliability of the Monaco TPS in accurately modelling dose distributions for open fields, thereby validating its robustness for clinical applications. However, discrepancies were identified in smaller FSs (3 x 3 cm² to 5 x 5 cm²) for PDDs and beam profiles, where MC simulations yielded higher doses.

CC models generally performed well for wedged fields, with PDDs and beam profiles closely matching measured data. Nonetheless, smaller wedged fields (e.g., 5 x 5 cm²) exhibited lower gamma pass rates, similar issues in small open fields suggest discrepancies. Previous studies have highlighted the limitations in small field dosimetry and the build-up region (Ding and Das, 2023;Da Silva *et al*., 2022), additional research is required to create effective strategies for addressing these issues. This includes investigating potential solutions to improve measurement accuracy and modelling approaches within the TPS to address the observed discrepancies. Despite these minor discrepancies, the Monaco TPS proved to be highly accurate for both open and wedged fields, particularly for larger FSs.

Accordingly, the OFs for different energies were analysed and it emerged that MC simulations yield higher values for the FSs smaller than 10 x 10 cm² and lower values for larger fields, while for CC simulations, results closer to the measured values were determined. Deviations in MC simulations were up to 2.69% for 6 MV and 2.19% for 18 MV at small (5 x 5 cm²) and large (40 x 40 cm²) FSs, respectively. For wedged fields, CC simulations showed deviations of 2.45% for 18 MV at 15 x 15 cm². Although these deviations slightly exceeded the ±2% tolerance recommended by AAPM TG 198, they are minor and do not significantly impact the overall accuracy of radiotherapy planning or treatment quality (Duchaine *et al*., 2022).

Reference dosimetry, carried out in accordance with the IAEA TRS-398 protocol, confirmed accurate calibration of Linacs, with doses closely matching expected values and deviations within ±1%. The SSD technique demonstrated a maximum deviation of 0.77% from the expected 1 Gy per 100 MU dose at dmax for a 10 x 10 cm² field at 100 SSD, adhering to calibration standards. Calibration for various photon energies consistently yielded doses above

1 Gy/MU, validating the Linac systems' accuracy. For wedge fields, doses at d_{max} were less than 0.28 Gy/MU, indicating proper adjustments for field configurations.

The evaluation of CT scans using the Catphan phantom revealed that Monaco TPS RED values were lower than expected in low HU regions, attributed to the phantom's limitations in density correction, but they were still within acceptable limits. Conversely, despite also not being ideal for homogeneity corrections, RED values from the Shane phantom closely matched those from the Monaco TPS. This finding suggests that the Monaco TPS can reliably convert CT data into RED values even with suboptimal phantoms. Gamma analysis with a 3%/3 mm criterion confirmed the clinical acceptability of the Monaco TPS for dose calculations and treatment planning despite the limitations of the Catphan phantom.

The IAEA audit methodology for IMRT/VMAT dosimetry of head and neck cases demonstrated that calculated and measured doses were within acceptable tolerances of 7% for the spinal cord and 5% for the PTV. A study on dose delivery accuracy in prostate cancer treatment using 3D-CRT and VMAT confirmed that both techniques-maintained dose accuracy within ±5% of the planned dose. These results affirm the efficacy and safety of both treatment methods in delivering precise radiation doses while minimising side effects.

PSQA using the PTW Octavius 4D phantom, following the TG 218 protocol, achieved a ≥95% passing criterion with 3 mm DTA, 3% DD and 5% dose suppression. All plans across different energies met these criteria, validating the PSQA process as effective in ensuring accurate and safe radiation treatment. Additionally, optimization of MLC leaf transmission factors consistently produced values below 0.5%, aligning with prior studies (Schneider *et al*., 2023;Boyer *et al*., 2001b) and meeting AAPM guidelines. DLG values for various photon energies were accurately determined using ionisation chamber readings and linear fitting techniques, contributing to precise dose modelling in TPS.

In conclusion, this study provides rigorous validation of the Monaco TPS for clinical implementation. The system demonstrates high accuracy in dose calculations for both open and wedged fields, particularly for standard and large field sizes. While minor discrepancies persist in small fields, these findings highlight the need for further refinement to enhance dosimetric accuracy in complex clinical scenarios.

6. References

Abuhaimed, A. & Martin, C. J., 2023. Assessment of organ and size-specific effective doses from cone beam CT (CBCT) in image-guided radiotherapy (IGRT) based on body mass index (BMI). *Radiation Physics and Chemistry,* Volume 208, p. 110889.

Afrin, K. T. & Ahmad, S., 2020. 3D conformal, IMRT and VMAT for the treatment of head and neck cancer: a brief literature review. Journal of Radiotherapy in Practice. *Journal of Radiotherapy in Practice,* 21(2), pp. 259-262.

Agrawal, A., Hadi, R., Rath, S., Bharati, A., Rastogi, M., Khurana, R., Sahni, K., Sapru, S., Gandhi, A. K., Srivastava, A. K., & Mishra, S. P., 2020. Dosimetric comparison of 3-dimensional conformal radiotherapy (3D-CRT) and volumetric-modulated arc therapy (VMAT) in locally advanced cervical cancer. *Journal of Radiotherapy in Practice*, *21*(1), pp. 60–67.

Ahnesjö, A., 1989. Collapsed cone convolution of radiant energy for photon dose calculation in heterogeneous media. *Medical Physics,* 16(4), pp. 577-592.

Alfitra, L. S., Suwandi, N. & Arif, I., 2024. IMRT Planning Using 5, 7 and 9 Radiation Field Directions for Nasopharyngeal Cancer Cases. *Journal of Physics. Conference Series,* 2734(1), p. 012001.

Ali, J., Sohail, M., Samad, A., Ahmad, I., Soomro, H., Biradar, G., Naz, I., & Tariq, I., 2023. Comparison of Percentage Depth Doses with the Published Data for Co-60 Radiotherapy Machine at a Regional Cancer Hospital. *Journal of Physics and Its Applications*, *6*(1), pp. 24-30.

AL-Sa'd, M., Graham, J. & Liney, G. P., 2013. A software tool for 3D dose verification and analysis. *Journal of Physics Conference Series*, 444, 012087. https://doi.org/10.1088/1742-6596/444/1/012087

Anetai, Y., Sumida, I., Kumazaki, Y., Kito, S., Kurooka, M., Ueda, Y., Otani, Y., Narita, Y., Kawamorita, R., Akita, K., Kato, T., & Nakamura, M. (2022). Assessment of using a gamma index analysis for patient-specific quality assurance in Japan. *Journal of Applied Clinical Medical Physics*, *23*(10). https://doi.org/10.1002/acm2.13745

Antunes, P. C. G., De Tarso Dalledone Siqueira, P., Shorto, J. M. B. & Yoriyaz, H., 2023. Heterogeneous physical phantom for I-125 dose measurements and dose-to-medium determination. Brachytherapy. 23(1), p. 73–84.

Asgari, A., Ashoor, M., Sohrabpour, M., Shokrani, P., & Rezaei, A., 2015. Evaluation of various energy windows at different radionuclides for scatter and attenuation correction in nuclear medicine. *Annals of Nuclear Medicine*, *29*(4), pp. 375–383.

Bayat, F., Eldib, M. E., & Altunbas, C., 2022. Megavoltage cross-scatter rejection and correction using 2D antiscatter grids in kilovoltage CBCT imaging. *Medical Imaging 2018: Physics of Medical Imaging*, 48. https://doi.org/10.1117/12.2611202

Bencheikh, M., Didi, A., Maghnouj, A., Tajmouati, J., Benkhouya, Y., & Ouahdani, S. E., 2018. Empirical Law to Evaluate the Skin Dose with Photon Beam Energy and Irradiation Field Size. *Moscow University Physics Bulletin*, *73*(6), 683–686.

Benedict, S.H., Yenice, K.M., Followill, D., Galvin, J.M., Hinson, W., Kavanagh, B., Keall, P., Lovelock, M., Meeks, S., Papiez, L., Purdie, T., Sadagopan, R., Schell, M.C., Salter, B., Schlesinger, D.J., Shiu, A.S., Solberg, T., Song, D.Y., Stieber, V., Timmerman, R., Tomé, W.A., Verellen, D., Wang, L. & Yin, F.F., 2010. Report No. 101 - Stereotactic body radiation therapy: The report of AAPM Task Group 101. *Medical Physics*, 37, pp.4078–4101.

Beyzadeoglu, M., Ozyigit, G. & Ebruli, C., 2010. *Basic radiation oncology.* 1st ed. Berlin: Springer.

Boyer, A., Biggs, P., Galvin, J., Klein, E., LoSasso, T., Low, D., Mah, K., & Yu, C., 2001. *Basic* Brock, K. K. et al., 2017. Use of image registration and fusion algorithms and techniques in radiotherapy: Report of the AAPM Radiation Therapy Committee Task Group No. 132. *Medical Physics,* 44(7), pp. 43-76.

Brooks, F. M. D., Glenn, M. C., Hernandez, V., Saez, J., Mehrens, H., Pollard-Larkin, J. M., Howell, R. M., Peterson, C. B., Nelson, C. L., Clark, C. H., & Kry, S. F., 2024. A radiotherapy community data-driven approach to determine which complexity metrics best predict the impact of atypical TPS beam modeling on clinical dose calculation accuracy. *Journal of Applied Clinical Medical Physics*, *25*(5). https://doi.org/10.1002/acm2.14318

Chandrasekaran, M., 2012. [Online] Available at: https://livrepository.liverpool.ac.uk/9373/4/ChandrasekaranMek_Sept2012_9373.pdf [Accessed September 2012].

Clark, C., Gershkevitsh, E., Lechner, W., Van Dyk, J., Venencia, D., Bokulic, T., Kazantsev, P. and Wesolowska, P., 2019. *National "End-to-End" Audit Programme for dose delivery using intensity-modulated radiation therapy through on-site visits to radiation therapy institutions*. Technical report, International Atomic Energy Agency, Vienna, Austria.

Clements, M., Schupp, N., Tattersall, M., Brown, A., & Larson, R., 2018. Monaco treatment planning system tools and optimization processes. *Medical Dosimetry*, *43*(2), pp. 106-117.

Conway, J., Bragg, C., Cherry, P. & A., D., 1998. *Practical Radiotherarapy Physics and equipment. Treatment planning and computer systems.* 2nd ed. London: Greenwich Medical Media.

Da Silva, F. S. G., De Souza Castro, A. L. & Fonseca, T. C. F., 2022. Computer simulations applied to Small-Field dosimetry in radiotherapy. *Brazilian Journal of Radiation Sciences,* 10(3B). https://doi.org/10.15392/2319-0612.2022.1778

Danckaert, W., Ost, P. & De Wagter, C., 2023b. Accuracy and reliability of a commercial treatment planning system in nontarget regions in modern prostate radiotherapy. *Journal of Applied Clinical Medical Physics,* 24(8). https://doi.org/10.1002/acm2.14003

Das, I. J., Cheng, C., Watts, R. J., Ahnesjö, A., Gibbons, J., Li, X. A., Lowenstein, J., Mitra, R. K., Simon, W. E., & Zhu, T. C., 2008b. Accelerator beam data commissioning equipment and

procedures: Report of the TG-106 of the Therapy Physics Committee of the AAPM. *Medical Physics*, *35*(9), pp. 4186-4215.

Das, S., Kharade, V., Pandey, V., Kv, A., Pasricha, R. K., & Gupta, M. (2022). Gamma Index Analysis as a Patient-Specific Quality Assurance Tool for High-Precision Radiotherapy: A Clinical Perspective of Single Institute Experience. *Cureus*. https://doi.org/10.7759/cureus.30885

De Martino, F., Clemente, S., Graeff, C., Palma, G., & Cella, L. (2021). Dose Calculation Algorithms for External Radiation therapy: An Overview for Practitioners. *Applied Sciences*, *11*(15), 6806. https://doi.org/10.3390/app11156806

Ding, G. X. & Das, I. J., 2023. On the field size definition and field output factors in small field dosimetry. *Medical Physics on CD-ROM/Medical Physics,* 50(6), p. 3833–3841.

Dogan, N., Mihaylov, I. & Studenski, M., 2017. Commissioning and Quality. In: M. Ben, ed. *Clinical 3D Dosimetry in Modern Radiation Therapy.* Amsterdam: Taylor & Francis Group, p. 405.

Duchaine, J., Wahl, M., Markel, D. & Bouchard, H., 2022. A probabilistic approach for determining Monte Carlo beam source parameters: II. Impact of beam modeling uncertainties on dosimetric functions and treatment plans. *Physics in Medicine and Biology,* 67(4), p. 045006.

Van Dyk, J., Rosenwald, J.-C., Fraass, B., Cramb, J., Ionescu-Farca, F. & Sharpe, M. B., 2006. *IAEA Technical Reports Series No. 430: Commissioning and Quality Assurance of Computerized Planning Systems for Radiation Treatment of Cancer.* Medical Physics. DOI: https://doi.org/10.1118/1.2167371.

Van Esch, A., Tillikainen, L., Pyykkonen, J., Tenhunen, M., Helminen, H., Siljamäki, S., Alakuijala, J., Paiusco, M., Iori, M., & Huyskens, D. P., 2006. Testing of the analytical anisotropic algorithm for photon dose calculation. *Medical Physics*, *33*(11), pp. 4130-4148.

Ese, Z., Erni, D., & Zylka, W., 2023. Accuracy of CT numbers and electron density calibration for mixtures of materials with low and high-atomic numbers. *Current Directions in Biomedical Engineering*, *9*(1), pp. 411-414.

Ezzell, G. A., Burmeister, J. W., Dogan, N., LoSasso, T. J., Mechalakos, J. G., Mihailidis, D., Molineu, A., Palta, J. R., Ramsey, C. R., Salter, B. J., Shi, J., Xia, P., Yue, N. J., & Xiao, Y., 2009. IMRT commissioning: Multiple institution planning and dosimetry comparisons, a report from AAPM Task Group 119. *Medical Physics*, *36*(11), pp. 5359-5373.

Fattori, G., Hrbacek, J., Regele, H., Bula, C., Mayor, A., Danuser, S., Oxley, D. C., Rechsteiner, U., Grossmann, M., Via, R., Böhlen, T. T., Bolsi, A., Walser, M., Togno, M., Colvill, E., Lempen, D., Weber, D. C., Lomax, A. J., & Safai, S. (2022b). Commissioning and quality assurance of a novel solution for respiratory-gated PBS proton therapy based on optical tracking of surface markers. *Zeitschrift Für Medizinische Physik*, *32*(1), pp. 52-62.

Fontenot, J. D., Alkhatib, H., Garrett, J. A., Jensen, A. R., McCullough, S. P., Olch, A. J., Parker, B. C., Yang, C. J., & Fairobent, L. A., 2014. AAPM Medical Physics Practice Guideline 2. a: Commissioning and quality assurance of X-ray-based image-guided radiotherapy systems. *Journal of Applied Clinical Medical Physics*, *15*(1), pp. 3-13.

Fraass, B., Doppke, K., Hunt, M., Kutcher, G., Starkschall, G., Stern, R., & Jake, V. D. (1998). American Association of Physicists in Medicine Radiation Therapy Committee Task Group 53: Quality assurance for clinical radiotherapy treatment planning. *Deep Blue (University of Michigan)*. http://hdl.handle.net/2027.42/134846

Fu, J., Bai, J., Liu, Y. & Ni, C., 2020. Fast Monte Carlo dose calculation based on deep learning. *2021 14th International Congress on Image and Signal Processing, BioMedical Engineering and Informatics (CISP-BMEI)*, pp. 721-726. https://doi.org/10.1109/cisp-bmei51763.2020.9263502

Gallo, J. J., Kaufman, I., Powell, R., Pandya, S., Somnay, A., Bossenberger, T., Ramirez, E., Reynolds, R., Solberg, T., & Burmeister, J., 2015. Single-fraction spine SBRT end-to-end testing on TomoTherapy, Vero, TrueBeam, and CyberKnife treatment platforms using a novel anthropomorphic phantom. *Journal of Applied Clinical Medical Physics*, *16*(1), pp. 170-182.

Gardner, S., Kim, J. & Chetty, I. J., 2019. Modern Radiation therapy planning and delivery.. *Hematology-oncology Clinics of North America,* 33(6), pp. 947-962.

Garibaldi, C., Jereczek-Fossa, B. A., Marvaso, G., Dicuonzo, S., Rojas, D. P., Cattani, F., Starzyńska, A., Ciardo, D., Surgo, A., Leonardi, M. C., & Ricotti, R., 2017. Recent advances in radiation oncology. *Ecancermedicalscience*, *11*. https://doi.org/10.3332/ecancer.2017.785

Geurts, M. W., Jacqmin, D. J., Jones, L. E., Kry, S. F., Mihailidis, D. N., Ohrt, J. D., Ritter, T., Smilowitz, J. B., & Wingreen, N. E. (2022). AAPM MEDICAL PHYSICS PRACTICE GUIDELINE 5.b: Commissioning and QA of treatment planning dose calculations—Megavoltage photon and electron beams. *Journal of Applied Clinical Medical Physics*, *23*(9). https://doi.org/10.1002/acm2.1364

Giada, S., Andrea, B., Matteo, O., Daniele, L., Domenico, F., Adriana, B., Valentina, B., Valeria, T., Roberto, S., & Mauro, I. (2023). TUNING AND VALIDATION OF THE NEW RADCALC 3D MONTE CARLO BASED PRE-TREATMENT PLAN VERIFICATION TOOL. *Journal of Mechanics in Medicine and Biology*, *23*(06). https://doi.org/10.1142/s021951942340047x

Gondré, M., Marsolat, F., Bourhis, J., Bochud, F., & Moeckli, R. (2021). Validation of Monte Carlo dose calculation algorithm for CyberKnife multileaf collimator. *Journal of Applied Clinical Medical Physics*, *23*(2). https://doi.org/10.1002/acm2.13481

Goodall, S., Rowshanfarzad, P. & Ebert, M., 2023. Correction factors for commissioning and patient specific quality assurance of stereotactic fields in a Monte Carlo based treatment planning system. *Physical and Engineering Sciences in Medicine,* 46(2), pp. 735-745.

Goodall, S., Rowshanfarzad, P. & Ebert, M. A., 2023. Correction factors for commissioning and patient specific quality assurance of stereotactic fields in a Monte Carlo based treatment planning system. *Physical and Engineering Sciences in Medicine/Physical and Engineering Sciences in Medicine.,* 46(2), pp. 735-745.

Gulliksrud, K., Stokke, C. & Martinsen , A. C. T., 2014. How to measure CT image quality: Variations in CT-numbers, uniformity and low contrast resolution for a CT quality assurance phantom. *Physica Medica,* 30(4), pp. 521-526.

Hanley, J., Dresser, S., Simon, W., Flynn, R., Klein, E. E., Letourneau, D., Liu, C., Yin, F., Arjomandy, B., Ma, L., Aguirre, F., Jones, J., Bayouth, J., & Holmes, T., 2021. AAPM Task Group 198 Report: An implementation guide for TG 142 quality assurance of medical accelerators. *Medical Physics*, *48*(10). https://doi.org/10.1002/mp.14992

Hrbacek, J., Depuydt, T., Nulens, A., Swinnen, A., & Van Den Heuvel, F. (2007). Quantitative evaluation of a beam-matching procedure using one-dimensional gamma analysis. *Medical Physics*, *34*(7), 2917–2927. https://doi.org/10.1118/1.2745239

Huq, M. S., 2010. *Implementing 3D Conformal Radiotherapy and IMRT in Clinical Practice: Recommendations of IAEA-TECDOC-1588.,* Vienna: International Atomic Energy Agency IAEA.

Hussain, A. & Muhammad, W., 2017. *"Treatment Planning in Radiation Therapy," in An Introduction to Medical Physics.* M. Maqbool: Ed. Springer International Publishing.

Hussein, M., Angerud, A., Saez, J., Bogaert, E., Lemire, M., Barry, M., Patallo, I. S., Shipley, D., Clark, C. H., & Hernandez, V., 2023. Improving the modeling of the Agility multi-leaf collimator. *arXiv (Cornell University)*. https://doi.org/10.48550/arxiv.2305.11787

Hussein, M., Clark, C. & Nisbet, A., 2017. Challenges in the calculation of the gamma index in radiotherapy – Towards good practice. *Physica Medica,* Volume 36, pp. 1-11.

Huszank, R., Szilágyi, E., Szoboszlai, Z. & Szikszai, Z., 2019. Investigation of chemical changes in PMMA induced by 1.6 MeV He+ irradiation by ion beam analytical methods (RBS-ERDA) and infrared spectroscopy (ATR-FTIR). *Nuclear Instruments and Methods in Physics Research Section B Beam Interactions With Materials and Atoms,* Volume 450, p. 364–368.

IAEA, 2001. *Absorbed dose determination in external beam radiotherapy: An international code of practice for dosimetry based on standards of absorbed dose to water. Technical Reports Series No. 398.,* Vienna, Austria: Technical report, International Atomic Energy Agency.

IAEA-TECDOC-1583, 2008. *Commissioning of radiotherapy treatment planning system: testing for typical external beam treatmet technique,* Vienna: IAEA.

Jeong, H., Han, Y., Kum, O. K. C. & Park, J., 2011. DEVELOPMENT AND EVALUATION OF A PHANTOM FOR MULTI-PURPOSE DOSIMETRY IN INTENSITY-MODULATED RADIATION THERAPY. *Nuclear Engineering and Technology,* 43(4), p. 399–404.

Kang, J., Lafata, K., Kim, E., Yao, C., Lin, F., Rattay, T., Nori, H., Katsoulakis, E., & Lee, C. I., 2024. Artificial intelligence across oncology specialties: current applications and emerging tools. *BMJ Oncology*, *3*(1), e000134. https://doi.org/10.1136/bmjonc-2023-000134

Kavousi, N., Nedaie, H. A., Gholami, S., Esfahani, M., & Geraily, G., 2019. Evaluation of Dose Calculation Algorithms Accuracy for Eclipse, PCRT3D, and Monaco Treatment Planning Systems Using IAEA TPS commissioning tests in a Heterogeneous Phantom. *DOAJ (DOAJ: Directory of Open Access Journals)*. https://doi.org/10.22038/ijmp.2018.33695.1416

Kazantsev, P., Lechner, W., Gershkevitsh, E., Clark, C. H., Venencia, D., Van Dyk, J., Wesolowska, P., Hernandez, V., Jornet, N., Tomsej, M., Bokulic, T., & Izewska, J., 2019. IAEA methodology

for on-site end-to-end IMRT/VMAT audits: an international pilot study. *Acta Oncologica*, *59*(2), pp. 141–148.

Keall, P. J., Siebers, J. V., Jeraj, R. & Moha, R., 2000. The effect of dose calculation uncertainty on the evaluation of radiotherapy plans. *Medical Physics,* 27(3), p. 478–484.

Khan, F. M., 2014. *The Physics of Radiation Therapy.* 5th ed. Philadelphia, Lippincott Williams & Wilkins.

Kim, D. W., Park, K., Kim, H. & Kim, J. S., 2020. Progress in Medical Physics. *History of the Photon Beam Dose Calculation Algorithm in Radiation Treatment Planning Systems. Progress in Medical Physics, 31(3), 54–62.,* 32(3), pp. 54-62.

Kim, J., Han, J. S., Hsia, A. T., Li, S., Xu, Z., & Ryu, S., 2018. Relationship between dosimetric leaf gap and dose calculation errors for high definition multi-leaf collimators in radiotherapy. *Physics and Imaging in Radiation Oncology*, *5*, pp. 31-36. https://doi.org/10.1016/j.phro.2018.01.003.

Klein, E. E., Hanley, J., Bayouth, J., Yin, F., Simon, W., Dresser, S., Serago, C., Aguirre, F., Ma, L., Arjomandy, B., Liu, C., Sandin, C., & Holmes, T., 2009. Task Group 142 report: Quality assurance of medical accelerators. *Medical Physics*, *36*(9 Part 1), pp. 4197-4212.

Krisnanjani, N. A., Budi, N. W. S., Setiawati, N. E., Purwaningsih, N. S., Juwita, N. I., & Furaida, N. F. (2024). Dose distribution: Three-Dimensional conformal radiation therapy (3DCRT) with 2 and 4 directions in the treatment planning system for cervical cancer cases. *International Journal of Scientific Research in Science and Technology*, *11*(4), pp. 30–38.

Liu, L., Shen, L., Yang, Y., Schüler, E., Zhao, W., Wetzstein, G., & Xing, L. (2023). Modeling linear accelerator (Linac) beam data by implicit neural representation learning for commissioning and quality assurance applications. *Medical Physics*, *50*(5), pp. 3137-3147.

LoSasso, T., Chui, C. & Ling, C. C., 1998. Physical and dosimetric aspects of a multileaf collimation system used in the dynamic mode for implementing intensity modulated radiotherapy. *Medical Physics,* 25(10), p. 1919-1927.

Miften, M., Olch, A., Mihailidis, D., Moran, J., Pawlicki, T., Molineu, A., Li, H., Wijesooriya, K., Shi, J., Xia, P., Papanikolaou, N., & Low, D. A. (2018). Tolerance limits and methodologies for IMRT measurement-based verification QA: Recommendations of AAPM Task Group No. 218. *Medical Physics*, *45*(4). https://doi.org/10.1002/mp.12810

Mohindra, P., Sawant, A., Griffin, R. J., Lamichhane, N., Vlashi, E., Xu-Welliver, M., Dominello, M., Joiner, M. C., & Burmeister, J. (2019). Three discipline collaborative radiation therapy (3 DCRT) special debate: I would treat all early-stage NSCLC patients with SBRT. *Journal of Applied Clinical Medical Physics*, *20*(3), pp. 7-13.

Mukwada, G., Hirst, A., Rowshanfarzad, P. & Ebert, M. A., 2024. Development of a 3D printed phantom for commissioning and quality assurance of multiple brain targets stereotactic radiosurgery. *Physical and Engineering Sciences in Medicine,* 47(2), p. 455–463.

Narayanasamy, G., Saenz, D., Cruz, W., Ha, C. S., Papanikolaou, N., & Stathakis, S. (2016). Commissioning an Elekta Versa HD linear accelerator. *Journal of Applied Clinical Medical Physics*, *17*(1), pp. 179-191.

Nguyen, V. N., Wang, B. & Shi, C., 2016. A Sensitivity Dosimetry Study of the Setup Uncertainties during Machine Commissioning and Annual QA. *International Journal of Medical Physics, Clinical Engineering and Radiation Oncology,* 5(4), pp. 329-347.

Oh, K., Sengupta, B., Olanrewaju, A., Zhang, L., Nair, S. S., Mani, T., Palanisamy, M., KanduKuri, U. S., Netherton, T. J., Cardenas, C. E., Court, L. E., & Ford, E. C., 2023. Commissioning and dosimetric validation of a novel compensator-based Co-60 IMRT system for evaluating suitability to automated treatment planning. *Medical Physics*, *50*(7), pp. 4466-4479.

Portela, C. F. T. & Mourão, A. P., 2023. Dose profile evaluation for two fields of a 6 MV LINAC X-ray beam. *Seven Editora.*

Poudel, S., Kulshreshtha, A., Zakaria, G. & Hartmann, G., 2023. Monte Carlo calculations of dose profiles with the 'given profile" method and comparison with measurements. *Radiation Physics and Chemistry,* Volume 213, p. 111236.

Raina, P., Singh, R. & Barthakur, M., 2022. Intensity Modulated Radiation Therapy Plan (IMRT) verification using indigenous heterogeneous phantom. *In IntechOpen eBooks.*

Reitz, B., Gayou, O., Parda, D. S., & Miften, M., 2008. Monitoring tumor motion with on-line mega-voltage cone-beam computed tomography imaging in acinemode. *Physics in Medicine and Biology*, *53*(4),pp. 823–836.

Roy, A., Kumar, S. & Kuma, A., 2023. Formulation of tissue maximum ratio for high energy photons using a medical electron linear accelerator. *Nuclear and Particle Physics Proceedings,* Volume 152-155, pp. 339-340.

Saini, A., Singh, A., Pandey, V. & Kumar, P., 2022. Dosimetric comparison of photon beams using CIRS Thorax Phantom to evaluate Monaco radiotherapy treatment planning system. *ECS Transactions,* 107(1), p. 5729–5735.

Samei, E., Bakalyar, D., Boedeker, K. L., Brady, S., Fan, J., Leng, S., Myers, K. J., Popescu, L. M., Giraldo, J. C. R., Ranallo, F., Solomon, J., Vaishnav, J., & Wang, J., 2019. Performance evaluation of computed tomography systems: Summary of AAPM Task Group 233. *Medical Physics*, *46*(11). https://doi.org/10.1002/mp.13763

Saez, J., Bar-Deroma, R., Bogaert, E., Cayez, R., Chow, T., Clark, C.H., Esposito, M., Feygelman, V., Monti, A.F., Garcia-Miguel, J., Gershkevitsh, E., Goossens, J., Herrero, C., Hussein, M., Khamphan, C., Kierkels, R.G.J., Lechner, W., Lemire, M., Nevelsky, A., Nguyen, D., Paganini, L., Pasler, M., Pérez Azorín, J.F., Ramos Garcia, L.I., Russo, S., Shakeshaft, J., Vieillevigne, L. & Hernandez, V., 2023. Universal evaluation of MLC models in treatment planning systems based on a common set of dynamic tests. *Radiotherapy and Oncology*, 186, pp.109775. https://doi.org/10.1016/j.radonc.2023.109775.

Saini, A., Pandey, V. P., Singh, A., & Kumar, P., 2022. Dosimetric comparison of photon beams using CIRS Thorax Phantom to evaluate Monaco radiotherapy treatment planning system. *ECS Transactions*, *107*(1),pp. 5729–5735.

Santos, W. S., Xavier, D. A., Santos, C. J., Neves, L. P., Belinato, W., Valença, J. V., & Perini, A. P., 2023. Dosimetric evaluation in brachytherapy and teletherapy for prostate cancer using Monte Carlo simulation and anatomically realistic virtual anthropomorphic phantom. *Radiation Physics and Chemistry*, *209*, 111000. https://doi.org/10.1016/j.radphyschem.2023.111000

Schneider, L., Thewes, M. & Eckl, F., 2023. Transmission probability filter optimization for Agility MLC in Monaco treatment planning system. *Journal of Applied Clinical Medical Physics,* 24(9).

Sharma, R., Sharma, S. & Avasthi, D. K., 2020b. Assessing the accuracy of treatment planning system based radiotherapy structure volumes. *Journal of Radiotherapy in Practice,* 21(1), pp. 31-35.

Sharma, S., Chander, S., Subramani, V., Kumar, P., Bhaskar, S., Pathy, S., Thulkar, S., Gopishankar, N., Sairem, M., Binjola, A., N, D., S, P., & Agarwal, P., 2017. IMRT AND VMAT COMMISSIONING FOR VERSA HD LINEAR ACCELERATOR USING AAPM TG-119. *International Journal of Advanced Research*, *5*(4), 352–362

Shin, H., Noh, Y., Kim, H., Kim, C., Sung, K., & Kim, D. W., 2024. Correction method for depth and field size dependence in Octavius 1000 SRS patient-specific QA. *Radiation Physics and Chemistry*, *223*, 111892. https://doi.org/10.1016/j.radphyschem.2024.111892

Slama, L., Mahmood, T. & Mckernan, B., 2023. Curvature correction factors for the independent verification of dose monitor units of electron treatment plans calculated in Eclipse. *Research Square (Research Square).*

Smilowitz, J. B., Das, I. J., Feygelman, V., Fraass, B. A., Kry, S. F., Marshall, I. R., Mihailidis, D. N., Ouhib, Z., Ritter, T., Snyder, M. G., & Fairobent, L., 2015. AAPM Medical Physics Practice Guideline 5.a.: Commissioning ad QA of Treatment Planning Dose Calculations — Megavoltage Photon and Electron beams. *Journal of Applied Clinical Medical Physics*, *16*(5), pp. 14–34

Spirou, S. V. & Chui, C. S., 1998. A gradient inverse planning algorithm with dose-volume constraints.. *Medical physics,* 25(3), pp. 321-333.

Stelljes, T. S., Harmeyer, A., Reuter, J., Looe, H. K., Chofor, N., Harder, D., & Poppe, B., 2015. Dosimetric characteristics of the novel 2D ionization chamber array OCTAVIUS Detector 1500. *Medical Physics*, *42*(4), p. 1528–1537

Suwanraksa, C., Bridhikitti, J., Liamsuwan, T. & Chaichulee, S., 2023. CBCT-to-CT Translation Using Registration-Based Generative Adversarial Networks in Patients with Head and Neck Cancer. *Cancers (Basel),* 15(7), pp. 2017.

Teixeira, P. C. F. & Prata, M. A., 2023. Dose Variation Profiles of Small Fields with a 10 MV Photon Beam. *International Journal of Oncology Research,* 6(1).https://doi.org/10.23937/2643-4563/1710052

Thrower, S., Farhat, M., Curl, B., Cifter, G., Shanker, M., Beckham, T., Ghia, A., Swanson, T., Wang, C., Brock, K., & Chung, C. (2023). LMAP-13 THE IMPACT OF RADIATION TREATMENT DOSE TO THE TUMOR AND NORMAL TISSUES USING POST-OPERATIVE MRI VS. MR-SIMULATION FOR RADIOTHERAPY PLANNING OF HIGH-GRADE GLIOMA. *Neuro-Oncology Advances*, *5*(Supplement_3), iii12. https://doi.org/10.1093/noajnl/vdad070.044

Tsai, P., Yang, Y., Wu, M., Chen, C., Yu, F., Simone, C. B., Choi, J. I., Tomé, W. A., & Lin, H. (2024). A comprehensive pre-clinical treatment quality assurance program using unique spot patterns for proton pencil beam scanning FLASH radiotherapy. *Journal of Applied Clinical Medical Physics*, *25*(8). https://doi.org/10.1002/acm2.14400

Van Herk, M., Remeijer, P., Rasch, C. R. N. & Lebesque, J. V., 2000. The probability of correct target dosage: dose-population histograms for deriving treatment margins in radiotherapy. *International Journal of Radiation Oncology Biology Physics,* 47(4), p. 1121–1135.

Venselaar, J., Mijnheer, H. & Welleweerd, B. J., 2001. Tolerances for the accuracy of photon beam dose calculations of treatment planning systems. *Radiother Oncol,* Volume 60, pp. 191-201.

Visbal, J. H. W. (2023). ON THE CORRECTION OF DOSE PROFILE DISCREPANCIES BY INTRODUCING AIR IN THE DERIVATION OF AN ELECTRON SPECTRUM. *Ingeniería Investigación Y Desarrollo*, *23*(1), 14–18. https://doi.org/10.19053/1900771x.v23.n1.2023.14751

Wijesooriya, K., Kim, T., Evans, J. & Chen, Q., 2017. Quality assurance of IGRT. *In: Principles and Practice of Image-Guided Radiation Therapy of Lung Cancer*. Boca Raton: CRC Press, pp.101–123. ISBN 9781498736732.

Xing, J., Locke, A., Hamilton, R., Stea, B., & Robbins, J., 2022. A dosimetric analysis of single fraction lattice radiotherapy as a boost for the palliative treatment of bulky head and neck tumors. *International Journal of Radiation Oncology*Biology*Physics*, *114*(3), e448. https://doi.org/10.1016/j.ijrobp.2022.07.1675

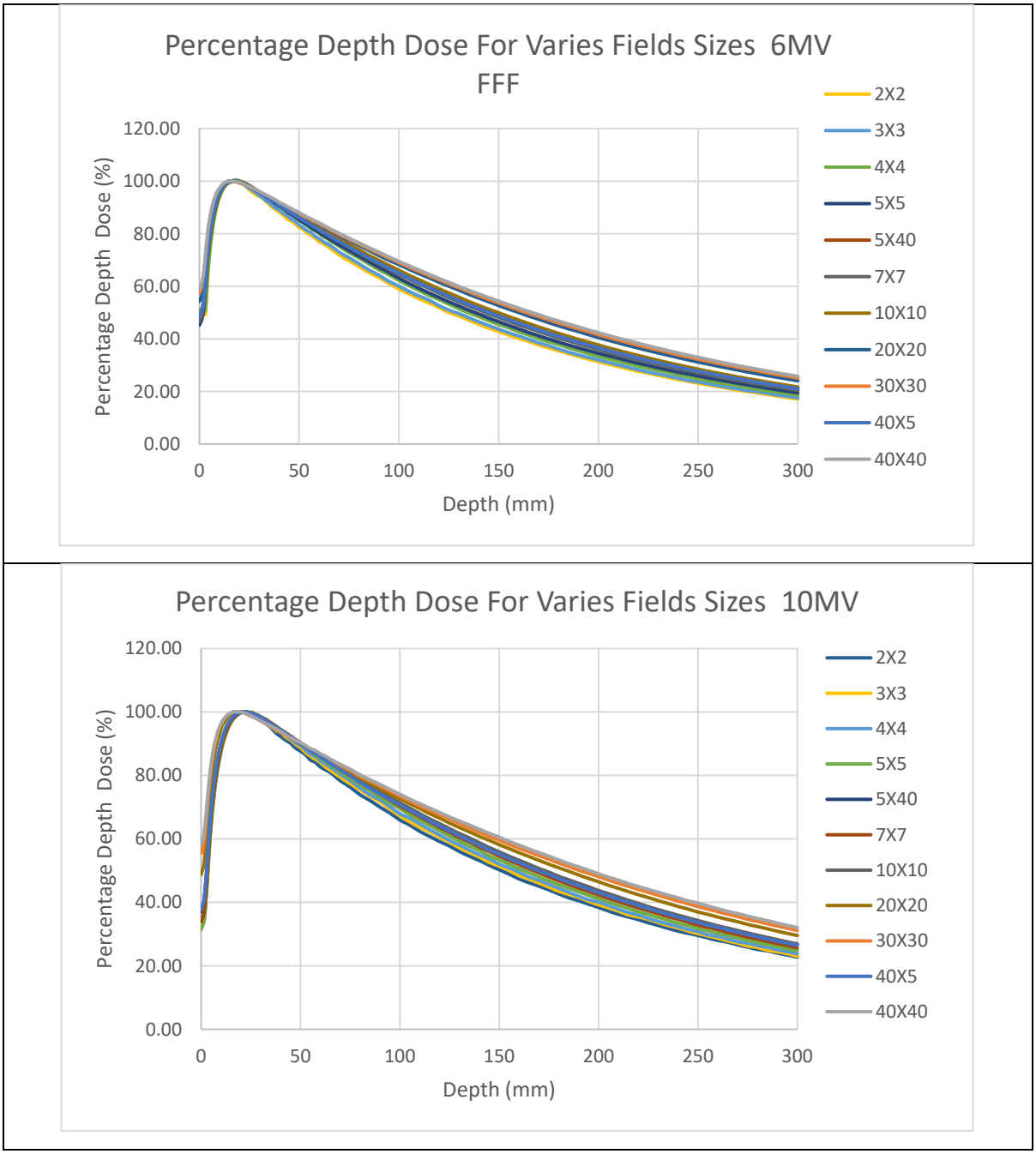
Zarb, F. & Rainford, L., 2014. Psychophysical evaluation of Catphan®600 CT image quality findings using human observers and software analysis. *Radiography,* 20(4), pp. 318-332.

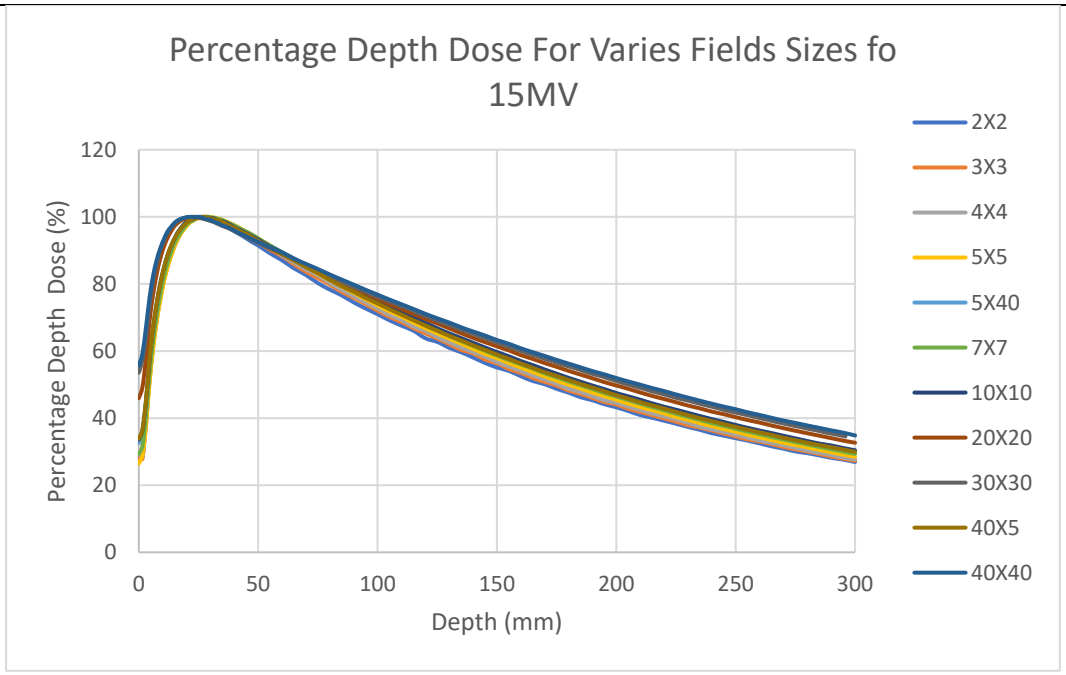
Zhao, J., Chen, Z., Wang, J., Xia, F., Peng, J., Hu, Y., Hu, W., & Zhang, Z., 2021. MV CBCT-Based Synthetic CT Generation using a deep learning method for rectal cancer adaptive radiotherapy. *Frontiers in Oncology*, *11*. https://doi.org/10.3389/fonc.2021.655325

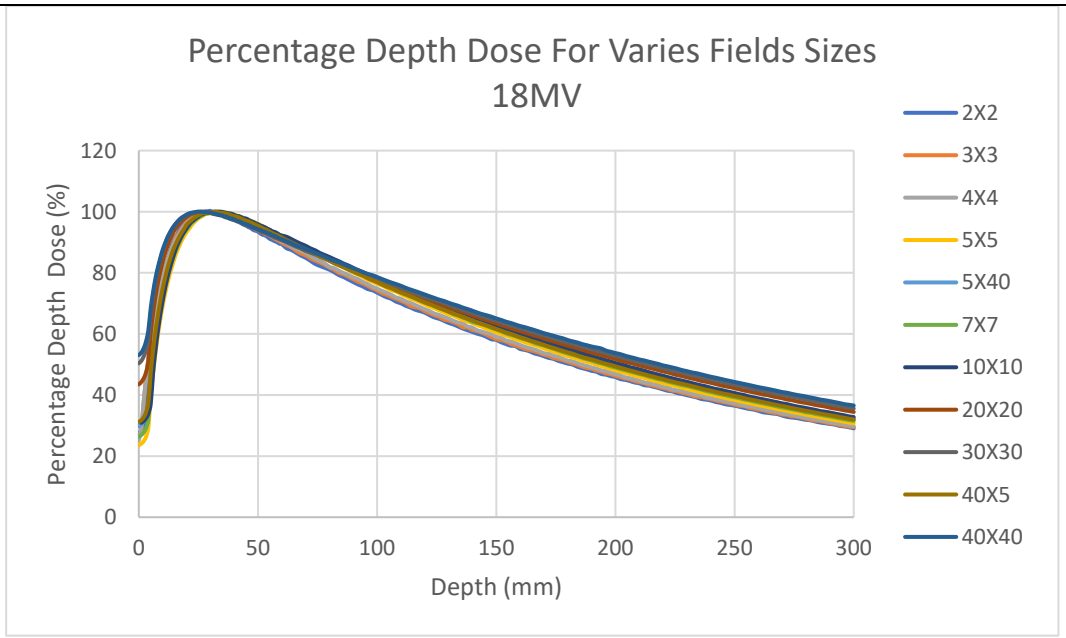
Zhao, W. & Xing, L., 2023. *Advances in treatment planning. In Principles and Practice of Image-Guided Abdominal Radiation Therapy.* 2 ed. Bristol, UK: IOP Publishing.

Zhou, P., Duan, A., Geng, M., Liu, Y., Li, J., Luo, J., & He, X. , 2022. The effect of minimum segment width of collimator on VMAT plan quality for rectal cancer using Monaco TPS. *Research Square (Research Square)*. https://doi.org/10.21203/rs.3.rs-1632761/v1

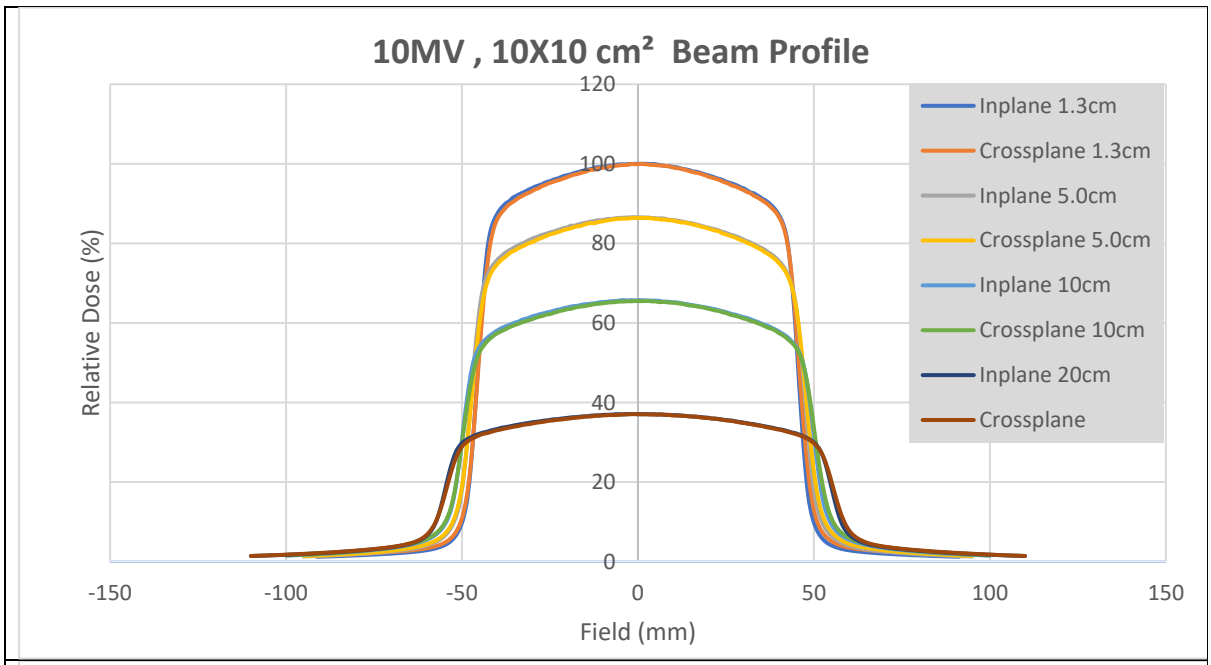
Appendix 1-Beam Data (PDDs)

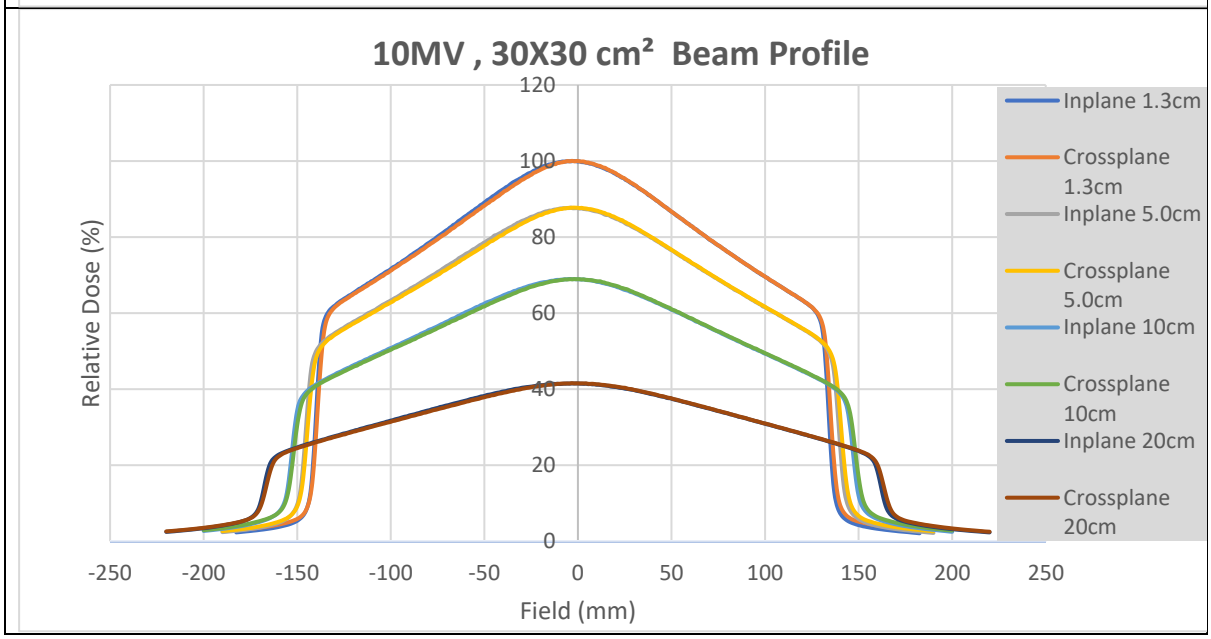


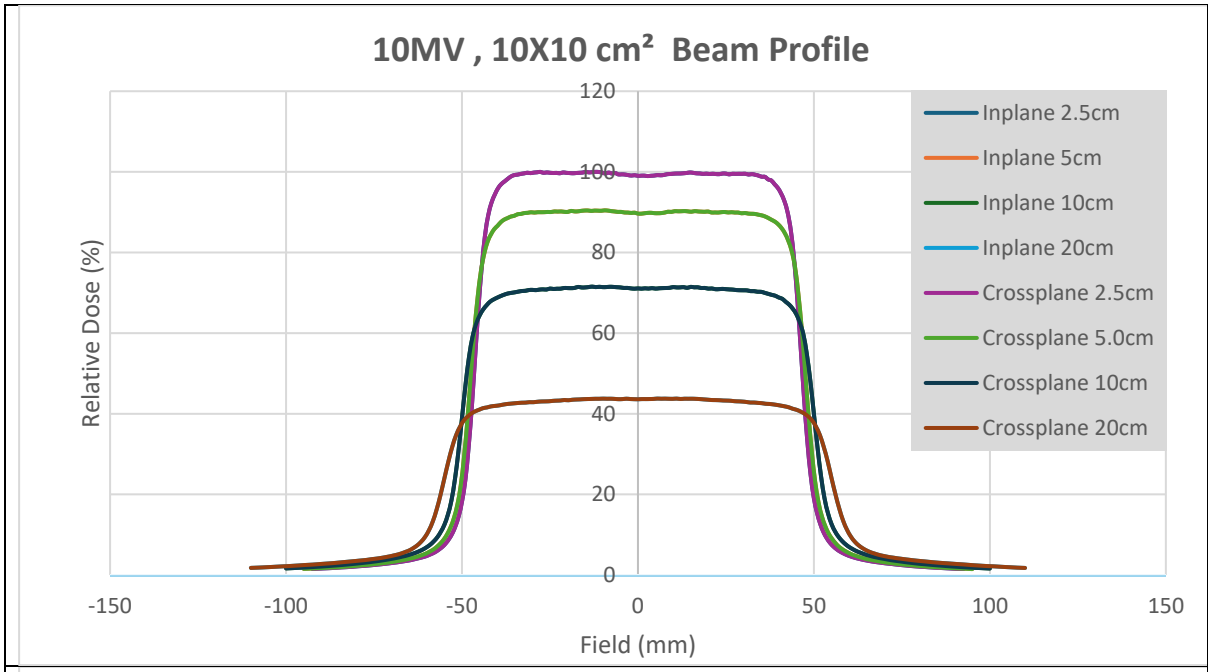

Percentage Depth Dose For Varies Fields Sizes fo 15MV
Percentage Depth Dose (%)
120
100
80
60
40
20
0
0
50
100
150
200
250
300
Depth (mm)
2X2
3X3
4X4
5X5
5X40
7X7
10X10
20X20
30X30
40X5
40X40

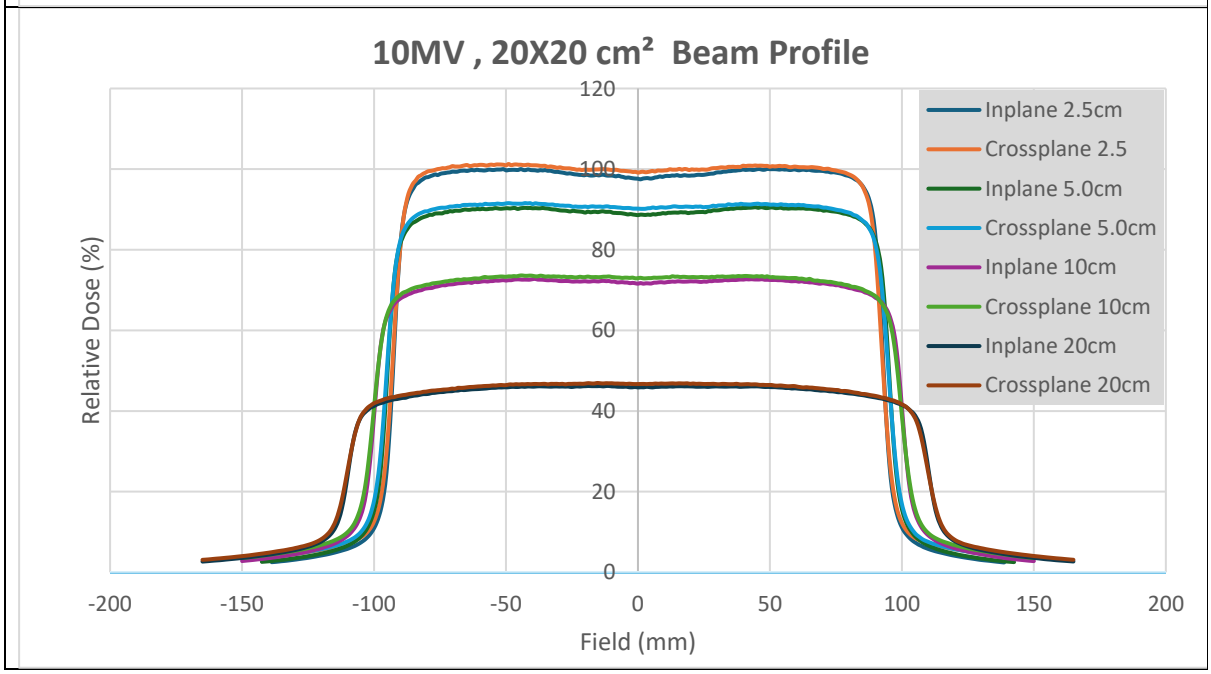

Percentage Depth Dose For Varies Fields Sizes 18MV
Percentage Depth Dose (%)
120
100
80
60
40
20
0
0
50
100
150
200
250
300
Depth (mm)
2X2
3X3
4X4
5X5
5X40
7X7
10X10
20X20
30X30
40X5
40X40

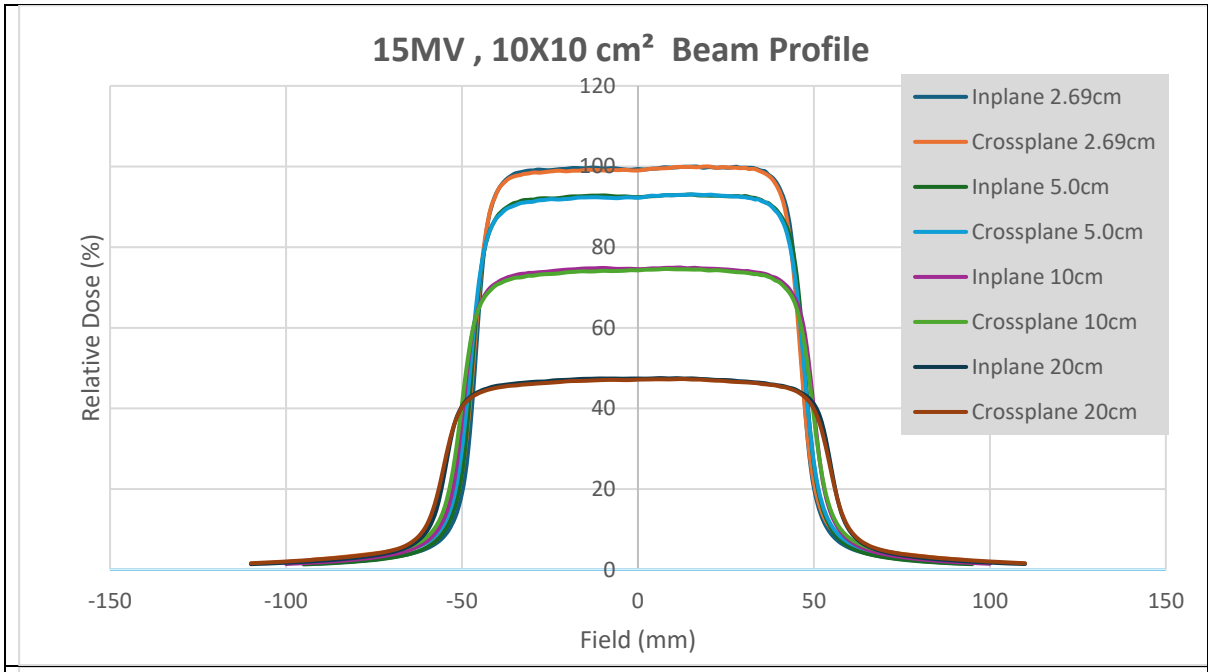
Appendix 2- Beam Data (Beam Profile)

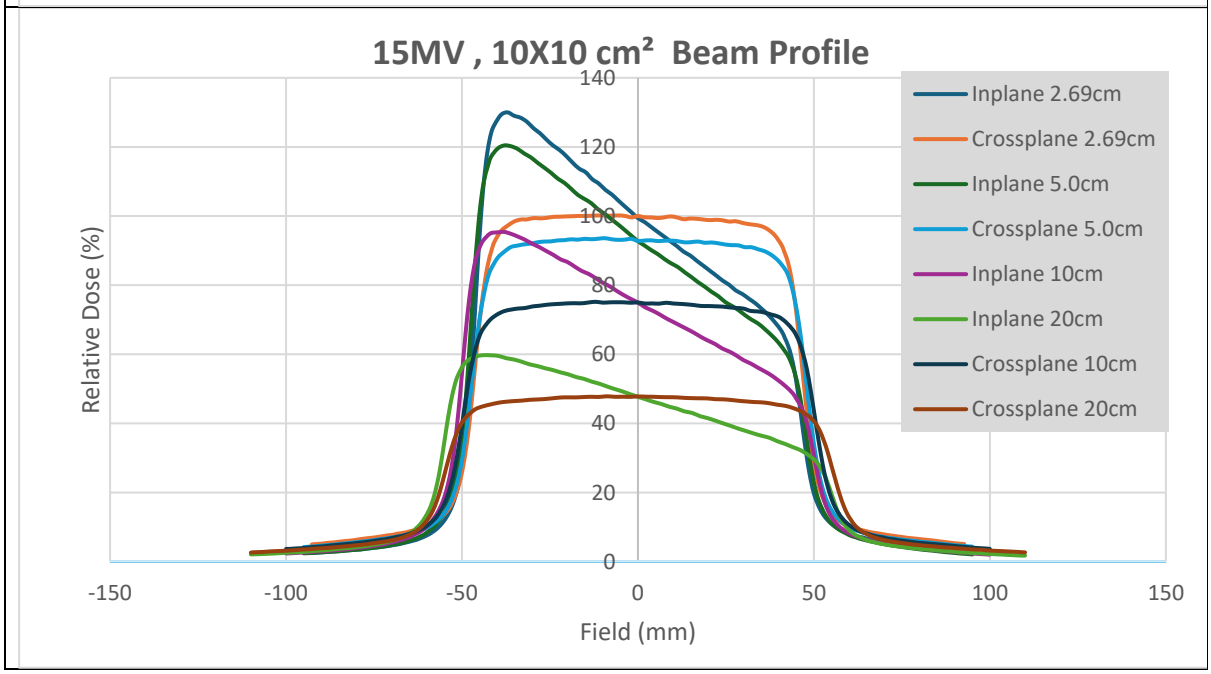


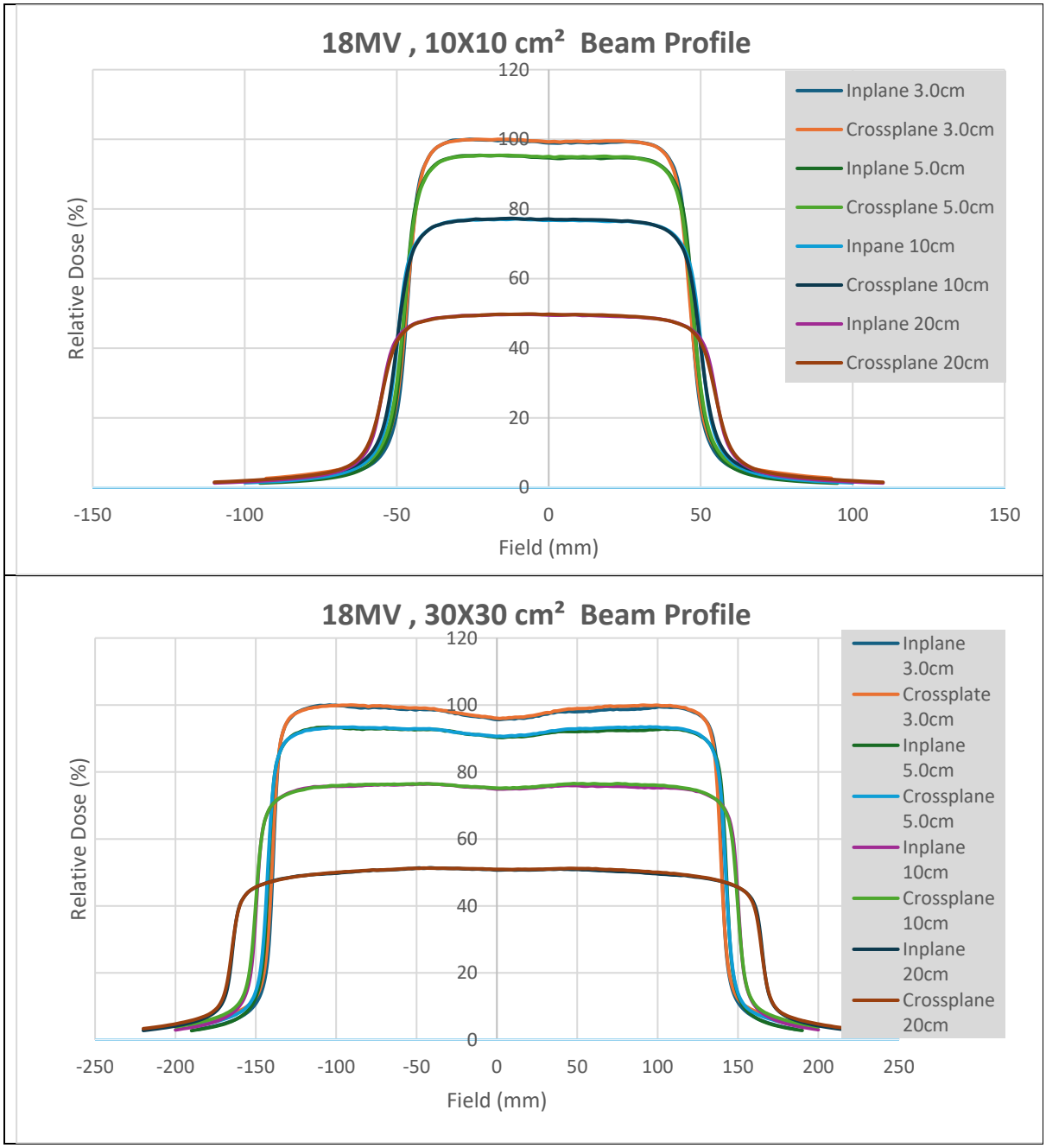



10MV , 10X10 cm² Beam Profile
Relative Dose (%)
120
100
80
60
40
20
0
-150
-100
-50
0
50
100
150
Field (mm)
Inplane 2.5cm
Inplane 5cm
Inplane 10cm
Inplane 20cm
Crossplane 2.5cm
Crossplane 5.0cm
Crossplane 10cm
Crossplane 20cm


10MV , 20X20 cm² Beam Profile
Relative Dose (%)
120
100
80
60
40
20
0
-200
-150
-100
-50
0
50
100
150
200
Field (mm)
Inplane 2.5cm
Crossplane 2.5
Inplane 5.0cm
Crossplane 5.0cm
Inplane 10cm
Crossplane 10cm
Inplane 20cm
Crossplane 20cm


15MV , 10X10 cm² Beam Profile
Relative Dose (%)
120
100
80
60
40
20
0
-150
-100
-50
0
50
100
150
Field (mm)
Inplane 2.69cm
Crossplane 2.69cm
Inplane 5.0cm
Crossplane 5.0cm
Inplane 10cm
Crossplane 10cm
Inplane 20cm
Crossplane 20cm


15MV , 10X10 cm² Beam Profile
Relative Dose (%)
140
120
100
80
60
40
20
0
-150
-100
-50
0
50
100
150
Field (mm)
Inplane 2.69cm
Crossplane 2.69cm
Inplane 5.0cm
Crossplane 5.0cm
Inplane 10cm
Inplane 20cm
Crossplane 10cm
Crossplane 20cm


18MV , 10X10 cm² Beam Profile
Relative Dose (%)
120
100
80
60
40
20
0
-150
-100
-50
0
50
100
150
Field (mm)
Inplane 3.0cm
Crossplane 3.0cm
Inplane 5.0cm
Crossplane 5.0cm
Inpane 10cm
Crossplane 10cm
Inplane 20cm
Crossplane 20cm
18MV , 30X30 cm² Beam Profile
Relative Dose (%)
120
100
80
60
40
20
0
-250
-200
-150
-100
-50
0
50
100
150
200
250
Field (mm)
Inplane 3.0cm
Crossplate 3.0cm
Inplane 5.0cm
Crossplane 5.0cm
Inplane 10cm
Crossplane 10cm
Inplane 20cm
Crossplane 20cm